



UNIVERSITA' DEGLI STUDI DI VERONA

DEPARTMENT OF

Neurosciences, Biomedicine and Movement Science

GRADUATE SCHOOL OF

Life and Health Sciences

DOCTORAL PROGRAM IN

*Biomolecular Medicine
Biochemistry Curriculum*

XXXV Cycle

Delivery of STAT3 through Extracellular Vesicles:
basis of a new possible Therapeutic Approach for the Treatment of
Autosomal Dominant Hyper-IgE Syndrome (AD-HIES)

S.S.D. BIO/10

Coordinator: Prof.ssa Lucia De Franceschi
Tutor: Prof.ssa Sofia Giovanna Mariotto
Co-Tutor: Dott.ssa Elena Butturini

Doctoral Student: Dott.ssa Ilaria Bettin

UNIVERSITA' DEGLI STUDI DI VERONA

DEPARTMENT OF

Neurosciences, Biomedicine and Movement Sciences

GRADUATE SCHOOL OF

Life and Health Sciences

DOCTORAL PROGRAM IN

*Biomolecular Medicine
Biochemistry Curriculum*


XXXV Cycle

Delivery of STAT3 through Extracellular Vesicles:
basis of a new possible Therapeutic Approach for the Treatment of
Autosomal Dominant Hyper-IgE Syndrome (AD-HIES)

S.S.D. BIO/10

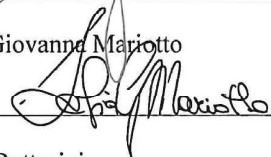
Coordinator: Prof.ssa Lucia De Franceschi

Signature



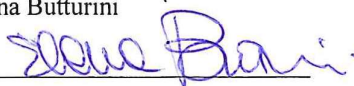
Tutor: Prof.ssa Sofia Giovanna Mariotto

Signature



Co-Tutor: Dott.ssa Elena Butturini

Signature



Doctoral Student: Dott.ssa Ilaria Bettin

Signature



This work is licensed under a Creative Commons Attribution-NonCommercial-NoDerivs 3.0 Unported License, Italy. To read a copy of the licence, visit the web page:
<http://creativecommons.org/licenses/by-nc-nd/3.0/>



Attribution — You must give appropriate credit, provide a link to the license, and indicate if changes were made. You may do so in any reasonable manner, but not in any way that suggests the licensor endorses you or your use.



NonCommercial — You may not use the material for commercial purposes.



NoDerivatives — If you remix, transform, or build upon the material, you may not distribute the modified material.

*Delivery of STAT3 through Extracellular Vesicles: basis of a new possible Therapeutic Approach
for the Treatment of Autosomal Dominant Hyper-IgE Syndrome (AD-HIES)*
Ilaria Bettin

PhD Thesis
Verona, 13th July 2023

Table of Contents

Abstract	3
List of Abbreviations.....	4
Introduction	6
1. Extracellular Vesicles: nomenclature and biogenesis.....	6
1.1. EVs nomenclature.....	6
1.2. EVs biogenesis.....	8
2. Isolation and characterization of Extracellular Vesicles.....	14
2.1. EVs Isolation	14
2.2. EVs characterization.....	17
2.2.1. Physical characterization.....	18
2.2.2. Molecular characterization.....	21
3. EVs in biomedical applications.....	23
3.1. EVs as Diagnostic Tools.....	23
3.2. Therapeutic potential of EVs: focus on EVs as Drug Delivery Systems	24
3.3. Innate therapeutic potential of EVs	31
3.4. Challenges ahead	32
4. Signal Transducer and Activator of Transcription 3.....	33
4.1. STAT3 structure	33
4.2. STAT3 signalling cascade	34
5. Autosomal Dominant Hyper-IgE Syndrome (AD-HIES).....	37
5.1. STAT3 role in T _H 17 cells development.....	37
Aim of the Thesis	39
Materials and Methods	41
1. Materials.....	41
2. Methods.....	42
2.1. Generation of the recombinant baculovirus for EGFP-STAT3 expression.....	42
2.2. Expression and purification of EGFP-STAT3 recombinant protein	44
2.3. Biophysical and functional characterization of EGFP-STAT3	46
2.4. Isolation of EVs from RO cells	47
2.5. Encapsulation of EGFP-STAT3 in RO cells EVs	48
2.6. Characterization of isolated EVs	49
2.7. Evaluation of the cellular uptake of EGFP-STAT3 loaded EVs.....	51
Results and Discussion.....	54
1. Purification of EGFP-STAT3 and STAT3 recombinant proteins.....	54
2. Biophysical and biochemical characterization of EGFP-STAT3 and STAT3 recombinant proteins.....	56

3. Isolation and characterization of EVs from RO cells	58
4. Encapsulation and characterization of EGFP-STAT3 loaded EVs.....	60
5. Evaluation of EGFP-STAT3 EVs uptake by MDA-MD-31 cells.....	65
Conclusions and Outlook	69
Appendixes	71
Appendix I	71
Appendix II	77
Bibliography	78

Abstract

Autosomal Dominant Hyper-IgE syndrome (AD-HIES) is a rare primary immunodeficiency and multisystem disorder characterized by recurrent infections, complex somatic features and increased innate immune response. Dominant negative mutations in the signal transducer and activator of transcription 3 (STAT3) gene underlie most AD-HIES cases. Impairment of STAT3 functionality leads to compromised development of T_H17 cells, a subset of CD4⁺ T cells responsible for host defence, resulting in the clinical features of AD-HIES. To date, no specific treatments are available, and the main therapeutic approaches are limited to supportive treatment and antimicrobial prophylaxis. Thus, the development of new therapeutic strategies represents an urgent need.

Here we proposed the restoration of STAT3 signalling by Extracellular Vesicles (EVs)-mediated administration of fully functional wild type STAT3. A novel recombinant fusion construct of STAT3 tagged with EGFP was produced using a baculovirus-based expression system and characterized from a biochemical and biophysical point of view. EGFP-STAT3 was encapsulated in EVs isolated from B-lymphoblastoid cells conditioned medium using a saponin-assisted method. The obtained EVs were characterized by fluorescence detection, western blotting, and Nanoparticle Tracking Analysis. In addition, the internalization of EGFP-STAT3 was demonstrated by proteolysis reaction. The EVs delivery potential of EGFP-STAT3 was successfully assessed in an *in vitro* cellular model using confocal microscopy.

The obtained results constitute the scientific background for further development of a new possible therapeutic approach for the treatment of AD-HIES.

List of Abbreviations

AD-HIES	Autosomal Dominant-HyperIgE Syndrome
ARMM	Arrestin domain-containing protein 1 (ARCC1)-mediated microvesicles
AU	Absorbance Unit
a.u.	arbitrary unit
BCA	Bicinchoninic acid Assay
BSA	Bovine Serum Albumin
CCM	Cell Conditioned Medium
CD	Circular Dichroism
DDS	Drug Delivery Systems
DLS	Dynamic Light Scattering
EGFP-STAT3	Enhanced Green Fluorescent Protein Signal Transducer and Activator of Transcription 3
ESCRT	Endosome Sorting Complexes Required for Transport
EVs	Extracellular Vesicles
FBS	Fetal Bovine Serum
HRP	Horseradish Peroxidase
ILVs	Intraluminal Vesicles
JAK2	Janus Kinase 2
MW	Molecular Weight
MWCO	Molecular Weight Cut-Off
MRW	Mean Residue Weight
MVs	Microvesicles
MVBs	Multi Vesicular Bodies
NTA	Nanoparticle Tracking Analysis
PBS	Phosphate Buffer Saline
PCR	Polymerase Chain Reaction
PEG	Polyethylene Glycol
PMSF	Phenylmethylsulfonyl Fluoride
PVDF	Polyvinylidene Difluoride
RT	Room Temperature
SD	Standard Deviation
SEC	Size Exclusion Chromatography
SEM	Standard Error Measurement

SOE PCR	Short Overlap Extension Polymerase Chain Reaction
SDS	Sodium Dodecyl Sulphate
SDS-PAGE	Sodium Dodecyl Sulphate PolyAcrylamide Gel Electrophoresis
SNAP	Soluble <i>N</i> -ethylmaleimide-Sensitive Factor Attachment Protein
SNARE	SNAP receptor
STAT3	Signal Transducer and Activator of Transcription 3
TCEP	Tris(2-CarboxyEthyl)Phosphine
TEV	Tobacco Etch Virus
TFF	Tangential Flow Filtration
UC	Ultracentrifugation
UF	Ultrafiltration
VPS4A	Vacuolar Protein Sorting-associated protein 4A
VTA1	Vacuolar protein sorting-associated protein 1
WB	Western Blot

Introduction

1. Extracellular Vesicles: nomenclature and biogenesis

The existence of cell-derived membrane extracellular vesicles (EVs) in mammalian tissues and fluids was known from the late 1960s when the first EVs images were captured. At the time, these particles were considered merely inert cellular debris and referred to as “platelet dust” (1). In the following decades, other publications described structures consistent with EVs and the first discussions on the existence and nature of these vesicles arose (2). Some of the key EV milestones from 1940s are outlined in Fig.1.

In the early 1980s, two independent groups described the secretion of transferrin receptors via the release of intraluminal vesicles from reticulocytes. These seminal works gave the first evidence of the EVs secretion pathways but also suggested that EVs could be used by cells for the disposal of obsolete molecules (3). In 1996, Raposo and colleagues discovered that EVs secreted from Epstein-Barr virus-transformed B-cells could stimulate adaptive immune responses suggesting that EVs were more than waste carriers, instead, they were likely to play a role in cell-to-cell communication (4). This and other discoveries published in these years catalysed the attention of the scientific community on EVs, their physiological and pathological role and their potential as biomarkers and therapeutics.

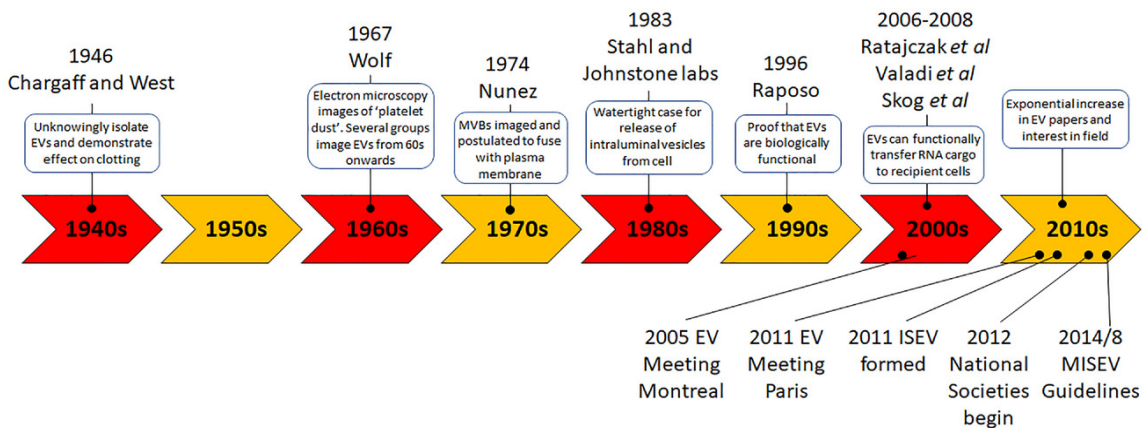


Fig. 1. Timeline of the selected milestones in the EV field. Adapted with permission from (3).

1.1. EVs nomenclature

In the early days, the scientific community used to recognize and stratify EVs into three main subtypes, namely exosomes, microvesicles (MVs) and apoptotic bodies, differentiated mainly on the available information regarding biogenesis mechanism and biophysical properties. In the later years, several other types of EVs have been described leading to a more and more complicated and intricate landscape (5).

This new knowledge led to the proposal of a new biogenesis-based classification in which EVs can be distinguished into two major subtypes: exosomes, if of endosomal origin, and ectosome, if released from the plasma membrane (6) (Fig. 2).

Exosomes (~50-200 nm diameter), are first generated when the endosomal membrane buds inwardly to form intraluminal vesicles (ILVs) in multivesicular compartments (multivesicular bodies (MVBs)) and are later secreted upon fusion of these compartments with the plasma membrane (7) (Fig. 2, right panel).

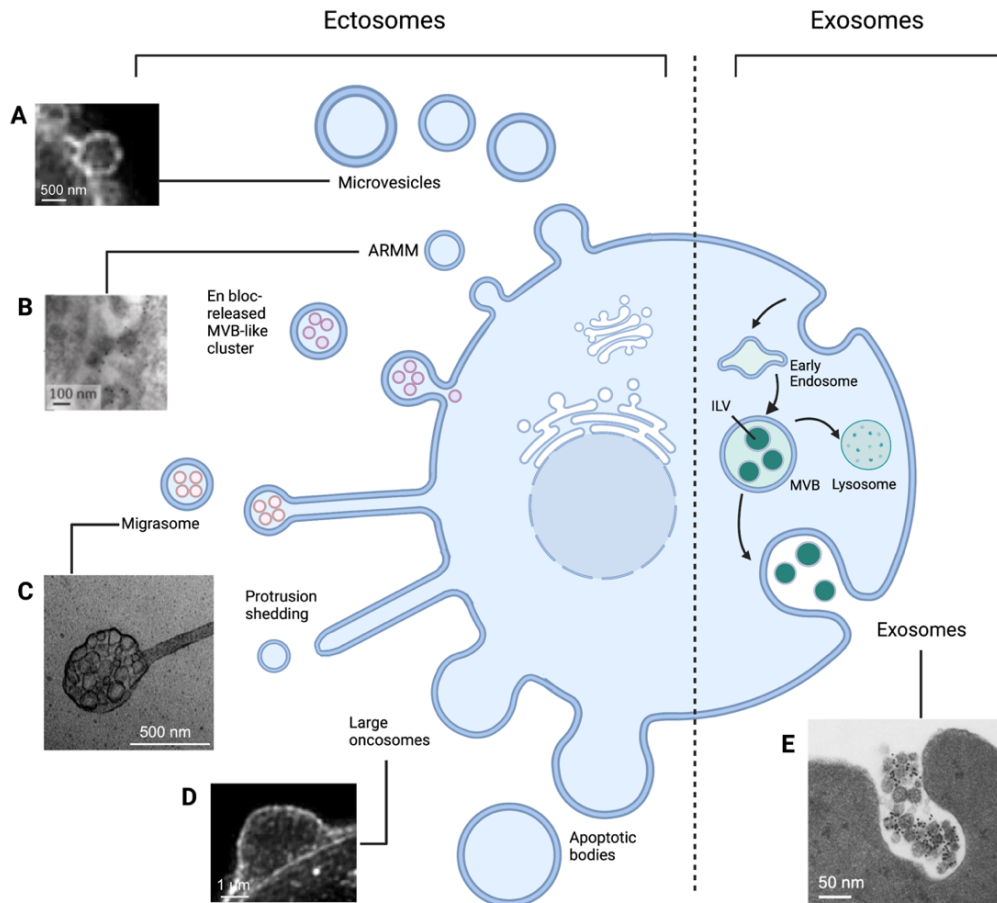


Fig.2. Schematic representation of the heterogeneity of EVs. Different types of ectosomes, left panel, with microscopy images. Exosomes, right panel. (A) Microvesicles released from colon cancer cells, observed by Structured Illumination Microscopy upon immunostained for Annexin1. Adapted with permission from (8). (B) Arrestin domain-containing protein 1 (ARCC1)-mediated microvesicles (ARMM) expressing ARCC1 fused with m-Cherry, detected by transmission electron microscopy, gold-labelled with anti-mCherry. Adapted with permission from (9). (C) Transmission electron microscope image of the pomegranate-like structures typical of migrasomes. Adapted with permission from (10). (D) Large oncosomes released from colon cancer cells, observed by Structured Illumination Microscopy upon immunostaining for Annexin1. Adapted with permission from (8). (E) Immuno-electron microscopy image of exosomes labelled with gold anti-transferrin receptor antibody. Adapted with permission from (9).

Differently, ectosomes are generated by outward budding of the plasma membrane, in a similar manner to retroviruses, as described by (11) (Fig. 2 left panel). Various subpopulations of ectosomes have been characterized, including microvesicles (MVs). These vesicles vary in size from 200 to 1000 nm diameter (Fig. 2 A) and constitute one of the main ectosome subpopulations.

Smaller vesicles (~100 nm) budding from the plasma membrane have been described, these are called arrestin domain-containing protein 1-mediated microvesicles (ARMM) (12) (Fig. 2 B). Large oncosomes can also be included among ectosomes (13). These large vesicles (1-10 μm) are typically released by cancer cells and are responsible for horizontal propagation of oncogenes (14) (Fig. 2 D). Lately, a plethora of low-abundance distinct EVs subtypes have been reported, such as migrasomes (10) (Fig. 2 E), exophers, cilia-derived vesicles, and *en bloc*-released MVB-like small EV clusters, which are still under characterization (6). In addition, apoptotic bodies (~1-5 μm) are formed during programmed cell death in a tightly regulated manner. Apoptotic bodies are difficult to distinguish from other large EVs, but they appear to contain relatively more genomic DNA than other EVs (15).

However, as stressed by the International Society of Extracellular Vesicles (ISEV), owing to the lack of markers of specific biogenetic routes and the overlapping size of different EVs subtypes, it is highly difficult to assign one or the other term. For this reason, in the Minimal Information for Studies of Extracellular Vesicles (MISEV) guidelines, it has been encouraged the use of “operational terms” if a portion of the population is isolated within a specific study. For instance, the terms “small” EVs and “large” EVs may be used within a particular study, provided that a clear definition of how the isolation procedures allowed the size differentiation is given (16).

In this thesis, since we did not focus on the isolation of a specific EVs subpopulation, the term Extracellular Vesicles (EVs) will be used, as endorsed by ISEV.

1.2. EVs biogenesis

Investigations on EVs biogenesis have been considerably hampered by the unavailability of efficient isolation methods (17). Indeed, preparations obtained by most current protocols are highly heterogeneous, being composed of EVs of endosomal and non-endosomal origin in different proportions according to the chosen isolation method (18). As already partially described above, overlapping ranges of size, similar morphology, and density among different types of EVs make the characterization of the specific mechanisms behind the biogenesis of both exosomes and ectosomes extremely challenging (17).

Nonetheless, researchers have succeeded in shedding some light on the cell biology of EVs, mainly using microscopy and biochemical techniques. Current knowledge on EVs biogenesis is mainly focused on exosomes and MVs, which, despite presenting different biogenesis processes, share common finely tuned membrane trafficking machinery (19).

Exosome biogenesis, transport, and release

Proteins meant to be secreted can be internalized from the plasma membrane (Fig. 3, step 1, in grey, and 2a, green) or reach the endosomal compartment from the Golgi apparatus (Fig. 3, step

2b, green), forming what is called early endosomes (EE). At this stage, cargo recycling and translocation to the plasma membrane or retrograde transport to the Golgi is also possible (20).

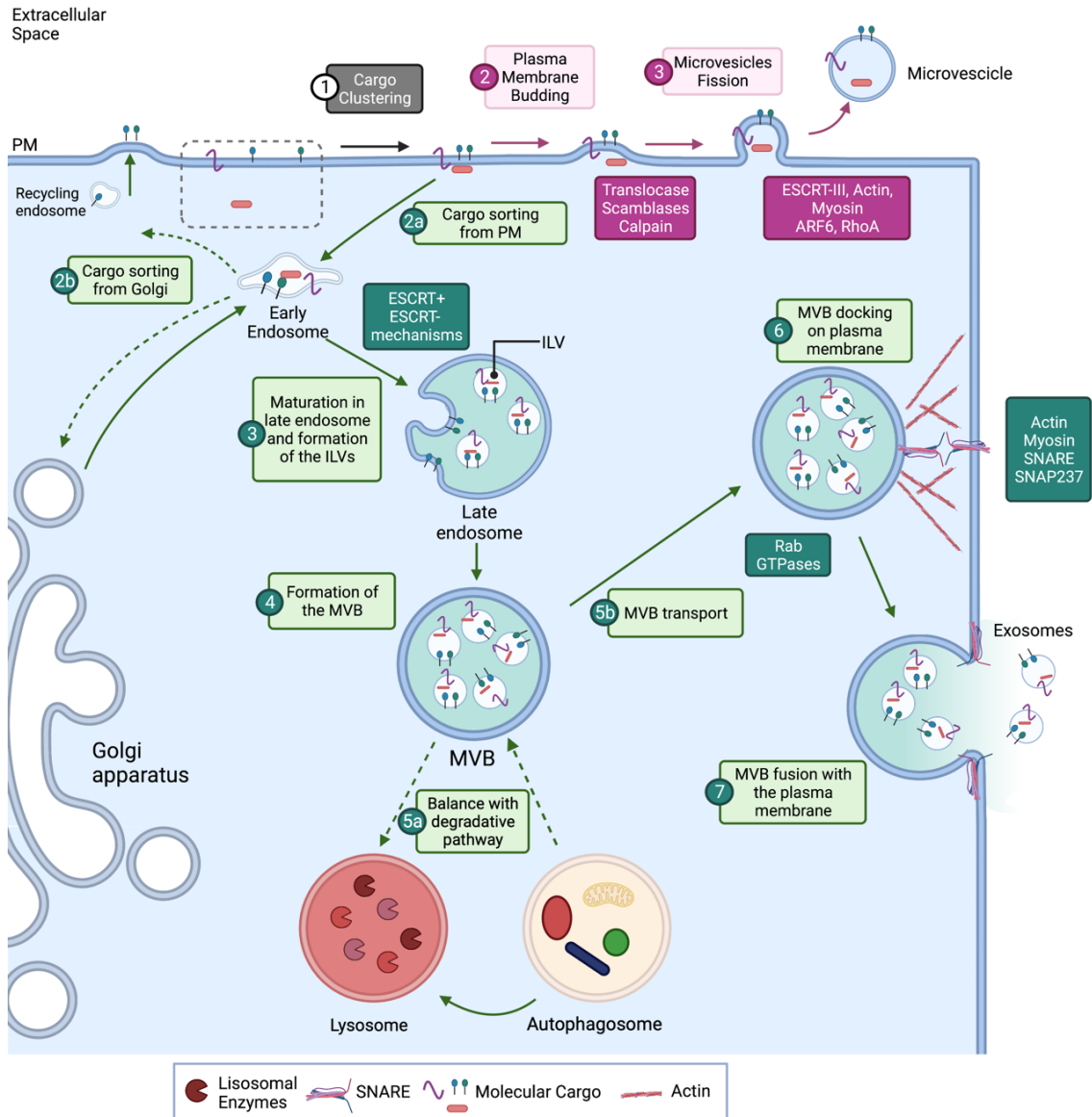


Fig. 3. Biogenesis of exosomes and microvesicles. The biogenesis pathway starts with a common step of cargo clustering (Step 1, grey). In the case of exosome biogenesis (green boxes), the cargo is targeted to the EE from the plasma membrane and/or the Golgi apparatus (Step 2 a-b, green); eventually, this EE can be recycled and fused back with the plasma membrane. The early endosome matures in the late endosome (Step 3, green) and later in MVB (Step 4, green), which presents in its lumen the ILVs formed by inward invagination of the endosome limiting membrane. The MVB can fused with Lysosomes or Autophagosomes (Step 5a, green) or can be transported to the plasma membrane (Step 5b, green) where its docking (Step 6, green) and fusion (Step 7, green) determine the release of exosomes in the extracellular space. During microvesicle biogenesis, the plasma membrane undergoes a rearrangement in protein and lipidic composition that leads to the membrane budding (Step 2, magenta), other protein machineries (dark magenta box) induce membrane fission and the release of the microvesicles (Step 3, magenta). ILVs, intraluminal vesicles; MVBs, multivesicular bodies; PM, plasma membrane. Figure partially inspired from (21). Illustration created with Biorender.com.

Early endosomes undergo a maturation process in which Intra Luminal Vesicles (ILVs) are formed through inward budding of the endosomal membrane (Fig. 3, step 3, green). ILVs further mature leading in turn to the formation of the late endosome and, later, of the Multi Vesicular

Bodies (MVBs) (22). Once MVBs are formed, they can fuse with lysosomes or autophagosomes, resulting in the degradation of their content, (Fig. 3, step 5a, green) or with the plasma membrane to release the exosomes in the extracellular space (21) (Fig. 3, step 5b-7, green). In this latter case, MVs are engaged in intracellular transport towards the plasma membrane (Fig.3, step 5b, green). The transport and fusion of MVBs to the plasma membrane require their association with the cytoskeleton (e.g., actin and microtubules), molecular motors (e.g., dynein, kinesins and myosins) and small GTPases (for example, Rab GTPases) proteins (21). Indeed, cytoskeletal proteins support both short- and long-range movements of MVBs along with molecular motor proteins (23), whereas Rab proteins have been suggested to serve in the docking of MVBs to the plasma membrane by rearrangement of the sub-membrane cytoskeleton (24) (Fig. 3, step 6, green). The final stage, namely the fusion of MVBs with the plasma membrane, is mainly arranged by SNARE (soluble NSF attachment protein receptor proteins) and by synaptotagmin family members (25) (Fig. 3, step 7, green).

All sorting processes are orchestrated by a particular machinery, the endosome sorting complexes required for transport (ESCRT) (26). The ESCRT machinery comprises of four different subcomplexes (ESCRT 0-I-II-III) and accessory proteins (Alix, VPS4, and VTA-1) (27).

Microvesicle biogenesis and release

In stark contrast with exosomes, the mechanisms underlying Microvesicles (MV) biogenesis and release are far less defined (22).

According to current understanding, the molecular cargoes fated for secretion into MVs are gathered at the budding site by binding to the inner leaflet of the plasma membrane or through their affinity for lipid rafts (28).

During MVs biogenesis, the plasma membrane undergoes several distinct and localized rearrangements in terms of lipid components and protein composition, which are responsible for modulation of its curvature and rigidity perturbation (budding) (29). This reorganization also affects the local electrolytes level (14). Alterations in Ca^{2+} levels in plasma microdomains induce the activation of Ca^{2+} -dependent enzymes, such as aminophospholipid translocases, scramblases, and calpain, with the consequent translocation of membrane phospholipids and disruption of membrane lipid asymmetry (30).

The following fission is driven by the rearrangement of the actin and myosin cytoskeleton. Small GTPases ADP-ribosylation factor 6 (ARF6) and RhoA, along with calpain (31), have been identified as regulators of actin dynamics. Indeed, they both act as initiators of two different signalling cascades that culminate in the activation of the myosin light chain, actomyosin contraction, and MVs release (21).

Cargo recruitment and EVs composition

The selective recruitment of proteins to EVs is performed by several regulatory proteins. For example, ARF6 determines the incorporation of $\beta 1$ integrin receptors, MHC class I molecules, membrane type 1-matrix metallo-proteinase 1 (MT1-MMP) and the vesicular SNARE (v-SNARE) vesicle-associated membrane protein 3 (VAMP3) into tumour derived MVs (21).

In addition to transmembrane cargo, cytosolic proteins may also be sequestered into ILVs mainly as a result of co-sorting with other proteins, such as the chaperones heat shock 70 kDa protein (Hsp70) and heat shock cognate 71 kDa protein (Hsc70) (32). Ubiquitylated and farnesylated cytosolic proteins have also been identified in EVs (33).

Interestingly, membrane microdomains are also suggested to be involved in sorting of cytosolic proteins and nucleic acids (21). In addition to proteins, extracellular vesicles also enclose mRNAs and non-coding RNAs, such as microRNAs, as well as DNA sequences (34). Fig. 4 summarizes the principal molecular cargo of the EVs.

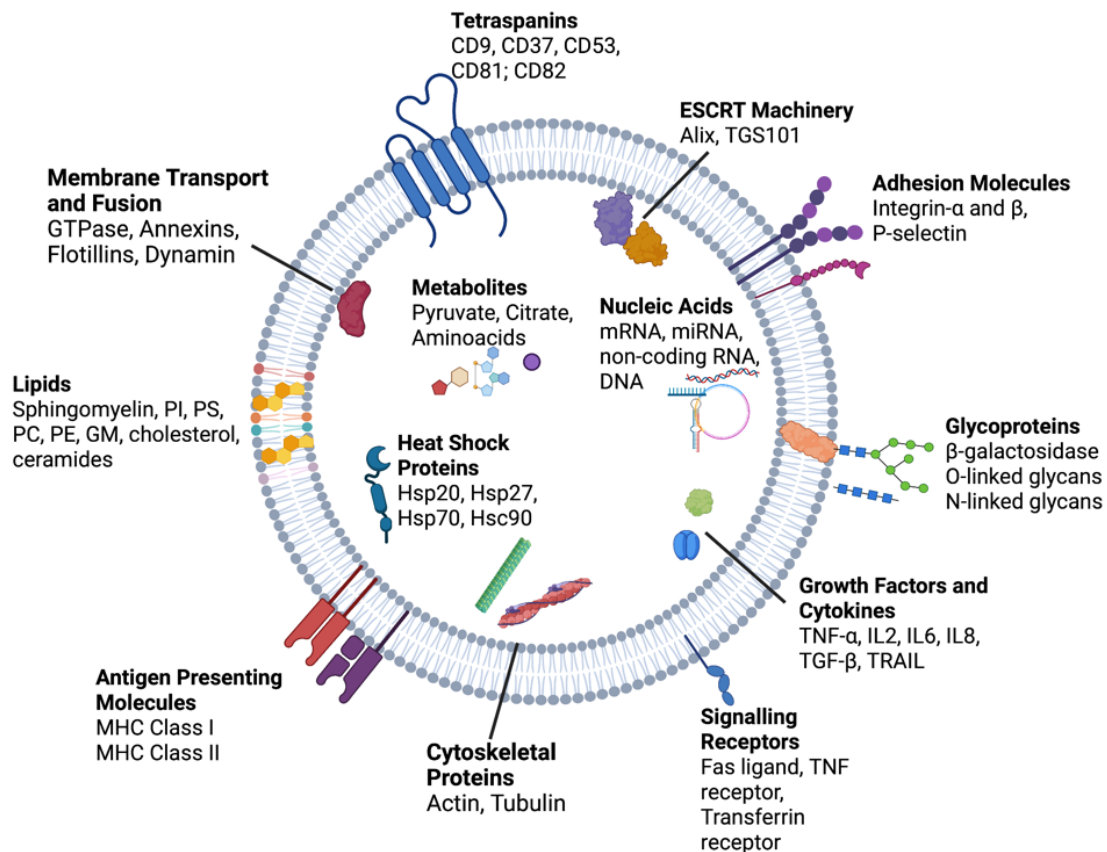


Fig. 4. Composition of EVs. EVs are composed of several types of proteins, lipids, and nucleic acids. Transmembrane proteins: tetraspanins, antigen presenting molecules, glycoproteins, and adhesion molecules. Cytosolic proteins: heat shock proteins (Hsp), cytoskeletal proteins, ESCRT components, membrane transport, fusion proteins, growth factors, and cytokines. Lipids: cholesterol, ceramides, sphingomyelin, phosphatidylinositol (PI), phosphatidylserine (PS), phosphatidylcholine (PC), phosphatidylethanolamine (PE), and gangliosides (GM). Nucleic Acids: mRNA, miRNA, non-coding RNA and DNA. Hsc, heat shock cognate; TSG, tumor susceptibility gene; TNF, tumor necrosis factor; TGF, Transforming growth factor; TRAIL= TNF-related apoptosis-inducing ligand. Figure inspired from (35).

1.3. EV uptake and cell-to-cell communication

A growing body of evidence supports the hypothesis of the importance of extracellular vesicles in intercellular communication (7). Clearly, to elicit a functional response and promote phenotypic changes in target cells, an interaction between EVs and target cells must occur (21). Two main types of interactions have been identified: EVs may interact via their surface ligands with receptors on cells (Fig. 5 A) and initiate intracellular signalling pathways, or they may deliver their cargo in the recipient cells (Fig. 5 B-F) (17,22).

In both cases, the mechanisms underlying EVs targeting remain poorly defined (17), although they are most likely determined by highly specific interactions between EVs ligands and cell receptors (21). For instance, Tetraspanines CD9 and CD81 present on EVs surfaces have been shown to contribute to EVs uptake in dendritic cells through interaction with cellular integrin $\alpha V\beta 3$. At the same time, integrins on the surface of EVs have been found to interact with intercellular adhesion molecules (ICAMs) on the surface of dendritic cells (36). Interestingly, extracellular matrix protein may mediate the interaction between EV integrins and the target cells, acting like a “zipper” (37). Lastly, the lipid composition of EVs may affect internalization, for example, phosphatidylserine can be specifically recognized by Tim4 (T-cell immunoglobulin- and mucin-domain-containing molecule) (38).

EVs can directly fuse with the plasma membrane (Fig. 5 B) or be internalized by endocytosis (Fig. 5 C-F) if the EVs cargo needs to be delivered to the cytosol (39). Despite some studies describing examples of direct fusion with the plasma membrane (40), most of experimental evidence supports the predominant involvement of endocytosis (22).

1.4. Delivery of content in recipient cells

Very little is known about the post-internalization fate of extracellular vesicles, but most likely EVs would chase the classical endosomal pathway (35). Once internalized, EVs are targeted to the early endosomes, where they are sorted toward recycling endosomes and then re-secreted (Fig. 5 H) or toward lysosomes (Fig. 5 G) while passing through MVBs and late endosomes (41). Once fused with lysosomes, they eventually undergo degradation, hindering the delivery of EV cargo (42,43).

However, since countless EV-mediated functional effects are observed in cells, EVs should be able to bypass lysosomal degradation (44). How EVs actually manage to fuse with the early endosome membrane and release their content is still largely unknown, and some authors have proposed membrane fusion triggered by acidification (17) (Fig. 5 I). Moreover, a new role for lysosomes has been suggested as a functional site for EVs (44). Nonetheless, it cannot be ruled out that EVs content delivery may take place by “simple” fusion of EVs with the plasma membrane allowing the direct release of the cargo in the cytosol (17).

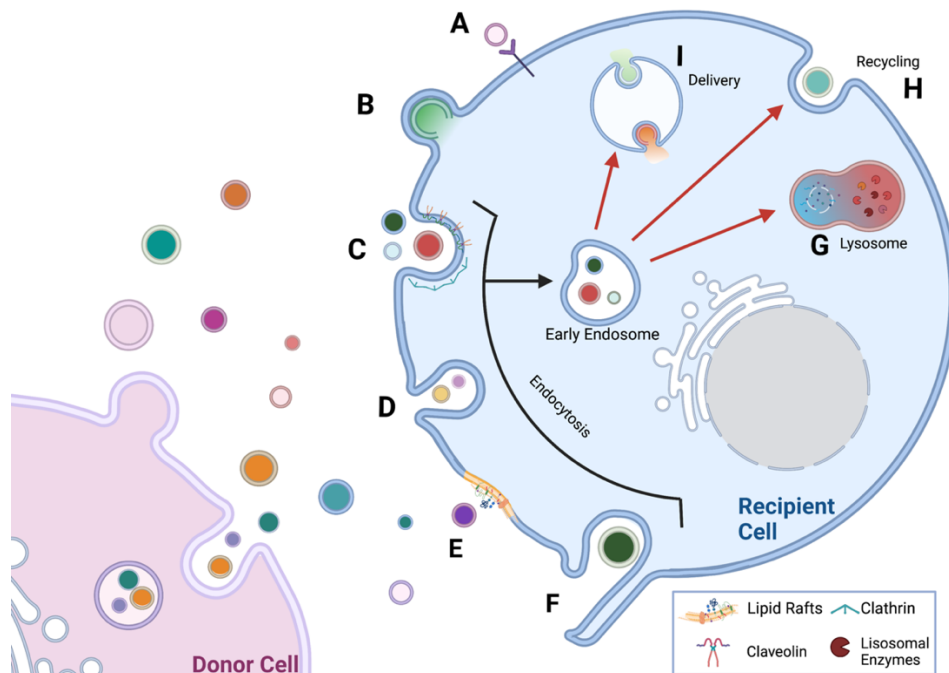


Fig. 5. EVs uptake and cell-to-cell communication. (A) Interaction of EVs with a specific receptor on the recipient cell surface triggers specific signalling inside the cell. (B) Fusion with the plasma membrane of the recipient cell with direct release of the EVs content in the cytosol. Different endocytotic mechanisms: (C) Clathrin- and caveolin-mediated endocytosis. (D) Phagocytosis, (E) lipid raft-mediated internalization, and (F) macropinocytosis. When EVs are internalized through an endocytotic mechanism they may be targeted to endosomes. At this stage, they can be targeted to lysosomes for degradations (G), recycled, and re-secreted in the extracellular space (H), or they may release their content in the cytosol, escaping the endosomal route (exact mechanism not yet clarified) (I). Figure inspire by (17).

2. Isolation and characterization of Extracellular Vesicles

2.1. EVs Isolation

EVs are secreted by the parental cells in the extracellular space. In an *in vitro* setting, they will be secreted in the culture medium, while in an *in vivo* context, their fate is far more complex. As a result, since EVs are secreted by almost all body cell types (45), they can be found in several types of body fluids, such as blood, urine, broncho-alveolar lavage fluid, cerebrospinal fluid, and milk (46). These matrices contain not only EVs but also a variety of other components, such as proteins, nucleic acids, sugar, and lipids, or other molecules, depending on the material source. Thus, the EVs have to be isolated from the “contaminants” non-EVs components in the preparations (47).

EVs isolation is undoubtedly one of the main hurdles in EVs research, regardless of the experimental question or purpose proposed by researchers. An ideal isolation method should provide evidence of high recovery and high specificity, being both effective and efficient. Unfortunately, obtaining EVs preparations characterized by high particle yield, absence of contaminants and which, at the same time, show preserved integrity and biophysical features is not a reachable goal with the technologies available as of this writing. Therefore, it is very important to emphasize that there is no “one method-fit-all” solution, but the choice of isolation method(s) will be mainly related to the aim of the research (46,48).

A particularly important note must be made regarding EVs isolation from mammalian cell cultures. Mammalian cells are usually cultured in media supplemented with Fetal Bovine Serum (FBS) or serum derived from other species (e.g., goat, horse, human, pig), which contain EVs and other protein aggregates that may be co-isolated with EVs from cells (49). This could lead to misinterpretation of the results of the following experiment and potentially introduce a source of xeno-immunisation, which can strongly impact therapeutic applications (50). Therefore, in most EVs isolation protocols from cell culture, before the harvesting of the conditioned medium, the cells are cultivated for 24-48 hours in medium without FBS (7-9). Alternatively, some groups used EV-depleted FBS media, mainly obtained by ultracentrifugation for prolonged periods (up to 18 hours) (47). Another proposed solution is to use serum-free, chemically defined supplements to avoid any possible contamination from FBS-derived EVs, extracellular proteins and RNAs (51).

Regardless of the chosen isolation method, the initial matrix is usually subjected to one or more pre-clearance steps, which comprise a series of consecutive runs at different centrifugal forces and durations. In the case of conditioned medium from *in vitro* cultured cells (CCM), the first centrifugation is usually performed at a low speed in the range of $300 \times g$ to remove cells and other large particles (52), followed by another centrifugation step at a higher speed, up to 10,000

× g, to further deplete the medium of particles, such as cellular debris (47). In the case of biofluids, given their higher viscosity, a dilution usually in phosphate buffer is performed on the initial matrix, and the centrifugation steps are carried out at increased speed and length (47). EVs are then isolated from the clarified matrices using one of the listed methods.

Ultracentrifugation

Ultracentrifugation (UC) is the most commonly used technique for EVs isolation according to a worldwide survey performed by the ISEV in 2019 (53). Upon application of centrifugal force, the particles present in the sample sediment according to their size and density over time. The larger and heavier the particles, the higher will be the sedimentation rate and the lower the force required for their pelleting. Instead, for smaller particles, such as EVs, higher forces – faster centrifugation rates are required to achieve their precipitation (54). Usually, centrifugation is performed at approximately 100,000-120,000 × g for 2 hours but numerous different protocols, ranging from 1 hour to overnight centrifugation, can be found in the literature (55,56).

Density Gradient Ultracentrifugation

Density Gradient Ultracentrifugation (DG UC) has been used to increase the purity of UC-based EVs preparations (57,58). This technique is based on the observation that particles of different densities can be fractionated in a density gradient medium upon ultracentrifugation (59). Specifically, a density gradient is generated by layering solutions of gradually decreasing density from the bottom to the top of the tube (60). The sample is applied on the top of the medium and ultracentrifuged for a prolonged period, from 16 to 90 hours (61). Each component moves in the discontinuous gradient until it reaches a layer having the same density (isopycnic separation). In an alternative approach, called moving-zone gradient UC, the gradient medium has a lower density than the particles; thus, particles move at a speed that is solely based on their size (62). Sucrose and iodixanol (commercially available as OptiPrep™) are the most commonly used gradient media.

Size Exclusion Chromatography

Another separation method employed in EVs research is Size Exclusion Chromatography (SEC). Traditionally, this technique has been widely used to separate the various macromolecules present in a sample according to their hydrodynamic volumes. In SEC, the stationary phase is composed of heterosporous polymeric beads that ultimately create a “maze” inside the column. The smaller the molecule, the greater the number of pores accessible to the molecules and, thus, the longer will be the retention time. In contrast, larger molecules have less to no access to the pores, travelling mainly through the volume among the pores, thus resulting in lower retention times (63).

Similarly, SEC has been reported to successfully separate EVs from soluble protein contaminants and other complexes present in initial samples (64). For EVs isolation purposes, the most commonly used stationary phases are cross-linked agarose beads, such as the commercially available Sepharose® CL-2B or CL-4B, but other matrices based on polyacrylamide and dextran beads have been proposed. Isolation of EVs through SEC has been employed in a variety of sample matrices, including but not limited to, plasma, urine, cell culture medium, and milk (65).

Filtration-based Method

Filtration is another size-based technique employed for both the isolation and concentration of EV-containing samples. In this technique, the separation of mixture components, according to a specific size range, is achieved using membranes with specified pore diameters. Two types of filtration are mainly used: ultrafiltration (UF) and tangential flow filtration (TFF).

In UF, the sample is forced through a membrane, which is generally placed in a container, by applying centrifugal force (66). In simple terms, molecules with a size smaller than the molecular weight cut-off (MWCO) migrate through the membrane while the larger molecules are retentate.

In TFF, the sample is applied on the membrane and displaced by a longitudinal flow passing across the membrane rather than through it, as in dead-end filtration (UF). Molecules with smaller sizes than the MWCO pass through the hollow fiber pores and are discarded, while molecules with larger sizes are kept in circulation, leading to a progressive concentration and enrichment of the larger molecules (67).

Polymeric Precipitation

Polymeric solutions have long been used for the precipitation of viral particles and macromolecules (63) and subsequently translated into EVs research. However, the mechanism underlying precipitation remains unclear. According to one of the most accredited theories, the addition of highly hydrophilic polymers leads to a decrease in EVs hydration, and thus, in their solubility (68). Indeed, in most protocols, mixing and overnight incubation of the sample with a polyethylene glycol (PEG) solution is followed by the sedimentation of EVs by centrifugation.

Affinity-based Techniques

The basic principle underlying these techniques is the highly specific interaction between an EVs membrane marker and a specific ligand (65,69). Typically, samples are incubated with ligands previously immobilized or conjugated to a solid surface, for example, magnetic beads, plates or affinity chromatography monolithic columns (65). After subsequential washing and elution steps, the EV-enriched sample is obtained (60). Antibodies targeting proteins present on EVs surfaces, such as tetraspanin CD9, CD63, and CD81 are commonly used, but EVs originating from specific cell types can be isolated if a specific marker is known (70).

Moreover, a plethora of other techniques has been developed and/or adapted for EVs isolation during the last few decades, including but not limited to flow field-flow fractionation, ion-exchange chromatography, and electrophoresis-based techniques. Moreover, several microfluidic devices that allow EVs separation from minimal sample volumes by applying the principles of already well-known techniques have been manufactured. For a detailed review, please refer to (65).

Method	Advantage	Disadvantage	Ref.
Ultracentrifugation	<ul style="list-style-type: none"> • Processing of high volumes of CCM • Minimal risk of contamination from separation reagents • Easily adaptable to other isolation methods 	<ul style="list-style-type: none"> • Poor recovery rate and coprecipitation of non-EV components • Possible disruption and aggregation of the components • Expensive equipment • Long run times • Poor scalability 	(71–73)
Density Gradient Ultracentrifugation	<ul style="list-style-type: none"> • Possibility to use isotonic solutions • Higher purity than 	<ul style="list-style-type: none"> • Significant workload • Expensive • Limited sample volume 	(69,74)
Size Exclusion Chromatography	<ul style="list-style-type: none"> • Samples not subjected to high pressure or shearing forces • Potential for separation of different evs subpopulations • low cost • Possibility of automatization 	<ul style="list-style-type: none"> • Co-isolation of particles with similar hydrodynamic volume. • Limited volume of the initial sample • The final dilution of the eluted EVs 	(63,65,75)
Ultrafiltration	<ul style="list-style-type: none"> • Simple, fast, and user-friendly technique 	<ul style="list-style-type: none"> • Risk of material loss and membrane fouling 	(73,76)
Tangential Flow Fractionation	<ul style="list-style-type: none"> • High scalability • Low impact on evs integrity 	<ul style="list-style-type: none"> • Requires optimization • Possibility of co-isolation of impurities 	(65)
PEG Precipitation	<ul style="list-style-type: none"> • Simple • Possibility of processing large volumes • Availability of commercial ready-to-use kits • No specialized laboratory equipment 	<ul style="list-style-type: none"> • Co-isolation of non-vesicular contaminants • PEG may interfere with downstream analyses • Longer processing time than UF and TFF 	(69,73)

Table 1. Overview of methods mainly used for the isolation and purification of EVs with their main advantages and disadvantages.

2.2. EVs characterization

A comprehensive and detailed characterization of EVs from a physicochemical and molecular point of view is of utmost importance, not only to assess the results of the isolation procedure, but also to gain information on EVs cargo, their role in cell-to-cell communication, and their diagnostic or/and therapeutic potential. As a result, in the Minimal Information for Studies of Extracellular Vesicles (MISEV) guidelines, recommendations on EVs characterization are listed and reviewed with critical analysis and helpful insights (48). Indeed, the assessment of EVs in terms of particle concentration and size, protein, lipid, and nucleic acid composition, and particle morphology is strongly encouraged, ideally combining multiple and orthogonal techniques (77).

2.2.1. Physical characterization

Light scattering techniques

Two main light scattering techniques are used in the EVs field, namely Dynamic Light Scattering (DLS) and Nanoparticle Tracking Analysis (NTA). When particles are present in a colloidal solution they move randomly in all directions in what is called Brownian motion. In particular, the smaller the particle, the faster will be the Brownian motion. Indeed, it is possible to calculate the particle size from Brownian motion by applying the Stokes-Einstein equation (78).

In both DLS and NTA, Brownian motion is measured by illuminating the suspension with a focused light beam and registering the scattered light. In DLS, the intensity fluctuations of the scattered light over time are registered by a detector (Fig. 6 A-B) and used to determine the diffusion coefficient of the particles, and thus their size distribution (Fig. 6 C) (79). DLS is a highly sensible technique and is particularly reproducible in the case of monodisperse homogeneous samples. Nonetheless, for the same reason, DLS is very sensitive to the presence of larger particles, resulting in a skewed particle distribution in polydisperse samples (such as EVs) (80).

In NTA, the scattered light of each particle is collected using a microscope and recorded by a camera (Fig. 6 D). The instrument software processes the captured videos (Fig. 6 E), tracking and calculating the diffusion coefficient of each tracked particle. As in the case of DLS, the diffusion coefficient, together with the temperature and viscosity of the liquid containing the particles, is used to calculate the particle size (hydrodynamic diameter). Simultaneously, the software is able to derive the particle concentration by counting the trackable particles in the field of view. In contrast with DLS, since each particle is tracked separately, the resulting estimation of the particle size distribution is not intensity-weighted but expressed as a function of particle number (81) (Fig. 6 F).

The main advantage of NTA is the possibility of determining particle concentration, which cannot be obtained by DLS. Moreover, several studies have provided evidence of better resolution and accuracy in sizing for NTA (82) compared to DLS in the analysis of polydisperse samples. NTA instruments also perform analysis in fluorescence mode, allowing to visualize, size and count fluorescent particles (83). EVs can be fluorescently labelled following different strategies, such as staining with non-specific membrane markers (for example, PKH67, DiI, BODIPY) (84), or with antibodies specifically recognizing EVs surface marker proteins (e.g., Alexa Fluor® or quantum dot conjugated anti-CD81 or -CD9) allowing the differentiation of different EVs-populations and potentially even their phenotyping (85). Moreover, fluorescent NTA measurements have been used to quantify EVs when fluorescent molecules are present in the intraluminal compartment (86).

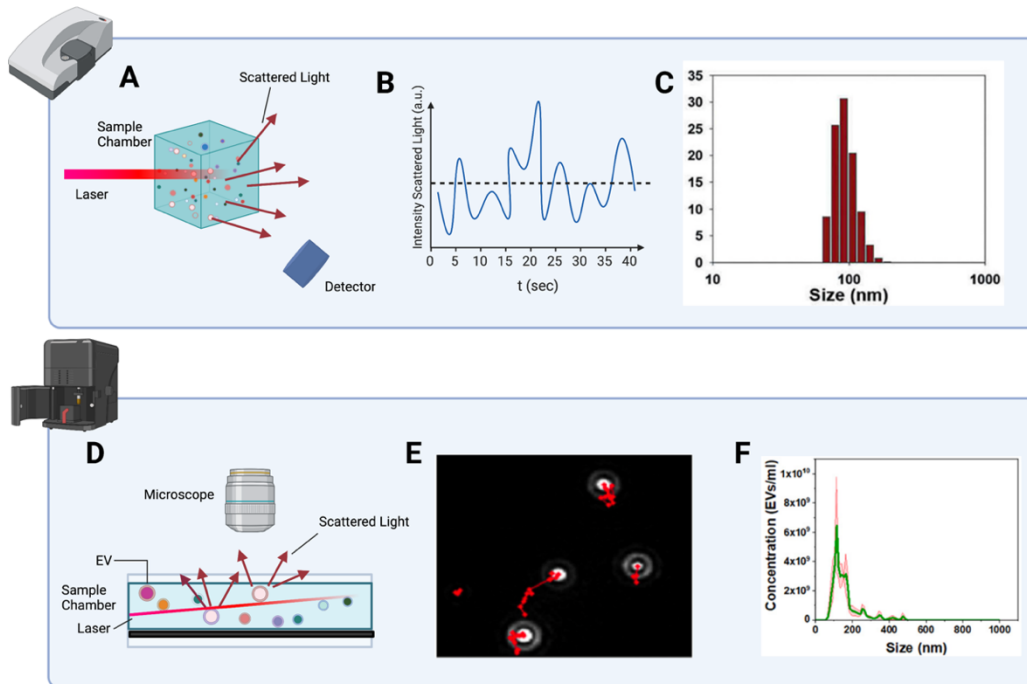


Fig. 6. Light scattering techniques for EVs characterization. Upper panel: Dynamic Light Scattering (DLS), (A) schematic representation of the optical setup, (B) representation of the recorded scattering intensity over time, and (C) typical DLS output for EVs. Adapted with permission from (87). Lower panel: Nanoparticle Tracking Analysis (NTA), (D) schematic representation of the basic setup, (E) tracking of the particle in the recorded video, (F) typical graph of the size distribution of the detected particles. (E) Adapted with permission from (88), and (F) adapted with permission from (89). (A) and (D) illustrations were created with Biorender.com.

Microscopy-based Techniques

Transmission Electron Microscopy (TEM) is widely used in EVs research. In TEM, a high-energy beam of electrons passes through a very thin sample, and an image revealing the finest details of the internal structure is formed on the fluorescent screen from the interaction between the sample and the electron (90) (Fig. 7 A).

Thus, TEM allows the detection and characterization of single EVs with high resolution (~ 1 nm) discriminating single EVs from non-EV particles of similar size (91) (Fig. 7 B). However, specimen preparation (drying and staining) may introduce morphological artifacts and prevent visualization of EVs in their native state (92). To circumvent this issue, cryo-TEM can be used (Fig. 7 C). In cryo-TEM, samples are directly applied on an EM grid, vitrified by flash freezing (water is transformed into a glass-like state but no ice crystals are formed), and then imaged keeping the sample in a special cooled holder (92). In this way, EVs can be visualized in their native hydrated structure (91), which is of an intact sphere, in contrast with the cup-shaped morphology visualized by TEM.

Additionally, for both TEM and cryo-TEM, immunophenotyping of EVs is also possible by incubating the sample with electron-opaque gold particles linked to an antibody directed against an EVs marker (91).

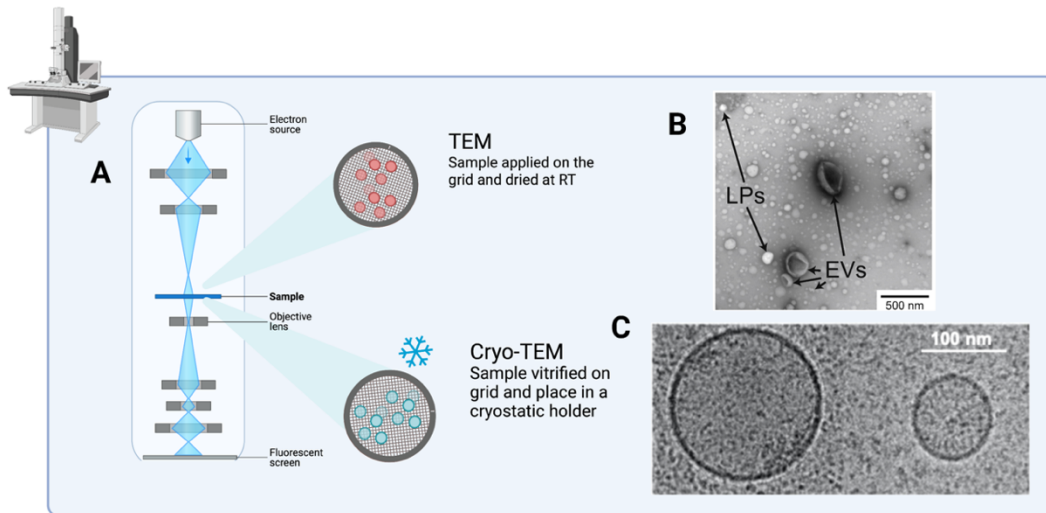


Fig. 7. Electron Microscopy techniques. (A) Schematic representation of an Electron Microscope, the Cryo-EM presents a cryostatic sample holder. (B) TEM image of EVs and lipoprotein particles (LPs) from the cell-depleted supernatant of a platelet concentrate, adapted with permission from (93). (C) Cryo-TEM of EVs isolated from HEK293T cells, adapted with permission from (86). Illustration (A) was created with Biorender.com.

Atomic Force Microscopy (AFM) has also been applied to determine vesicle size and morphology at nanometer-scale resolution (94). AFM allows the reconstruction of the 3D topography of a sample immobilized on a mica flat surface by recording variation in the distance between a gliding probing tip and the sample (89) (Fig. 8 A). If antibody-coated tips are used, this technique can also provide information on the protein content of the EVs membrane. Instead, if antibody-coated surfaces are used, the EVs subpopulation can be analysed. Nonetheless, this method has been questioned regarding the effect of the immobilization conditions on the shape of EVs (94). Moreover, this technique is quite demanding in terms of sample preparation and analysis since it allows for the analysis of one particle at a time (89).

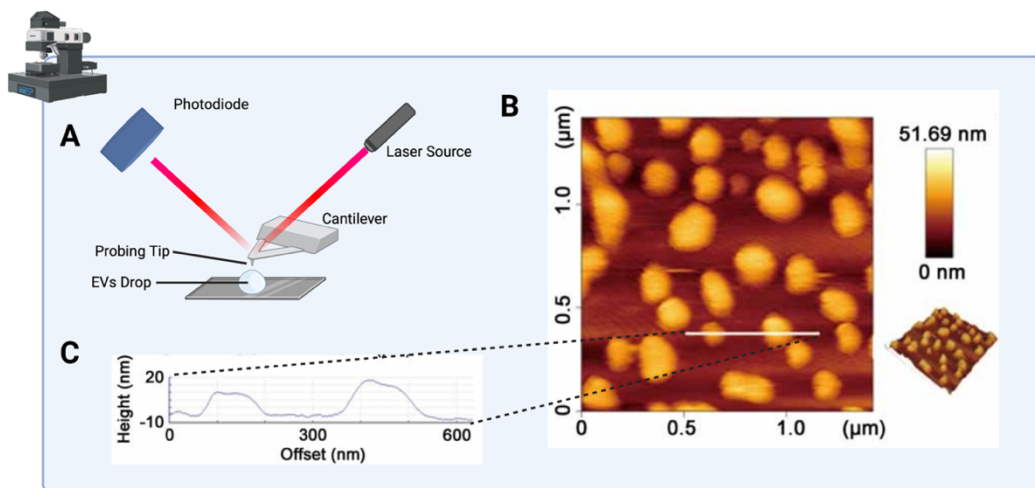


Fig. 8. Atomic Force Microscopy. (A) Schematic representation of the general components, (B) AFM image of exosomes on mica, with 3D topography, and (C) cross section following the line in the image. (B) and (C) adapted with permission from (95). Illustration (A) was created with Biorender.com.

Physical characterization of the EVs has also been performed using scanning electron microscopy and tunable resistive pulse sensing. This latter technique allows the measurement of particle size and concentration, but it can also be used to evaluate the zeta potential of nanoparticles (96). Nonetheless, these techniques are less commonly used (97).

2.2.2. Molecular characterization

Physical characterization of EVs preparations is typically combined with the characterization of the EVs molecular components, in terms of protein, lipid, and nucleic acids. EV sample protein quantification can be assessed on the bulk level by colorimetric assays (Bradford or bicinchoninic acid assay), fluorimetric assays or by global protein stain on SDS-PAGE (98). Each presents different sensitivities and accuracies (99). Importantly, since these methods cannot clearly differentiate EV-related proteins from contaminants, the results may be overestimated, especially if low-purity methods have been used for EVs isolation. Moreover, the results may vary remarkably depending on whether a lysis step has been performed before quantification (100). Protein bulk assessment is often used along with particle counting with NTA to determine the doses for *in vitro* and *in vivo* studies.

Detection of specific proteins expected to be present in EVs is strongly recommended to demonstrate the presence of EVs in the isolated preparations (101). This is usually performed by immunoblotting or by enzyme-linked immunosorbent assay (ELISA). Examples of EV-associated proteins are presented in Fig. 4. Moreover, to obtain suggestions on the degree of sample purity, the presence of contaminant proteins (e.g., GM130, Calnexin, Albumin, Fibronectin) can also be tested (2).

Flow cytometry is another technique that is used to detect and quantify specific EVs markers. This technique has long been used to simultaneously quantify and characterize large number of cells exploiting light scattering principles and fluorescence detection. However, most of the conventional flow cytometers are ideal for the detection of cells or particles with diameters > 300 nm. Thus, since the vast majority of EVs present a size smaller than 300 nm, analysis on single EVs cannot be performed (101). One proposed approach to circumvent this problem consists of immobilizing the EVs on beads, coated with antibodies directed against specific EVs markers, which are sized in the range of micrometers and therefore detectable by the instrument (98). Once mixed, the beads-EVs complex can be labelled with fluorescently conjugated antibodies (47) and analysed to obtain information on the EVs surface marker signature (102).

In the last decade, high-resolution flow cytometers have been developed to quantify and characterize EVs with sizes down to 40 nm after staining with fluorescent dyes and immunofluorescent antibodies (103). Moreover, imaging flow cytometry has been successfully employed to analyse single EVs. This novel application allows simultaneous

immunophenotyping, localization of EVs markers, and analysis of EVs morphology and shape (104).

Proteomic profiling of EVs samples, both from a qualitative and a quantitative point of view, is usually performed by mass spectrometry (MS) techniques since these techniques provide a larger amount of information than any other protein characterization method. Liquid chromatography coupled with tandem mass spectrometry (LC-MS/MS) is one of the most popular configurations for EVs analysis (105).

Nonetheless, nucleic acid content is also widely characterized, especially in terms of RNAs (106). Usually, the quantification of nucleic acid content is performed using spectrophotometric techniques, or fluorescence-based methods, including the RiboGreen assay, and quantitative reverse transcription (qRT)-PCR-based assays. Moreover, content and profiling investigations are carried out by next-generation sequencing or microarrays (107).

Recently, lipid content has gained increasing attention (108). Quantification of total lipids can be performed using different methods, such as colorimetric assays, by measuring the fluorescence of membrane intercalating dyes, by total reflection Fourier-transform infrared spectroscopy, or by thin layer or gas-liquid chromatography (48). The assessment of lipid composition mainly relies on MS techniques (109,110).

The principal biochemical techniques for the molecular characterization of EVs are summarized in Fig. 9.

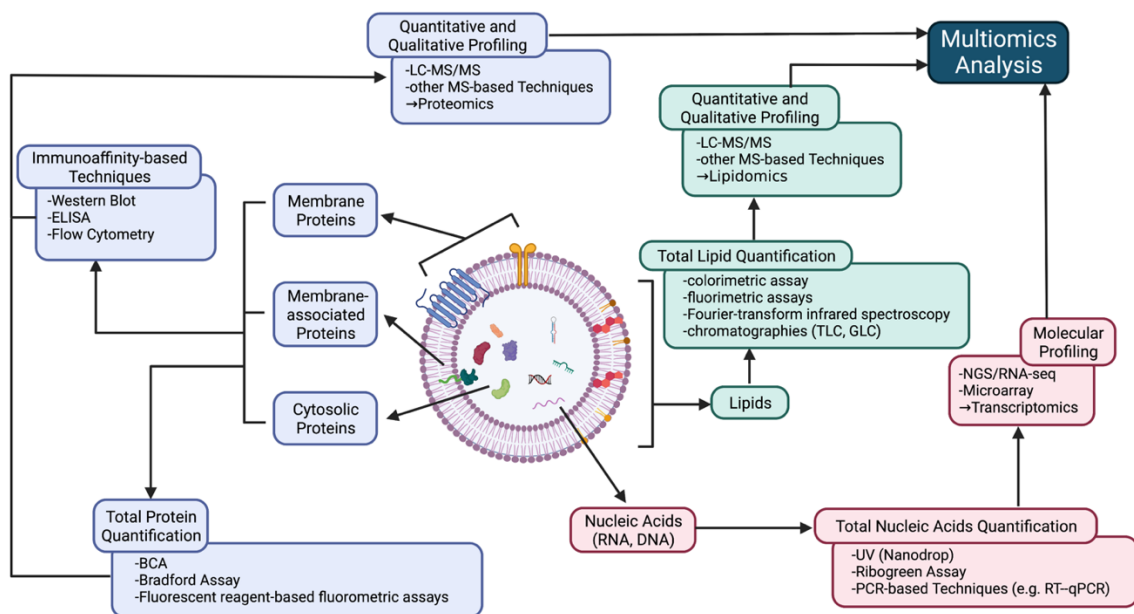


Fig. 9. Overview of Biochemical Techniques used for Molecular Characterization of EVs. In blue proteins, in red nucleic acids and in green lipids. Figure adapted with permission from (107). Illustration created with Biorender.com.

3. EVs in biomedical applications

EVs bear intrinsic features which are of huge interest in translational research and biomedical applications. These natural particles can transport macromolecules over long distances and elicit a biological response in recipient cells, making them exceptionally appealing as a potential new class of therapeutics (Fig. 10 B) and drug delivery systems (DDS) (Fig. 10 C) (111). Moreover, because of their peculiar composition, EVs have drawn attention as a diagnostic toolbox (34) (Fig. 10 A).

To date, 400 clinical trials in which EVs are used as diagnostic and therapeutic, especially unmodified EVs, have been reported on the ClinicalTrials.gov database (<https://clinicaltrials.gov/>, searched for “exosome OR extracellular vesicle”, last access 14.02.23, 11:16). Several companies have been founded pursuing the goal of commercializing EVs therapeutics (112).

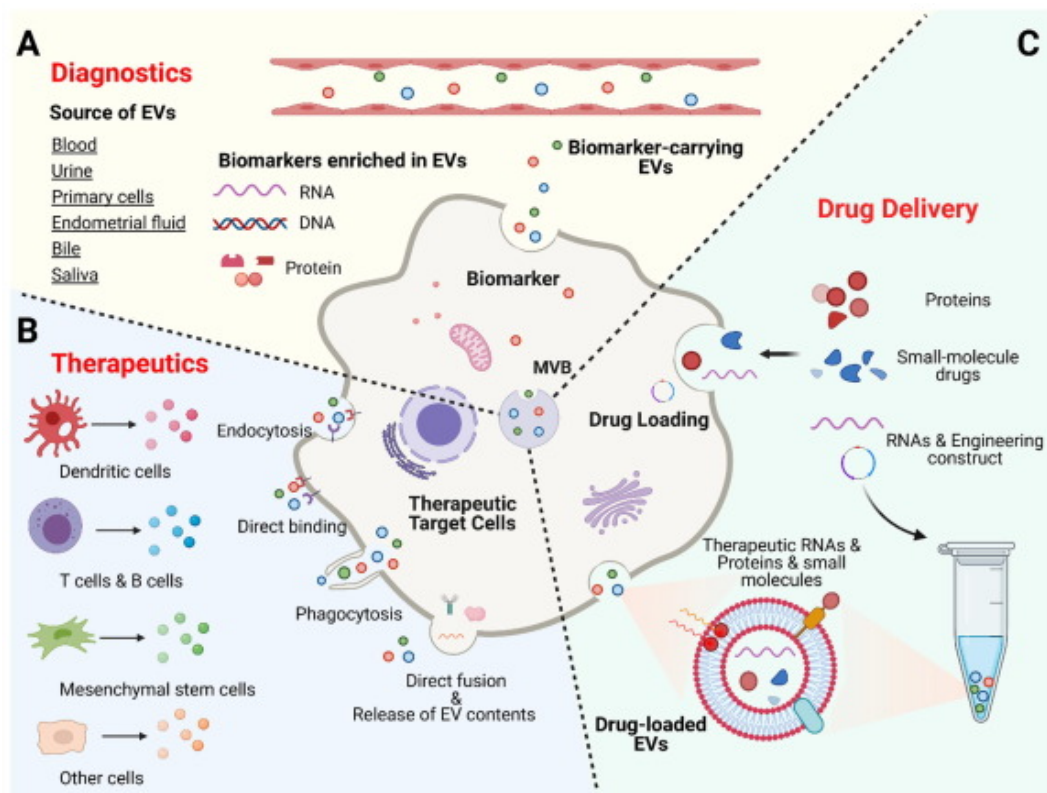


Fig. 10. Potential applications of EVs. (A) Diagnostic (and prognostic) potential of EVs obtained from various sources. (B) Therapeutic potential of EVs. (C) EVs as potential DDS. Adapted with permission from (113).

3.1. EVs as Diagnostic Tools

EVs have been proposed as powerful and convenient diagnostic tools for several diseases since their surface and content are heterogeneous and highly dependent on the cellular source, cellular activation state, and environmental conditions (114). As demonstrated by “omic” analyses of EVs isolated from the blood of patients affected by different diseases, EVs haul unique molecular

signatures related to the disease state and progress (115). These features can be extremely useful in the screening and early detection of diseases as well as in monitoring disease progression and response to specific treatments (116).

Moreover, as mentioned above, since EVs can be found in almost all biological fluids, they stand out as ideal candidates for liquid biopsies. In the majority of cases, EVs can be obtained with minimally invasive procedures that allow to minimize risks linked to solid biopsy and maximizing patient compliance, which could be particularly useful in the case of vulnerable populations (115).

3.2. Therapeutic potential of EVs: focus on EVs as Drug Delivery Systems

In the last decades, EVs have attracted wide interest in the field of drug delivery due to their potential to outperform conventional drug delivery systems, such as liposomes and nanoparticles (115). Ideally, a nanocarrier should improve the distribution of the therapeutic agent from both a spatial and temporal points of view, thereby enhancing its therapeutic efficacy while minimizing drug toxicity and side effects (117). Although liposomes are the most extensively studied and most successful synthetic nanocarriers, having managed to make the leap from the bench to the bedside, they still face many obstacles in the delivery of the drug to the designed target (117).

Indeed, once in the bloodstream, liposomes, like most synthetic nanoparticles, are readily subjected to opsonization and uptake by the reticuloendothelial system (RES), where they are cleared by resident macrophages through the endosomal-lysosomal pathway (118). In addition, liposomes may trigger the activation of the immune system and, in particular, of the complement system leading to an acute and dangerous hypersensitivity reaction called complement activation–related pseudoallergy (119).

As a result, implementation of the design of drug delivery vehicles is needed. As suggested by Witwer *et al.* in (120), this demand can be fulfilled by multifunctional systems presenting a “level of complexity comparable to the biological environment”.

Given that, at first glance, EVs can be considered a holy grail in the drug delivery field (120) since they can potentially succeed where conventional drug delivery systems fail. This initial enthusiasm has led to an outburst in EVs research, as shown by the increasing number of preclinical studies published in the last decade (113).

Why use EVs as Drug Delivery System

In a (very simplified) nutshell, EVs are sophisticated envelopes able to carry a huge collection of nucleic acids and proteins while protecting them from potentially degrading external factors (121). One of the first studies on the role of EVs in cell-to-cell communication, Ratajczak *et al.* showed that EVs from embryonic stem cells can shuttle mRNAs to hematopoietic progenitor cells, which were later translated into the encoded protein (122). Other following studies have demonstrated that EVs manage to functionally deliver their cargo (reviewed in (15,121)). This

potential of “delivery while shielding” is undoubtedly regarded as one of the major advantages for the delivery of drugs that otherwise will show suboptimal pharmacological properties (123). EVs show selective retention toward target cells by receptor-ligand pairing, which is strongly related to the specific properties of the parental as well as the recipient cells (124). In particular, different studies have shown that EVs from neoplastic cells display remarkable tropism towards organs housing their parental cells (125). In addition, comparative studies have reported more efficient cellular uptake of EVs than other synthetic nanocarriers (119).

EVs theoretically present a favourable safety profile. In fact, due to their biological origin, the immune system should be minimally reactive towards EVs (119). Toxicity profile analysis of engineered and native EVs from HEK293 cells performed on immunocompetent mice did not show any toxicity or appreciable immune response (126). Analogous results were obtained after administration of EVs from Expi293F cells to BALB/c mice (127). One strategy proposed to minimize the potential immunogenicity is the use of EVs in an autologous manner. EVs from patient cells, previously harvested and propagated in culture, can be loaded with the desired therapeutics and re-administered to the patient (46). Preclinical studies in animal models have been conducted following this strategy (128–130).

In close relation to this issue, EVs have been praised for their high stability in the circulation (118). However, a comprehensive understanding of the *in vivo* pharmacokinetic properties of EVs is still lacking (113). Nonetheless, rapid opsonization and clearance by the mononuclear phagocyte system can be avoided thanks to the presence of membrane-bound CD55, CD59, or CD47 proteins (131). Indeed, if CD55 and CD59 on the EVs surface were blocked, a remarkable increase in complement-mediated lysis was observed. On the other hand, CD47, a putative “don’t eat me” signal initially observed in stem cells and widely present in tumoral cells, has also been found on EVs secreted by fibroblasts, T cells, and MSCs (118).

Intriguingly, several studies have suggested that EVs can cross tissue, cellular and intracellular barriers (132), including the blood brain barrier (BBB) (133). It has been proposed that EVs can bypass biological barriers through transcytotic processes or small vessel opening (124), or by exploiting the enhanced permeability and retention (EPR) effect (134).

How to load Therapeutic on EVs

Obviously, an unavoidable prerequisite in the use of EVs as Drug Delivery Systems (DDS) is to find an efficient loading strategy, which, as recently highlighted by several authors, is not easily reachable to date (113,135).

Nonetheless, different strategies have been proposed for drug loading, whenever the drug would be a small molecule, a nucleic acid, or a protein. These strategies can be broadly divided into two different types: endogenous and exogenous approaches (Fig.11). In endogenous approaches, EVs

parental cells are exploited to incorporate and/or produce the desired therapeutic cargo and for its sorting in the EVs (119). On the other hand, in exogenous approaches the chosen active pharmaceutical ingredient (API) will be incorporated into or onto the isolated EVs (123).

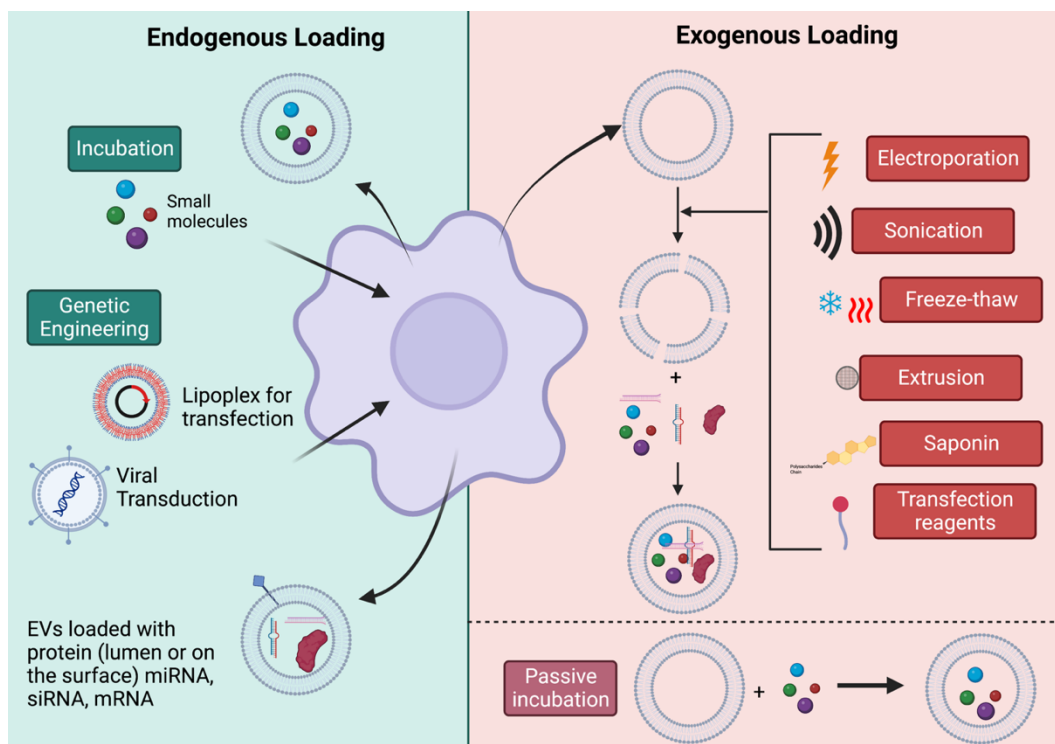


Fig. 11. EVs as Drug Delivery Systems: cargo loading. Strategies for loading of therapeutic molecules into EVs before EVs isolation, endogenous approaches (left panel) and after EVs isolation, exogenous approaches (right panel).

Endogenous approaches

Quite simply, cargoes can be incorporated in the EV-producing cells, which will later release EVs containing the desired molecules. This incorporation can be carried out by co-incubation of the API with cells, typically by adding it to the culture medium. Alternatively, cells can be manipulated by genetic engineering (viral transduction, plasmid, miRNA, and antagomiR transfection) to obtain EVs equipped with the protein/RNA of therapeutic interest (119). For instance, the transfection of mammalian plasmid encoding two enzymes defective in lysosomal storage disorders resulted in EVs enriched with these enzymes (136).

Moreover, further improvement in the loading efficiency has been obtained by fusion or interaction of the desired cargo with molecules naturally sorted inside the EVs. One possible strategy involves the use of the late-domain (L-domain) sorting pathway, as proposed in (137). In their work, WW-tagged Cre recombinase was successfully loaded inside EVs by exploiting the interaction between the WW-tag and the L-domain of the protein Ndfip 1, which was previously demonstrated to be involved in protein trafficking in early endosomes.

Another strategy exploits the biomolecular mechanism at the base of the ARMMs outward budding (138). Indeed, since overexpression of ARRDC1 increases ARMMs production, Wang and colleagues suggested to fuse the desired cargo (i.e. the tumour suppressor p53 protein) with ARRDC1 to induce its packaging in ARMMs. Very intriguingly, the authors also managed to deliver RNAs and the genome-editing CRISPR-Cas9/guide RNA complex. Moreover, all these cargoes were successfully delivered to the recipient cells, where they carried out the awaited biological tasks (139). Other strategies are briefly overviewed in Table 2.

Technology	Exploited EVs component	Exploited interaction	Cargo	Loading efficiency	Ref.
Blue light inducible loading system (EXPLOR)	CD9 fused with a truncated form of CIB1	CIB1-CRY2	mCherry, luciferase-mCherry, Bax-mCherry, super-repressor IκB (srIκB)-mCherry, Cre recombinase-mCherry All fused with CRY2	Luciferase: 40-fold increase compared to EVs loaded by extrusion	(140)
HIV-1 RNA-TAT peptide	TAR Lamp2a fused with RNA binding domain TAT peptide	TAR-TAT	pre-miR-199a pre loop modified in TAR RNA loop	65-fold increase compared with no TAT	(141)
Targeted Modular Loading (TAMEL)	and EV Lamp2b, CD63, Hspa8, modified Lamp2b All fused with MCP	MCP-bacteriophage MS2 RNA	mRNAs containing one or more bacteriophage MS2 RNA loops	4-fold for modified Lamp 2b 6- fold for CD63 no difference for Hspa8 compared with Lamp2b	(142)
Drug dimerization	inducible n-myristoylated DrmA	DrmA-DrnC	GFP, Cre recombinase, and CRISPR-Cas9 ribonucleoprotein (RNP) complex fused with DrnC	Expressed as increase in cargo protein/alix GFP: 15-fold Cre recombinase:2.5-fold Cas9: 9-fold	(143)

Table 2. Examples of engineering approaches for endogenous loading into EVs. CRY2, cryptochrome 2; CIB1, CRY-interacting basic-helix-loop-helix 1; MCP, MS2 bacteriophage coat protein. CRISP, Clustered Regularly Interspaced Short Palindromic Repeats. Partially adapted from (119).

Exogenous approaches

The exogenous approaches comprise two main strategies: passive and active loading. In passive loading, the free API in solution is incubated with EVs, enabling the incorporation of the drug into the EVs (144). This approach is generally more successful for loading of hydrophobic drugs, such as curcumin, doxorubicin, and paclitaxel, probably because these molecules are likely to distribute in the double layer rather than inside the vesicle (145).

Conversely, active loading relies on mechanical or chemical methods to induce destabilization of the double layer and favours the encapsulation of the desired therapeutic inside the EVs lumen (146). These approaches are mainly undertaken for biologicals since their relatively high molecular weight makes spontaneous diffusion in the EVs lumen negligible (147). Mechanical

methods comprise electroporation, sonication, freeze-thaw cycles, and extrusion, whereas chemical methods include the use of mild surfactant saponin, and transfecting agents (148).

The electroporation method applies a controlled electric field to the EVs suspension, inducing a temporary disruption of the double layer and allowing the transit of the desired cargo (149). Proteins, chemotherapeutic drugs, and RNAs have been encapsulated using this method with quite different degrees of success. Indeed, a set of various factors is probably responsible for electroporation efficiency, such as biochemical features of the cargo, cargo size, EV composition (thus its cell source) and, clearly, the set electroporation parameters (135). During sonication, ultrasounds are exploited to induce loosening of the membrane, promoting the diffusion of the API in the EV lumen (148). Although this method it is likely to be disruptive for EVs structure, membrane microviscosity seems to be restored in one hour post sonication (150). Some reports have suggested that ultrasonication may induce degradation and aggregation of mRNAs during loading procedure (147). Moreover, hypothetical effects on EVs composition and topography have not yet been investigated (135).

Freeze-thaw cycles can also be used to form pores in EVs membranes thanks to the formation of ice crystals during the freezing steps. Nonetheless, freeze-thaw cycles have been demonstrated to undermine the stability of proteins and nucleic acids, and an increase in EVs aggregation was also observed (151).

Extrusion methods are borrowed from the liposome field. The mixture of EVs and API is repeatedly pushed through a porous membrane (size 400 or 200 nm) and the applied shear force is responsible for membrane disruption (117).

Saponin is a natural surfactant which is able to interact with lipid double layers generating transient pores (152). Very interestingly, saponin-assisted permeabilization has been used for encapsulation of the enzyme catalase in the EVs derived from RAW 264.7 cells showing a higher encapsulation efficiency (18.5%) when compared with other methods such as passive incubation (4.9%) and freeze-thawing (14.7%), but lower than sonication (26.1%) (153). Moreover, it has been successfully used for encapsulation of another enzyme, β -glucuronidase (154,155). Nonetheless, this type of permeabilization has also been used for small molecules, such as doxorubicin (156) and the hydrophilic porphyrins (157). This method does not require specialist equipment or expertise, it is not expensive and, surprisingly, it does not affect EVs morphology (158), all of which represent notable advantages. On the other hand, whether saponin compromises the organization of some lipidic microdomains, and if this may impact the overall performance remains to be elucidated (135).

Lipid-based transfection reagents, such as lipofectamine or other commercially available reagents, have been successfully employed for loading of nucleic acids on isolated EVs. The

cationic lipids combined with the negatively charged nucleic acids form a complex with an excess of positive charges that can interact with the lipidic membrane of the EVs and be internalized (148,159).

Some examples of exogenous loading into EVs divided by API type are listed in Table 3.

	Target cells/model	EV source	Therapeutic cargo	Loading Method	Loading Efficiency	Ref.
SMALL MOLECULES	HeLa, HEK293	U937	Doxorubicin	Incubation, saponin-assisted, freeze-thaw	Incubation 24h RT: ~13%; Incubation 5 min 37°C: ~16.5%; Saponin-assisted: ~50%, Freeze-thaw: ~13%.	(156)
	Cisplatin resistant ovarian cancer A2780	Umbilical cord blood derived macrophage	Cisplatin	Sonication	Expressed as loading capacity: 28-30%	(160)
	Breast cancer MDA-MB231	MDA-MB-231, HUVEC, hMSC and hESCs	Porphyrins	Incubation, extrusion and electroporation	Expressed as fold increase of loading efficiency: from 0.6 to 36	(157)
	MRSA infection	RAW 264.7	Linezolid	Incubation	Expressed as loading capacity: 5%	(161)
	Glioblastoma U87 spheroids	hEnSCs	Atorvastatin	Freeze-thaw, sonication, incubation with Tween-20, incubation	Freeze-thaw: 10% Sonication: 20% Incubation with Tween-20: 28% Incubation: 20%	(162)
	Murine Lewis lung carcinoma 3LL-M27 mouse model of pulmonary metastasis	RAW 264.7	Paclitaxel	Incubation at RT, electroporation, and sonication	Expressed as loading capacity. Incubation: 1.44% Electroporation: 5.3% Sonication: 28.29%	(150)
NUCLEIC ACIDS	Leukaemia and breast cancer	hRBCs	Therapeutic RNAs (antisense oligonucleotide, CRISPR-Cas9 genome editing guide, Cas9 mRNAs)	Electroporation	24%	(163)
	Osteoarthritis	Chondrocytes	miR-140 mimic	Electroporation	60%	(164)
	Parkinson's Disease	Bone marrow hMSC	Antisense oligonucleotides	Electroporation	25.4%	(165)
	Huntington's disease	U87	Hydrophobically modified siRNAs	Incubation	70% max (EV-associated)	(166)
	B-cell lymphoma	HEK293T	CRISPR-Cas9 system-expressing plasmid	Electroporation	Not reported	(167)
PROTEINS	Batten Disease	IC21 macrophages	Tripeptidyl peptidase-1	Sonication, saponin-assisted.	Expressed as enzymatic activity per 10 ¹¹ particles.	(168)
	Not applicable	A549, HUVEC, RO cells (human B lymphoblastoid cells)	β-glucuronidase	Saponin-assisted	Not reported	(154)

Neuronal PC12, Parkinson Disease mouse model	RAW 264.7	Catalase	Incubation, saponin-assisted, sonication, freeze-thaw, extrusion	Incubation: 4.9% Saponin-assisted: 18.5% Sonication: 26.1% Freeze-thaw: 14.7% Extrusion: 22.2%	(153)
RAW 264.7, MDA-MB-231	MDA-MD-231	Cas9 protein complexed with PULSin nanoparticles	Incubation in sucrose buffer	Not reported	(169)
Breast cancer SK-BR-3, MCF-7, 4T1	SK-BR-3, MCF-7, 4T1	P53 conjugated with TPP tryphenilphosphonium	Electroporation	Expressed as μg protein in EVs after loading/ μg p53 initial: 73.5%	(170)

Table 3. Examples of studies on exogenous loading of EVs. hMSC=human mesenchymal stromal cells; hESC=human embryonic stem cell; MRSA=methicillin-resistant *Staphylococcus aureus*; hEnSCs= Human derived endometrial stem cells; hRBCs= Human red blood cells; HUVEC=human umbilical vein endothelial cells.

How to improve EVs performance as DDS

In an attempt to enhance the targeting ability of EVs and/or to improve their biodistribution (123), different surface engineering strategies have been proposed. Among the various developed methods (broadly reviewed in (147)), genetic engineering and chemical modifications are the most promising.

In a similar fashion to the endogenous cargo loading strategies mentioned above, membrane proteins specifically enriched in EVs (such as Lamp2a or platelet-derived growth factor (PDGF) receptor) are exploited to introduce targeting moieties on EVs surfaces (171).

In the first example of this approach, rabies viral glycoprotein (RVG) was used to achieve neuron-specific targeting. EV-producing cells were transfected with a plasmid encoding the RVG-Lamp2a fusion construct, leading to the release of EVs that successfully delivered the loaded siRNA to neuronal cells (172). Other works have proposed to fuse Lamp2a with a variety of other molecules to endow EVs with new and more specific targeting properties. For instance, cardiosphere-derived cells were engineered to release EVs on whose surface a cardiomyocyte specific peptide was expressed as a result of fusion with Lamp2a (173).

Chemical modifications rely on the covalent linkage of the desired moieties on the EVs surface. In case of chemically simple molecules, they can be directly linked to the EVs surface by reaction with the amino groups on the lysine side chain or N-termini of EVs surface proteins (174). Instead, for more complex molecules, an intermediate step of functionalization of the amino groups on EVs and of the surface modifier molecule, for example, with an activated ester or by diazotransfer, is required to achieve successful derivatization, often exploiting a biorthogonal chemistry strategy. Using this latter method, a peptide presenting high affinity to integrin $\alpha\nu\beta_3$ was successfully attached on EVs surface achieving targeted delivery to ischemic rat brain (175).

3.3. Innate therapeutic potential of EVs

As direct consequence of their nature and their role in body physiology and pathophysiology, EVs were straightforwardly investigated for their innate therapeutic potential (7).

A widely explored possibility is the use of EVs from Mesenchymal Stromal Cells (MSCs). MSCs-EVs have been suggested as the effectors of the beneficial outcomes of MSCs therapy in a variety of diseases, especially immunological diseases (176,177), and of their potential in tissue regeneration (178). Interestingly, the use of EVs is more convenient than cell therapy because EVs are non-replicative, non-mutagenic and seem to be less immunogenic than their originating cells (179).

Examples of preclinical studies employing MSC-EVs are presented in Table 4.

EV source	Therapeutic Indication	Main effects	Ref.
Human umbilical cord Wharton's jelly MSCs	Pulmonary hypertension	Inhibition of STAT3 signalling. Pleiotropic protective effect on the lung and inhibition of pulmonary hypertension.	(180)
Human Bone Marrow MSCs	Acute kidney injury	mRNA transfer from MSCs to tubular cells. induction of proliferation. Acceleration of functional recovery.	(181)
Human umbilical cord MSCs	Autoimmune Uveitis	Reduction of the T cell subsets infiltration in the eyes. Inhibition of chemoattractive effects of CCL2 and CCL21 on inflammatory cells.	(182)
Human induced pluripotent stem cells (hiPSCs)	Osteoporotic bone fractures	Enhancement of bone regeneration and angiogenesis in critical-sized calvarial defects in ovariectomized rats.	(183)
Murine adipose tissue and bone marrow MSCs	Transient global ischemia	Inhibition of COX-2 expression in hippocamp. Rescue of synaptic transmission and plasticity, improvement of spatial learning and memory in mice.	(184)

Table 4. Examples of MSC-derived EVs preclinical studies. For an extensive review please refer to (185).

Along with MSCs, other cell types with stem cell-like properties and their secreted EVs have also been investigated for therapeutic applications.

Notably, EVs released from immune cells hold promises in cancer therapy (148). Natural Killer (NK) derived EVs were found to exert a cytotoxic effect *in vitro* on a wide range of cancer cell lines, for instance, through the release of cytotoxic proteins, such as perforin, granzyme A and B, granulysin and Fas ligand, in acute lymphoblastic leukaemia and neuroblastoma cell lines (186). Moreover, EVs from human amniotic epithelial cells have been shown to positively contribute to wound healing (187), while EVs from endothelial progenitor cells (188) and embryonic stem cells (189) have been proven to be effective in promoting cardiac regeneration in myocardial infarction models.

Other “less conventional” sources of EVs have been demonstrated to bear innate therapeutic potential. For example, EVs isolated from milk were demonstrated to be effective in alleviating dextran sulphate sodium-induced ulcerative colitis in mice by exerting a regulatory effect on gut T_{reg} and T_H17 immune cells and reshaping the gut microbiota (190).

3.4. Challenges ahead

Although EVs are suggested as new biogenic therapeutic avenues, it must be born in mind that this field is only at its very beginning and that several are the issues that still need to be tackled (46,135,191).

First and foremost, one of the pending issues is the lack of standardisation in the methodology and reporting of EVs isolation, characterisation and loading, as recently outlined in a recent review paper (135). Nonetheless, other challenges are unavoidably linked to the preclinical studies, especially when it comes to the comparison with the other DDS (119,120,134). The EVs scientific community is unanimous in the call for proper studies on EVs pharmacokinetics (124) which is likely the result of a combination of several different factors (such as EV cell source and isolation procedures). This, in turn, leads to the need for a comprehensive characterization of potential interactions of the EVs with cells and tissues to achieve a strategic and successful design of new DDS (46). Moreover, deeper analyses and careful design will be needed to bring EVs therapeutics to clinical trials and, ultimately, to the market. Indeed, to move to clinical use, all the various steps from isolation to purification and storage need to adhere to Good Manufacturing Practices (GMP) (119).

4. Signal Transducer and Activator of Transcription 3

Signal transducer and activator of transcription 3 (STAT3) is a pleiotropic transcription factor responsible for the expression of genes involved in several physiological processes such as cell differentiation, angiogenesis, proliferation, apoptosis, metastasis, and immune responses (192).

4.1. STAT3 structure

Four STAT3 isoforms have been described so far, STAT3 α (92 kDa), the full-length isoform, and three truncated isoforms, namely STAT3 β , STAT3 γ and STAT3 δ . STAT3 β (84 kDa), is an alternatively spliced RNA form of STAT3 α in which 55 amino acids at the C-terminal are replaced by 7 additional amino acids (193); STAT3 γ (72 kDa) and STAT3 δ (64 kDa) are the results of post-translational limited proteolysis (194).

Two crystallographic structures of STAT3 have been solved and deposited the Protein Data Bank (PDB): the homodimer STAT3 β -DNA complex (1BG1) (195) (Fig. 12 A) and the unphosphorylated STAT3 core (137-688) fragment (3CWG) (196).

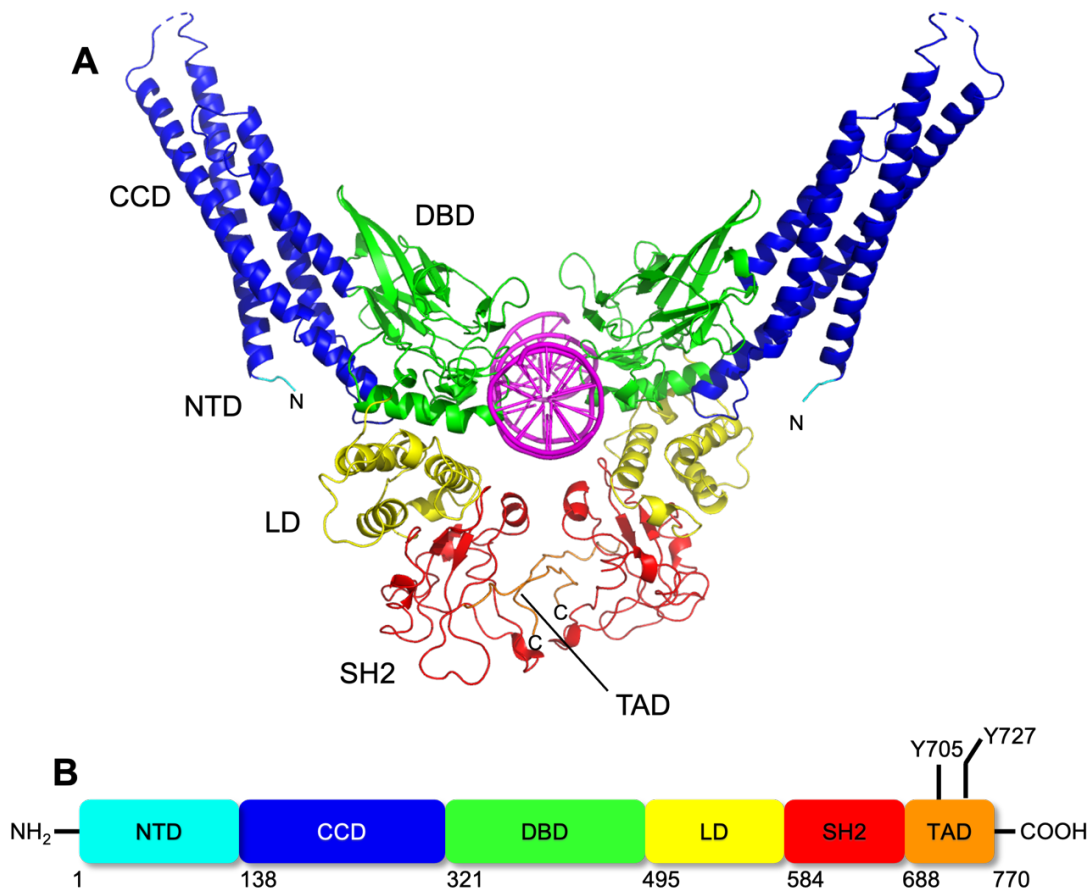


Fig. 12. STAT3 structure. (A) Three-dimensional representation of the STAT3 homodimer bound to a DNA double helix obtained from the crystallographic structure (pdb: 1GB1). The crystallized STAT3 comprised residue from 127 to 722. (B) Schematic representation of the six domains of STAT3, NTD (cyan), CCD (blue), DBD (green), LD (yellow), SH2 (red) and TAD (orange). The same colours have been used to indicate the domains in the three-dimensional structure. In magenta is represented the DNA double helix.

As the other members of the STAT family, STAT3 presents six structured and functionally conserved domains (195) (Fig. 12 B).

- N-terminal domain (NTD): residues 1-137. It is responsible for the tetramerization of two pTyr705 phosphorylated STAT3 dimers which is required for cooperative DNA binding (197,198). Moreover, it mediates the dimerization of unphosphorylated STAT3 (199) and the interaction with other proteins to form complexes implicated in transcriptional regulation (198).
- Coiled-coil domain (CCD): residues 138-320. Arranged in a bundle of four antiparallel helices connected by short loops, this domain present a large hydrophilic surface (195). It is essential for the recruitment of STAT3 to the cytokine receptor, its subsequent activation (200) and nuclear translocation (201).
- DNA binding domain (DBD): residues 321-465. The domain sequence is organized in an eight-strand β -barrel secondary structure and, as suggested by the name, it mediates the recognition and the binding of the protein to a specific DNA sequence (202).
- Linker domain (LD): residues 466-583. A small helical domain, formed by two helix-loop-helix modules, is involved in the proper rearrangements of DBD and SH2 domains which may affect pSTAT3-dependent transcription (203).
- Src homology 2 (SH2) domain: residues 584-688. This domain consist of a central three-stranded β -pleated sheet flanked by one α -helix and two β -strands (195) which form a binding pocket with a conserved Arg residue (Arg609). This Arg residue mediates the interaction with the phosphate groups of the activated receptor as well of other pTyrSTAT3 leading, respectively, to the docking of STAT3 to the receptor or the formation of homo- or hetero- STAT dimers (204).
- C-terminal transcriptional activation domain (TAD): residues 689-770. This domain is involved in the transcriptional activation and its length and composition varies among the different isoforms. It contains the key residue Tyr 705 which, upon phosphorylation, interacts with the SH2 domain of another monomer, leading to the formation of the dimer. In this domain another important residue is the Ser 727, whose phosphorylation contributes to the maximal activation of STAT3 transcription (205).

4.2. STAT3 signalling cascade

The STAT3 signalling pathway is complex and a tightly regulated cascade. Under physiological condition, STAT3 is present in its latent form in the cytoplasm until cytokines, hormones or growth factors (e.g., IL-6, IL-10, IL-11, endothelial growth factor, vascular endothelial growth

factor, tumor necrosis factor α) interact with specific receptors on the cell surface triggering STAT3 activation (206).

In the canonical STAT3 signalling pathway (Fig. 13), the interaction between the cytokines, hormones or growth factors and their cognate receptor induces a ligand-receptor complex organization followed by a rapid transphosphorylation of the Janus tyrosine kinases (JAKs) associated to the intracellular receptor domain. These JAKs kinases (JAK1, JAK2 and Tyr2) in turn phosphorylate a specific tyrosine residue (pTyr) on the cytoplasmatic tail of the receptor setting up the docking site for STATs. At this stage, STAT3 is recruited to pTyr domains on the activated receptor through its SH2 domain. JAKs, now in close proximity to STAT3, can phosphorylate STAT3 at Tyr 705 (207). Phosphorylated STAT3 proteins form homodimers or heterodimer with the other STATs family protein members in a tail-to-tail fashion and, thanks to the interaction with the importin- α 3, translocate into the nucleus where they bind to specific DNA targets (206,208). Here, STAT3 dimer cooperates with other transcriptional coactivators and transcription factors to drive the gene expression.

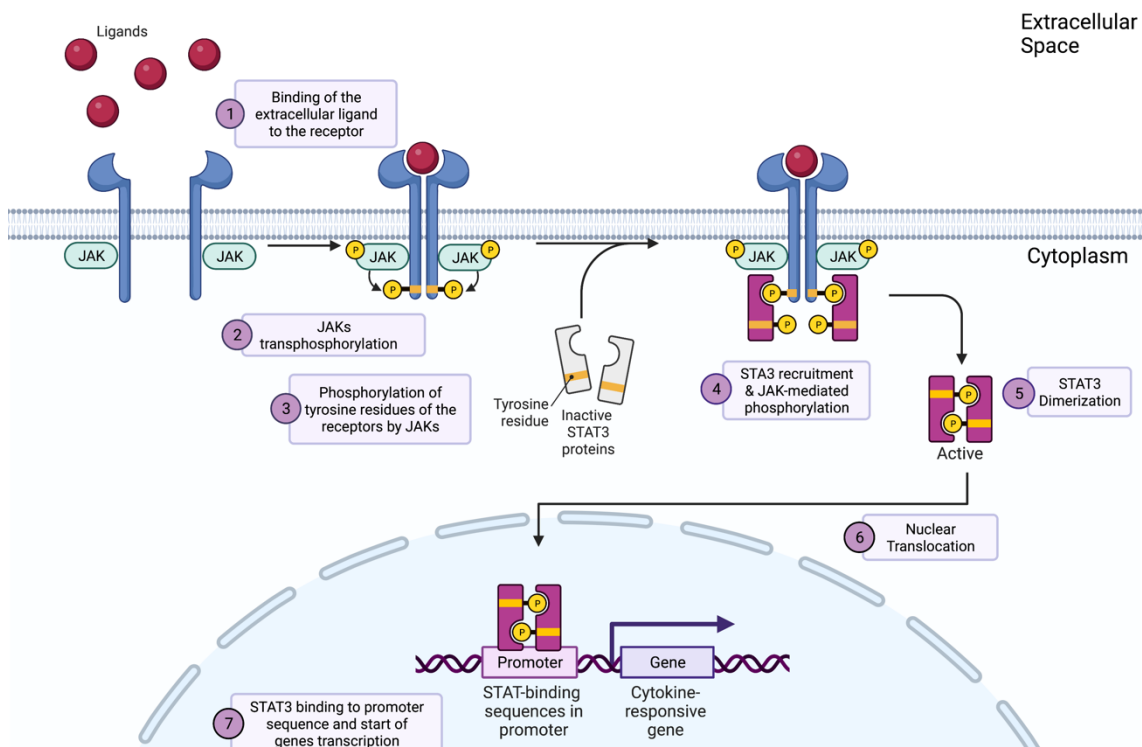


Fig. 13. STAT3 Canonical Pathway. (1) STAT3 pathways is initiated by the binding of cytokines or growth factors to the specific receptor on cell surface. (2) JAKs kinases, associated to the receptor, are activated through phosphorylation (3) leading to the phosphorylation of the receptor itself. (4) The cytoplasmic STAT3 protein associates with the receptor and is phosphorylated by the JAKs. (5) Phosphorylated STAT3 form active dimers and (5) translocate in the nucleus. (6). Here (7) the dimer can bind the promoter and start the transcription. Illustration created with Biorender.com.

Under physiological conditions, STAT3 signalling is a rapid and transient signalling cascade that can last from half to several hours. STAT3 dimers are dephosphorylated by nuclear protein tyrosine phosphatases (e.g., TC45, TC-PTP). Once unphosphorylated, STAT3 associates with the nuclear export factor, e.g., the Chromosome Region Maintenance 1 (CRM1), through its hydrophobic Nuclear Export Signal (NES) elements and it is shuttled back to the cytoplasm where it can be reactivated (209).

Since the STAT3 signalling is a tightly regulated process, along with the dephosphorylation of the dimer in the nucleus, other mechanisms contributed to its downregulation. Indeed, the family of Suppressor Of Cytokine Signalling proteins (SOCS), the protein inhibitors of activated STATs (PIAS), and other members of the protein tyrosine phosphatases (PTPs) family are involved in negative modulation of STAT3 transcriptional activity at various levels of the STAT3 pathway (210).

5. Autosomal Dominant Hyper-IgE Syndrome (AD-HIES)

Hyper-IgE Syndrome (HIES) or Job's syndrome is a rare primary immunodeficiency and multisystem disorder (211). It was first described in 1966 when the first report was made about two young girls who presented “cold” abscesses caused mainly by *Staphylococcus aureus* (212). Later, in 1972, Buckley et al. added high plasma immunoglobulin E (IgE) levels to the clinical features, from which derived the denomination HIES (213).

Along with the immunologic (elevated serum IgE) and infectious disease manifestations, such as eczema, rashes, skin abscesses, and recurrent sinopulmonary infections, non-immunological features have been reported (211). These include craniofacial abnormalities, osteoporosis, hyperextensibility, scoliosis, vascular abnormalities and parenchymal brain lesions. Moreover, HIES patients present an increased risk of developing malignancies (214–217).

Currently, HIES patients are pharmacologically treated with long-term administration of systemic antibiotics and antifungals to prevent and manage infections. A subpopulation of HIES patients is treated with immunoglobulin substitution therapy; however this is not a general therapy (218,219). Finally, a few patients were treated with bone marrow transplantation, but the results are unclear (220,221).

HIES is divided into autosomal dominant (AD-HIES) and autosomal recessive (AR-HIES), both leading to a failure of T_H17 CD4⁺ T cell differentiation. Heterozygous loss-of-function (LOF) mutations in *STAT3* encoding gene have been identified in AD-HIES patients' cells (222).

Since the first report of *STAT3* mutations involved in AD-HIES (223,224), 114 mutations in the *STAT3* gene have been reported (225). The vast majority of the mutations identified in AD-HIES patients are missense mutations located in coding exons, which mainly affect the DNA binding domain (DBD) and the Src homology 2 (SH2) domain (226). Thus, these mutations hinder the binding of *STAT3* to the DNA and its dimerization, converging in a loss of function (LOF) of the transcription factor. This LOF, in turn, leads to the perturbation of cytokine type and level and in the failure of T_H17 CD4⁺ cell differentiation (227, 228). In the future, therapies targeting *STAT3* signalling are expected.

5.1. *STAT3* role in T_H17 cells development

STAT3 plays an extremely complex role in the immune system contributing to both innate and adaptative immune response (210,229). Importantly, *STAT3* regulates the transcription of genes crucial for the development, differentiation and survival of several hematopoietic cells including CD4⁺ T cells, B cells, myeloid cells, and granulocytes (230).

In particular, it has been demonstrated that *STAT3* is required for the generation of T_H17 cells from their progenitor naïve CD4⁺ T cells (231). The development of T_H17 cells can be

summarized as depicted in Fig. 14. IL-6 mediated stimulation of the naïve CD4+ T cells activates STAT3 signalling pathway, resulting in IL-21 expression and release. The subsequent binding of IL-21 on its receptor on the same cell surface reinforces STAT3 activation in a positive feedback and leads to the expression of the Retinoic acid-related Orphan nuclear Receptors (ROR γ t and ROR α) and of hallmark cytokines of the T_H17 lineage (232). In turn, ROR γ t and ROR α induce the expression of the IL-23 receptor, making the cells responsive to IL-23, a cytokine mainly released by antigen-presenting cells essential for stabilization and/or amplification of the T_H17 phenotype (233).

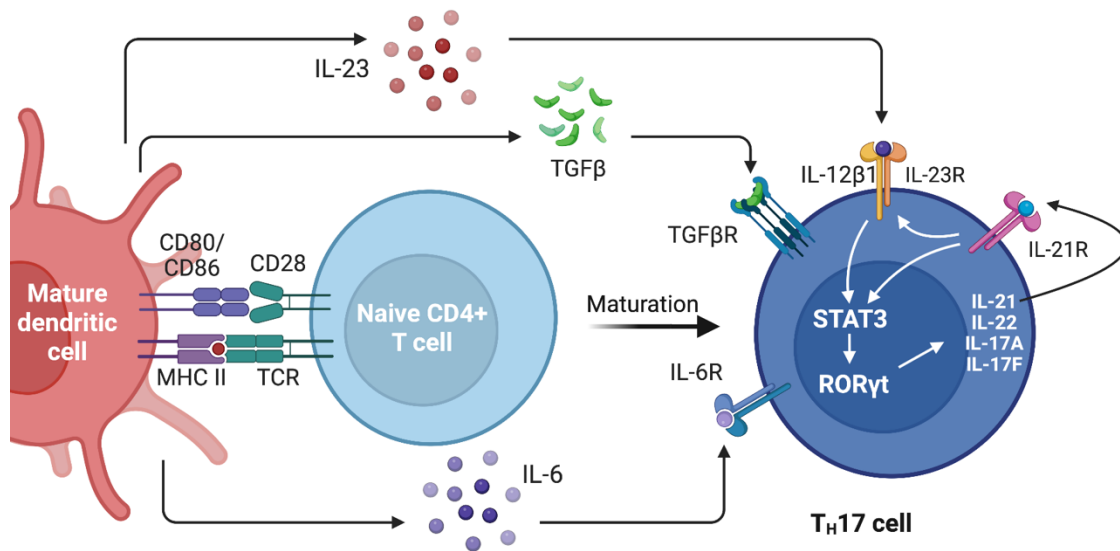


Fig. 14. Development of T_H17 cells from CD4+ Naïve T-cells. CD, Cluster of Differentiation; MHC I and II, Major Histocompatibility Complex I and II. TGF- β , Transforming Growth Factor β . ROR γ t, Retinoic acid-related Orphan nuclear Receptor γ . Figure created with Biorender.com, inspired by (230).

T_H17 cells are instrumental in the host defence against certain extracellular bacteria (e.g., *Staphylococcus aureus* and *Klebsiella pneumoniae*) and fungi (e.g., *Candida albicans*) (234). Indeed, IL-17 and the other released pro-inflammatory factors, such as IL-21, IL-22 and granulocyte macrophage–colony-stimulating factor (GM-CSF) promote neutrophil maturation and chemotaxis. Moreover, they are responsible for the production of many antimicrobial peptides and proteins (235).

Aim of the Thesis

AD-HIES is a rare primary immunodeficiency and multisystem disorder characterized by developmental abnormalities, poor wound healing, and recurrent infections (222). In 2007, heterozygous loss-of-function (LOF) mutations of STAT3 were identified in AD-HIES patients' cells. These mutations in the *STAT3* gene impaired STAT3 function, resulting in the failure of T_H17 CD4⁺ cell differentiation (224,236,237).

To date, no specific treatments are available, and the main therapeutic approaches are limited to the prevention and management of infections with long-term administration of systemic antibiotics and antifungals (238). Indeed, a new strategy aimed at acting more directly on the underlying causes of the disease would be beneficial for AD-HIES patients, lowering the risk of infections, the use of medications, and hospitalizations.

In this attempt, the restoration of STAT3 signalling, through the administration of fully functional wild type STAT3 to CD4⁺ T cells from AD-HIES patients, could compensate for the loss of function of the mutated protein forms and enhance the differentiation into T_H17 cells. To achieve effective delivery of STAT3, we propose the use of Extracellular Vesicles (EVs) as a Drug Delivery System (DDS). These biogenic particles hold interesting promise as DDS owing to their potential to overcome the lack of effective delivery systems for high molecular weight biological drugs such as proteins (146).

A schematic representation of the proposed approach is given in the illustration on the next page (Fig.15).

In particular, in this thesis, the foundations for the development of such approach have been laid. Indeed, the research activity has been focused on:

- Production and characterization of a novel fusion construct of STAT3 in which STAT3 were fused with EGFP allowing easy tracking of the protein by fluorescence detection.
- Isolation and characterization of EVs from cell conditioned media of a particular type of B-lymphoblastoid cells.
- Exogenous loading of EGFP-STAT3 protein inside the isolated EVs by saponin-assisted encapsulation and characterization of the obtained EGFP-STAT3 EVs.
- Evaluation of EGFP-STAT3 EVs uptake in a cellular model (MDA-MD-231).

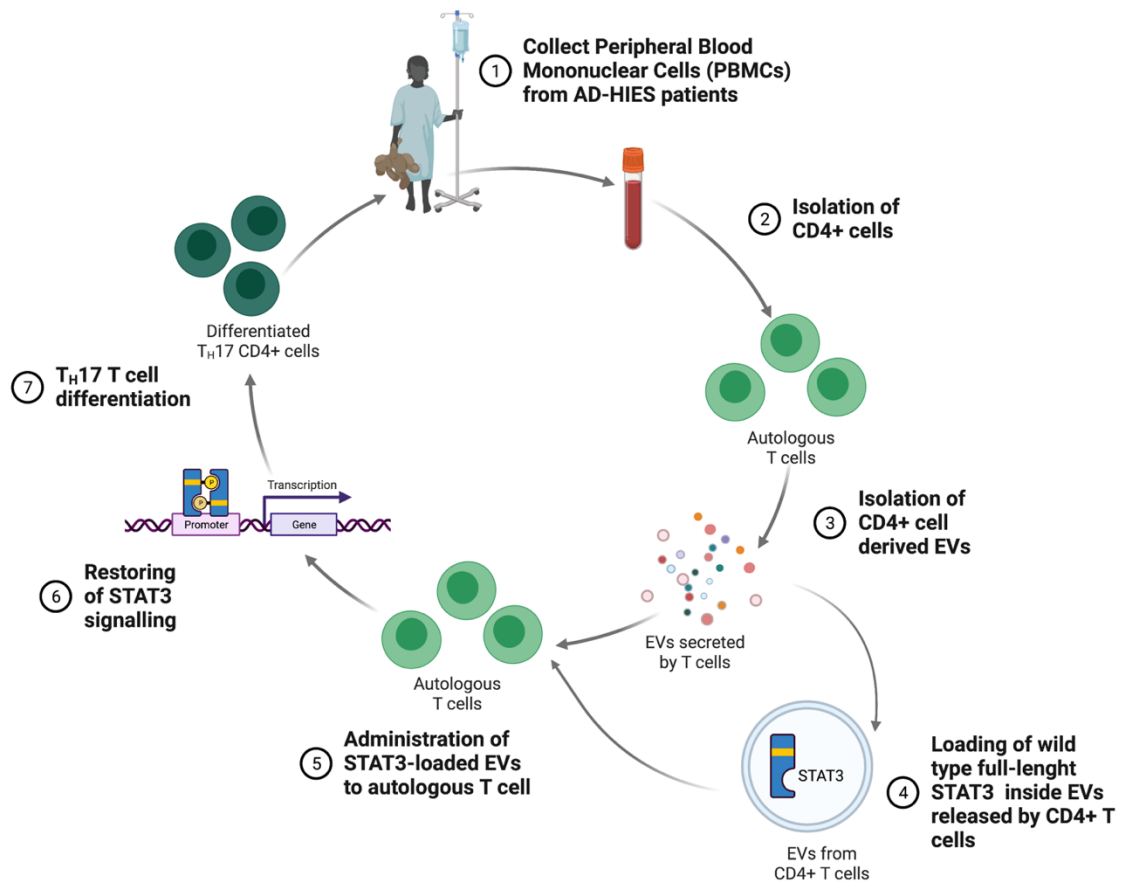


Fig. 15. Proposed approach for STAT3 signalling restoration in AD-HIES patients by use of EVs as delivery vesicles for the full-length wild type STAT3. Illustration created with Biorender.com.

Materials and Methods

1. Materials

All chemicals used were of the highest analytical grade, purchased from Sigma-Aldrich, unless stated otherwise. Roswell Park Memorial Institute (RPMI) 1640 and Dulbecco's Modified Eagle Medium (DMEM) cell culture mediums, penicillin, streptomycin, gentamycin, sodium pyruvate, Dulbecco's phosphate-buffered saline (DPBS), Insulin-Transferrin-Selenium-Ethanolamine (ITS - X) and Fetal Bovine Serum (FBS) were obtained from Thermo Fisher Scientific.

Primers	Sequence
F1	5-ATGCATCATCATCATCATCATCATCATCATATGGTGAGCAAGGGC-3'
R2	5'-GCCCTGAAAATACAGGTTTTTCGGATCCCTTGTACAGCTCGTC-3'
F3	5'-GAAAACCTGTATTTTCAGGGCATGGCCCAATGGAATCAG-3'
R4	5'-TCACATGGGGGAGGTAGCGCACTC-3'
F Polyhedrin	5'-AAATGATAACCATCTCGC-3'
R SV40 polyA	5'-GGTATGGCTGATTATGATC-3'
F pUC/M13	5'-CCCAGTCACGACGTTGAAAACG-3'
R pUC/M13	5'-AGCGGATAACAATTTACACAGG-3'

Table 5. Primers used for cloning and construction of EGFP-STAT3 recombinant bacmid. F1, R2, F3 and R4 were purchased from Eurofins Genomics, the others were part of the Bac-to-Bac® TOPO® Expression System kit.

Kit	Manufacturer	# Catalog
Bac-to-Bac® TOPO® Expression System	Invitrogen	A11101
ExpiSf™ Expression System	Gibco	A33841
Pierce™ BCA Protein Assay Kit	Thermo Scientific	23225
QuantiPro™ BCA Assay kit	Sigma-Aldrich	QPBCA
Total Exosome Isolation Reagent (from cell culture media)	Invitrogen	4478359
GenElute™ Gel Extraction Kit	Sigma-Aldrich	NA1111
GenElute™ Plasmid Miniprep Kit	Sigma-Aldrich	PLN70
GenElute™ Plasmid Midiprep Kit	Sigma-Aldrich	PLD35

Table 6. Commercial kits used.

Antibodies	Manufacturer	# Catalog	Dilution
Anti-pTyr705 STAT3	Santa Cruz Biotechnology	sc-8059	1:500
Anti-STAT3	Santa Cruz Biotechnology	sc-8019	1:1000
Anti-STAT3	Santa Cruz Biotechnology	sc-482	1:1000
Anti-CD63	Santa Cruz Biotechnology	sc-365604	1:1000
Anti-rabbit IgG HRP-linked antibody	Cell Signalling Technology	7074S	1:2000
Anti-mouse IgG HRP-linked antibody	Cell Signalling Technology	7076S	1:2000

Table 7. List of antibodies with the respective dilution used.

2. Methods

2.1. Generation of the recombinant baculovirus for EGFP-STAT3 expression

Construction of EGFP-STAT3 cDNA

The full-length cDNA coding for human STAT3 (STAT3 α) from the pOTB-STAT3 vector (ImaGENES) was amplified using the F1 and R2 primers (see Material section) by Short Overlap Extension (SOE) PCR to obtain the full-length STAT3 construct with a TEV (*Tobacco Etch Virus*) protease cleavage site at the N-terminus. Moreover, the EGFP gene was amplified from the pEGFP-N1 (Clontech) using the F3 and R4 primers, which inserted a 10 \times poly-Histidine sequence at the N-terminus.

To fuse EGFP and STAT3 templates, the same PCR procedure was carried out employing the F1 and R4 primers. PCR reactions were performed with Pfu Core High Fidelity (Jena Bioscience), a thermostable proofreading polymerase able to generate blunt-end products. Compositions of PCR reaction mixes and cycling parameters are reported in Table 8.

PCR reaction mix		PCR parameters		
Pfu	0,7 μ L	Step	T	Time
Template	1 μ L	1. Initial denaturation	94°C	3 min
F primer	1,5 μ L	2. Denaturation	94°C	30 sec
R primer	1,5 μ L	3. Annealing	55°C	30 sec
dNTP 100 μ M	1,5 μ L	4. Extension	72°C	2 min 30 sec
X-Buffer 10X	5 μ L	5. Final extension	72°C	7 min
Sterile H ₂ O	35 μ L	6. Hold	4°C	Hold

Table 8. PCR for EGFP-STAT3 SOE PCR. PCR reaction mixture composition and thermocycler parameters for the construction of EGFP-STAT3 cDNA.

PCR products were purified by agarose gel electrophoresis (0.8% agarose gel) and then extracted from the gel with a GenElute™ Gel Extraction Kit (Sigma-Aldrich).

Cloning of EGFP-STAT3 gene into pFastBac™ TOPO® Vector

The obtained blunt-end EGFP-STAT3 insert was cloned inside the pFastBac™ TOPO® Vector, following the manufacturer's instruction and using an insert:vector molar ratio of 2:1 and a reaction time of 30 min.

The resulting reaction mixture was used to transform the One Shot® Mach1™ T1^R Chemically Competent *E.coli* cells, which were later plated on a selective LB agar solid medium (100 μ g/mL Ampicillin) and grown overnight at 37°C.

On the following day, each colony was resuspended in 10 μ L of sterile mQH₂O and screened by PCR, using F Polyhedrin and R4 primers, to check for positive transformants. PCR reactions were

performed using DreamTaq Green DNA Polymerase (Thermo Fisher). The PCR mix was assembled as indicated in Table 9.

PCR reaction mix		PCR parameters		
DNA polymerase Master Mix	10 μ L	Step	T	Time
Colony suspension	5 μ L	1. Initial denaturation	94°C	3 min
F primer	1 μ L	2. Denaturation	94°C	30 sec
R primer	1 μ L	3. Annealing	55°C	30 sec
Sterile H ₂ O	3 μ L	4. Extension	72°C	1 min
		5. Final extension	72°C	7 min
		6. Hold	4°C	Hold

Table 9. Colony PCR. PCR reaction mixture composition and thermocycler parameters for colony screening PCR.

Positive clones were identified by electrophoresis and amplified in 3 mL of LB+100 μ g/mL Ampicillin and grown overnight at 37° under constant agitation. On the following day, the plasmid DNA was isolated using the GenElute™ Plasmid Miniprep Kit (Sigma-Aldrich) and properly quantified.

The identity of the purified plasmid was confirmed by DNA sequencing (performed by Eurofins Genomics) using F Polyhedrin, F3, and R SV40 polyA primers.

Generation of the EGFP-STAT3 recombinant bacmid

DH10Bac™ *E.coli* competent cells were transformed with EGFP-STAT3 pFastBac™ TOPO® Vector by heat shock and grown for 4 h at 37°C in SOC medium (0.5% (w/v) Yeast Extract, 2% (w/v) Tryptone, 10 mM NaCl, 2.5 mM KCl, 10 mM MgCl₂, 10 mM MgSO₄, 20 mM Glucose) in a shaking incubator. A 10-fold dilution of the cells was plated on LB agar selective medium which contained 50 μ g/mL kanamycin, 7 μ g/mL gentamicin, 10 μ g/mL tetracycline, 100 μ g/mL X-gal, and 40 μ g/mL IPTG. Plates were incubated at 37°C for 48 hours.

After the incubation time, white colonies were screened by colony PCR in a reaction mixture prepared as indicated in Table 9 using F pUC/M13 and R2 primers. As described above, the PCR mixtures were analyzed by electrophoresis to identify the positive clone(s).

One of the positive clones was inoculated in 3 mL of LB+50 μ g/mL kanamycin, 7 μ g/mL gentamicin, and 10 μ g/mL tetracycline, and grown for 5 hours, at 37°C, in a shaking incubator. Subsequently, 50 mL of fresh medium were added to the culture and grown overnight, at 37°C, with continuous shaking. The following day, the plasmid DNA was isolated using the GenElute™ Plasmid Miniprep Kit (Sigma-Aldrich) and properly quantified.

To further confirm the correct insertion of the gene in the bacmid, three PCR reactions were performed with different combinations of primers: F pUC/M13+R4, F1+R pUC/M13, F pUC/M13+R pUC/M13, setting the thermocycler as indicated in Table 8.

Baculovirus P0 generation

To generate the baculovirus, ExpiSf9 cells were cultured in ExpiSf CD medium (ThermoFisher) until cell density reaches $5-10 \times 10^6$ viable cells/mL and 90% cell viability. Then, cells were transfected with EGFP-STAT3 bacmid DNA using the ExpiFectamine™ transfection reagent (ThermoFisher) following the manufacturer's instructions.

After 96 hours the cell suspension was centrifuged at $300 \times g$ for 5 min and the supernatant containing the newly generated baculovirus (P0) was harvested.

Baculovirus P0 was used to infect other cells for amplification and P1 generation, which was later used for the following infections and protein expression experiments. In detail, insect cells were seeded in a 125 mL flask with a final density of 5×10^6 cells/mL in a 25 mL medium final volume. On the following day, the cells were infected with 500 μ L of P0 viral stock. After 72 hours the virus was harvested as for P0.

2.2. Expression and purification of EGFP-STAT3 recombinant protein

EGFP-STAT3 protein expression

On the day before infection, cells were seeded in a 500 mL flask with a final density of 5×10^6 cells/mL in 100 mL medium and ExpiSf™ Enhancer (ThermoFisher), an adjuvant for maximizing protein yield, was added. On the following day, the insect cells were infected with 500 μ L of P1 viral stock and incubated for 72 hours at 27°C in a shaking incubator.

An overview of the various steps for the setting up of the Baculovirus Expression System for EGFP-STAT3 is given in Fig. 16.

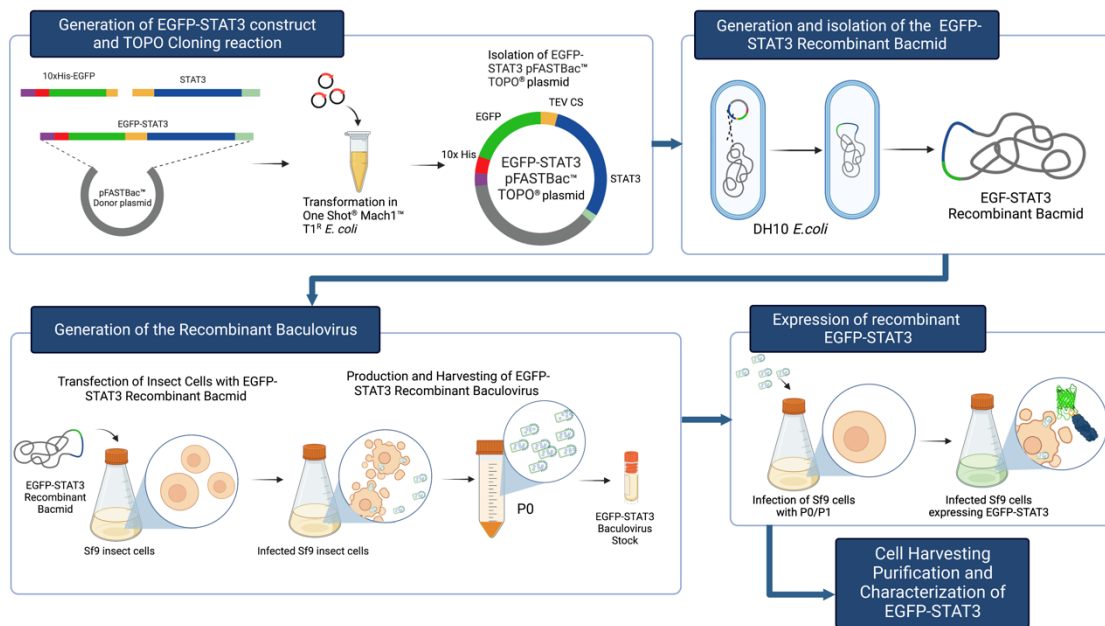


Fig. 16. Schematic representation of the workflow for the cloning and generation of EGFP-STAT3 Recombinant Baculovirus. Created with BioRender.com.

EGFP-STAT3 protein purification

Cells were harvested by centrifugation of the cellular suspension at $300 \times g$ for 10 min and consequently resuspended in 30 mL ice-cold buffer composed of buffer A (20 mM Tris HCl pH 7.5, 300 mM NaCl, 20 mM Imidazole, 0.2% (v/v) NP40, 0.5 mM TCEP) supplemented with 100 units of DNase (Roche) to eliminate nucleic acids and reduce suspension viscosity, 5 mM MgCl₂ as DNase cofactor, 1 mM PMSF, 1 tablet of SigmaFast™ Protease Inhibitor (Sigma-Aldrich) and 0.1 mM Na₂VO₃. The resuspended cells were transferred in a 15 mL Dounce homogenizer on ice to complete the lysis process until the pellet was homogeneously resuspended.

The crude extract was centrifuged for 30 min at $14,000 \times g$ and 4°C and the supernatant was loaded on a 5 mL home-packed Ni²⁺-column pre-equilibrated with buffer B (20 mM Tris HCl pH 7.5, 300 mM NaCl) supplemented with 20 mM Imidazole. After the complete loading of the protein extract, the column was extensively rinsed with buffer B+20 mM Imidazole, followed by a washing step with buffer B, supplemented with 50 mM Imidazole, to get rid of unspecific component bound on the resin. EGFP-STAT3 was eluted with buffer B added with 250 mM Imidazole and the flow through was collected until the resin colour turned from green to blue. The resin was then washed with buffer B containing 1M Imidazole. Aliquots from each purification step were collected and analyzed by SDS-PAGE. The fractions containing EGFP-STAT3 were pooled and concentrated by several ultrafiltration steps with an Amicon® Ultra-15 ultrafiltration device with a 50 kDa cut-off (Millipore). The protein solution was then loaded on a PD10 desalting column (Cytiva Life Science) to completely remove Imidazole and exchange the buffer in buffer C (20 mM Tris HCl pH 7.5, 150 mM NaCl, 0.5 mM TCEP). All the purification steps were carried out at 4°C.

The protein spectrum in the 550-220 nm region of the UV-Vis was recorded with a V-550 UV-Vis spectrophotometer (Jasco) and the absorbance value at 280 nm was used to quantify the protein concentration applying the Lambert-Beer's Law. The extinction coefficient was computed with the ProtParam tool upon entering the EGFP-STAT3 aminoacidic sequence (239).

The protein solution was then aliquoted and stored at -80°C or used for further experiments.

STAT3 protein purification

To obtain the STAT3 protein, the TEV protease (produced in the Laboratory of Prof. Capaldi) was added to the EGFP-STAT3 solution to obtain a substrate:enzyme ratio of 15:1 (w/w). The reducing agent TCEP was also added to the sample to a final concentration of 1 mM. The reaction mixture was incubated for 90 min at room temperature (RT) followed by overnight incubation at 4°C without agitation.

On the following day, the reaction mixture was centrifuged at $20,000 \times g$ for 10 min on a benchtop centrifuge to remove any precipitate. Imidazole was added to the supernatant to a final

concentration of 20 mM and loaded on a home-packed IMAC column (2.5 ml of Ni²⁺ resin) pre-equilibrated with buffer C+20 mM Imidazole. Subsequently, the column was washed with the same buffer and the flow through (around 5 ml), containing the cleaved STAT3, was collected. STAT3 was concentrated by ultrafiltration to 1 ml, quantified and subjected to Size Exclusion Chromatography (SEC) to separate the cleaved STAT3 from any coeluted proteins with a home-packed Sephadex G200 column (30cm × 10mm). The column was equilibrated with buffer C and the chromatographic run was performed using a 0.2 mL/min flow rate with detection at 280 nm in an ÄKTA prime plus system (Pharmacia). Fractions of 0.5 mL were collected with an automatic sampler collector. Aliquots from each purification step were analysed by SDS-PAGE. The obtained protein solution was quantified as described for EGFP-STAT3, using the extinction coefficient computed by ProtParam starting from the STAT3 aminoacidic sequence, aliquoted and stored at -80°C or used for further experiments.

2.3. Biophysical and functional characterization of EGFP-STAT3

The obtained proteins, EGFP-STAT3 and STAT3, were characterized from a biophysical and functional point of view.

Circular Dichroism

Circular Dichroism (CD) spectra were registered both in the Far and Near UV spectrum region (250-200 nm and 320-250 nm) with a J715 spectropolarimeter (Jasco) equipped with a Peltier system to keep the sample compartment at 25°C. Far UV spectra were registered in 1 mm quartz cuvette with a protein concentration of 1.65 μM (STAT3) and 1 μM (EGFP-STAT3) in buffer C (20 mM Tris HCl pH 7.5, 150 mM NaCl, 0.5 mM TCEP). Near UV spectra were recorded using a 10 mm quartz cuvette with a protein concentration of 3.3 μM (STAT3) and 4 μM (EGFP-STAT3) in the same buffer.

Spectra acquisitions were performed using the following parameters: bandwidth of 1 nm; response of 4 sec; sensitivity standard; data pitch of 1nm; scanning speed of 50 nm/min; 3 accumulation (for Far UV), 5 accumulation (for Near UV). Thermal denaturation experiments were performed by monitoring the circular dichroic signal at 208 nm at 1 μM (EGFP-STAT3) and 3.3 μM (STAT3) concentrations on a 15–90 °C linear temperature gradient, with a temperature slope of 1.5 °C/min.

Mean residue ellipticity $[\theta]_{MRW}$ (deg cm² dmol⁻¹) was calculated according to the formula $[\theta]_{MRW}=(\theta/10)(MRW/lc)$, where θ is the registered ellipticity (in mdeg), MRW is the mean residue weight of the protein, l is the pathlength (in cm) and c is protein concentration (in mg/ml) (240,241). Secondary structure estimation has been performed using BeStSel online tool (242,243).

STAT3/JAK2 kinase assay

STAT3/JAK2 (Janus Kinase 2) kinase assay was performed for both EGFP-STAT3 and STAT3 using recombinant JAK2 active protein (Upstate Biotechnology), as previously described (244–246). In detail, 5 µg of EGFP-STAT3 or STAT3 were incubated with 0.5 µg of recombinant JAK2 active protein in 20 mM Tris HCl pH 7.5, 50 mM MgCl₂, 100 µM ATP. The reaction mixture was incubated for 1 hour at RT under mild agitation. Negative controls were performed by incubation of EGFP-STAT3 in 20 mM Tris HCl pH 7.5, 50 mM MgCl₂. The reactions were quenched by addition of reducing Laemmli Sample Buffer followed by heating at 95°C for 5 min and the samples were loaded on 7.5% SDS polyacrylamide gel. The gel was run at a constant voltage of 100 V. The separated proteins were transferred on a PVDF membrane (Immobilon P, Millipore) by wet tank blotting.

The membrane was blocked with 5% (w/v) Bovine Serum Albumin (BSA) solution in Tris-buffer saline supplemented with 0.1% (v/v) Tween 20 (TBS-T) at RT for 1h under gentle agitation. Then, it was incubated overnight at 4°C with the anti-pTyr705 STAT3 antibody (Santa Cruz Biotechnology, sc-8059; 1:500). After washing with TBS-T, the membrane was incubated with a Horseradish Peroxidase (HRP)-conjugated anti-mouse secondary antibody (Cell Signaling Technology, 7076S; 1:2000) at RT for 1 h. After washing with TBS-T, the immunoreactive proteins were detected with Immobilon® ECL Ultra Western HRP Substrate (Millipore) using ChemiDoc XRS Imaging System (BioRad).

The membrane was subsequently stripped, washed, blocked with 5% BSA in TBS-T and hybridized overnight at 4°C with an anti-STAT3 antibody (Santa Cruz Biotechnology, sc-482; 1:1000). The following passages were performed as described above.

2.4. Isolation of EVs from RO cells

RO cells culture

Human B lymphoblastoid cells RO (DSMZ, ACC 452) were initially cultured in RPMI 1640 cell culture medium supplemented with 10% (v/v) Fetal Bovine Serum (FBS), 100 UI/mL penicillin, 100 µg/mL streptomycin in 5% CO₂ incubator at 37°C.

When cells had reached 90% viability the FBS was gradually replaced with 1% (v/v) Insulin-Transferrin-Selenium-Ethanolamine (ITS-X) medium supplement and 1 mM Sodium Pyruvate. Briefly, cells weekly counted and seeded at a density of 0.35×10^6 cells/mL in a volume of 45 mL/flask. After 3 days 25 mL of the supernatant (hereinafter called cell conditioned medium (CCM)) were harvested and replaced by 50 mL of fresh medium. On day 7, 50 mL of the CCM were harvested, and the cells were counted again (247). The CCM, used for EVs isolation, was stored at -80°C, for up to 2 months.

RO cell culture has been established and optimised in the lab of Prof. G. Fuhrmann (248). It should be noted that the choice to use the RO cells for EVs isolation was the result of the attempts to obtain at the same time an appreciable amount of CCM, an FBS-free culture and, to minimize the immunogenicity of the EVs. RO cells grow in suspension, allowing to obtain up to ~75 mL/week CCM from a single T75 flask. They can be adapted, by a stepwise switch, to a serum-free media by using the already cited IST-X supplement. Finally, they were obtained from a patient with severe combined immunodeficiency, not expressing MHC class II complexes (249), suggesting that the derived EVs may be low in immunogenicity (248).

Isolation and purification of EVs

Isolation and purification of EVs were performed following the protocol described in (155,247), with some modifications. 400mL of RO cells CCM was first centrifuged at $300 \times g$ for 10 min to remove any cells, transferred to a new falcon tube and centrifuged again at $9500 \times g$ for 30 min to get rid of any possible cellular debris. The supernatant was then subjected to two following filtration passages, at $0.45 \mu\text{m}$ and $0.22 \mu\text{m}$, using PVDF sterile syringe filters. The filtered CCM was then ultracentrifuged at $100,000 \times g$ for 2h at 4°C using 70mL Polycarbonate Bottles suitable for a Type 45 Ti rotor in an Optima XPN-80 Ultracentrifuge (Beckman Coulter Lifescience). The resulting EV-containing pellet was resuspended in 1 mL of PBS and purified by SEC for further experiments.

SEC was performed using a 40 mL Sepharose CL-2B (Cytiva Life Science) home-packed column equilibrated with degassed autoclaved PBS filtered at $0.22 \mu\text{m}$. The same buffer was used as mobile phase with the aid of a peristaltic pump (flow 1 mL/min). Fractions of 1 mL were collected to a total of 40 mL. Between runs, the column was washed with at least 2 column volumes of degassed autoclaved mQH_2O and equilibrated with 2 column volumes of degassed autoclaved PBS filtered at $0.22 \mu\text{m}$.

The collected SEC fractions were analysed for protein content and particle size distribution as afterwards described. The EVs SEC-fractions were gathered and concentrated by polymeric precipitation with the Total Exosome Isolation Reagent (Invitrogen™) following the manufacturer's instructions. These procedures were carried out to achieve a sample volume feasible for the downstream experiments.

2.5. Encapsulation of EGFP-STAT3 in RO cells EVs

The EGFP-STAT3 was loaded into isolated EVs using a saponin-assisted encapsulation technique (153,154). Briefly, the pellet from the ultracentrifugation passage was resuspended directly in the EGFP-STAT3 solution (2 mg total protein). After 10 min incubation at RT, an aqueous solution of saponin was added to the mix at a final concentration of 0.1 mg/mL. The EVs-EGFP-STAT3-

saponin mixture was then incubated for 30 min at 25°C under gentle agitation, and 30 min at 25°C without agitation. This cycle was repeated a total of 2 times.

2.6. Characterization of isolated EVs

Nanoparticle Tracking Analysis (NTA)

To determine the particle size and concentration in the eluted SEC fractions, NTA analyses were carried out with two instruments depending on in which lab the experiment had been performed (in Verona or during the abroad stay in Erlangen, Germany). Both instruments were used for analysis in scatter and fluorescence mode (when applicable).

NS300 NanoSight (Malvern Panalytical) was used to perform NTA experiments in Verona. Each fraction was diluted in degassed autoclaved 0.22 µm filtered PBS (dilution factors ranging from 1:20 to 1:200) in 1 mL total volume and injected into the instrument. For each sample, 3 videos of 60 seconds each were recorded, and the camera level was set to give a clear sharp image of the particles. The acquired video were analyzed using NanoSight 2.3 software with a detection threshold from 3 to 5 and only the measurement within the linear range of the instrument have been considered (81).

ZetaView MPX-220 Duo-NTA (ParticleMetrix) was used to carry out the experiment in Erlangen. Each day, before the starting of the analysis, alignment with 100 nm standard polystyrene standard beads (Particle Metrix) diluted 1:250,000 (v:v) was performed. Furthermore, to ensure a sharp and focused image during fluorescence measurement, YG488 fluorescently conjugated polystyrene standard beads (Invitrogen) diluted 1:250,000 (v:v) were analyzed in fluorescence mode. Each fraction eluted from the SEC column was diluted (dilution factors ranging from 1:100 to 1:1000) in degassed, autoclaved, 0.22 µm filtered PBS to 1 mL final volume. Measurements were performed at 25°C. Scattering capture settings were: sensitivity 80, shutter 100, minimum trace length 15, 488 nm laser. Fluorescence capture settings were: sensitivity 95, shutter 100, minimum trace length 7, 488 nm laser and 500 nm filter.

Protein concentration assessment

Protein concentration of each fraction eluted from the SEC column was measured by Bicinchoninic acid assay (BCA) using commercial kits (QuantiPro™ BCA Assay kit, Sigma-Aldrich, or Pierce BCA Protein Assay Kit, ThermoFisher) following the manufacturer's instructions. Before each measurement, a calibration curve (500, 250, 125, 62.5, 31.25, 15.62 and 0 µg/mL) made with standard Bovine Serum Albumin (BSA) was prepared in triplicate. Each fraction was measured in duplicate. The measurements were performed with a Multiplex M Nano microplate reader (Tecan).

EGFP-STAT3 quantification

EGFP-STAT3 was quantified by measuring the fluorescence emission of EGFP at 535 nm upon excitation at 485 nm. A six-point calibration curve (100, 50, 15, 12.5, 6.25 and 0 $\mu\text{g/mL}$) was prepared in triplicate starting from an EGFP-STAT3 solution at known concentrations. 80 μL of each fraction were added to a black 96-wells plate and the fluorescence was measured with a Multiplex M Nano microplate reader (Tecan). Each fraction was measured in duplicate.

Protein Slot Blot

The assay was performed using a Bio-Dot[®] SF Microfiltration Apparatus (BioRad) following the manufacturer's instructions. 100 μL from each fraction were loaded on each well and blotted on a nitrocellulose membrane (Bio-Rad). The membrane was blocked with 5% BSA (w/v) in TBS-T at RT for 1h under gentle agitation and incubated overnight at 4°C with primary anti-CD63 antibody (Santa Cruz Biotechnology, sc-365604, 1:1000). The following steps were performed as described in paragraph 2.3.

Western Blot (WB)

The EVs pellets from Polymeric Precipitation were resuspended 10 μL of 2 \times reducing Laemmli Sample Buffer and heated at 95°C for 5 min. The samples were then diluted to get 1 \times concentration of the sample buffer and run on a 10% SDS-PAGE gel. Gel run and blotting were performed as described above in paragraph 2.3.

The membrane was then probed using the primary antibody against STAT3 (Santa Cruz Biotechnology, sc-8019; 1:1000). The immunocomplexes on the membrane were revealed as described above in paragraph 2.3.

Assessment of protein encapsulation

Fluorescence-positive fractions were gathered and subjected to the precipitation step. The new pellet was resuspended in 100 μL of PBS buffer and the total protein amount was determined by BCA.

The sample was then divided in 4 aliquots and each one was subjected to a different treatment. The first aliquot was lysed upon treatment with SDS. The second one was lysed with SDS and, subsequently, was subjected to proteolysis upon treatment with Proteinase K. The third one was treated only with Proteinase K while and the fourth one was used as a control. To lyse the EVs, aliquots 1 and 2 were firstly incubated for 30 min at 25°C under mixing at 400 rpm in a thermal mixer in 1% (v/v) SDS solution. Afterwards, aliquots 2 and 3 were incubated for 1h at 37°C under mixing in presence of Proteinase K (QIAGEN) to induce proteolysis. Proteinase K was used in a final EVs proteins-Proteinase K ratio of 1:100 (w/w).

After the treatments, reducing Laemmli sample buffer was added to 1 \times final concentration. The aliquots were heated at 95°C for 5 min and loaded onto 10% SDS polyacrylamide gel. SDS-PAGE

and WB were performed as described in paragraph 2.3, using a primary antibody against STAT3 (Santa Cruz Biotechnology, sc-8019, 1:1000).

2.7. Evaluation of the cellular uptake of EGFP-STAT3 loaded EVs

MDA-MD-231 cell culture

Human breast cancer cell line MDA-MD-231 (ATCC HTB-26) were cultured in DMEM supplemented with 10% FBS, 100 UI/mL penicillin, 100 µg/mL streptomycin, and 40 µg/mL gentamycin in a 5% CO₂ atmosphere at 37°C.

Staining of EVs

EVs (EGFP-STAT3 loaded or unloaded) were subjected to an additional labelling step with DiD, a carbocyanine fluorescent dye. In detail, 1 µL of DiD solution (Molecular Probes Inc.) was added to the EVs suspension directly after ultracentrifugation, for unloaded EVs, or after incubation with EGFP-STAT3, for loaded EVs. The mixture was incubated for 30 min at 30°C and then purified by SEC as described in paragraph 2.4. The labelling has been evaluated by measuring the fluorescence emission of DiD at 670 nm upon excitation at 640 nm with a Multiplex M Nano microplate reader (Tecan). Each fraction was measured in duplicate.

Treatment of MDA-MD-231 cells with EGFP-STAT3 EVs

9×10^5 cells/well were seeded in 24-wells plate in 500 µL medium volume and left overnight in the incubator. After 24 hours, the medium was removed, the cells were washed twice with sterile DPBS and the suspension of EGFP-STAT3 DiD-stained-EVs (1.5×10^8 particles in fresh medium) was added to the cells. At selected times (1h, 2h, 5h, 24h) the medium containing the EVs was temporarily replaced with Hanks' Balanced Salt Solution (HBSS) and observed under a fluorescence microscope (Zeiss Axiovert AX10) using a bright field and a fluorescence filter (Zeiss Filter set 38, Excitation 470 nm, Emission 525nm). Representative images were captured with the hardware camera and processed using ZEN software (Zeiss microscopy) and ImageJ (Rasband, W.S., ImageJ, U. S. National Institute of Health, Bethesda, Maryland, <http://rsb.info.nih.gov/ij/>, 1997–2008).

Immunofluorescence and confocal analysis

MDA-MD-231 cells were seeded on glass coverslips in 24-wells plate (9×10^5 cells/well) and let adhere overnight. On the following day, the medium was replaced with EGFP-STAT3 DiD-stained EVs solution (1×10^9 total particles in 500 µL fresh medium). Untreated cells were used as control.

After the treatment, the supernatant was removed, and the cells were washed twice with DPBS and fixed with 4% (v/v) paraformaldehyde (PFA) for 10 min at RT. The PFA excess was removed, and the glass slides were washed twice with DPBS for 10 min under gentle agitation. Fixed cells

were permeabilized with 0.1% (v/v) Triton X-100 in DPBS for 5 min and blocked with 5% (w/v) BSA + 0.05% (v/v) Triton X-100 in DPBS for 1h at RT under agitation. Nuclei staining were performed with 4',6-diamidino-2-phenylindole (DAPI, ThermoFisher, 1:1000) for 15 min at RT. After washing, the coverslips were mounted on the glass slides with Dako Fluorescence Mounting Medium (Agilent).

Confocal analyses were performed with a confocal laser-scanning fluorescence microscope Leica SP5 (Leica Microsystem) using a 488 nm laser for excitation of EGFP-STAT3, 405 nm laser for DAPI and 633 nm laser for DiD. Images were captured at 40× magnification and processed using Adobe Photoshop and ImageJ software.

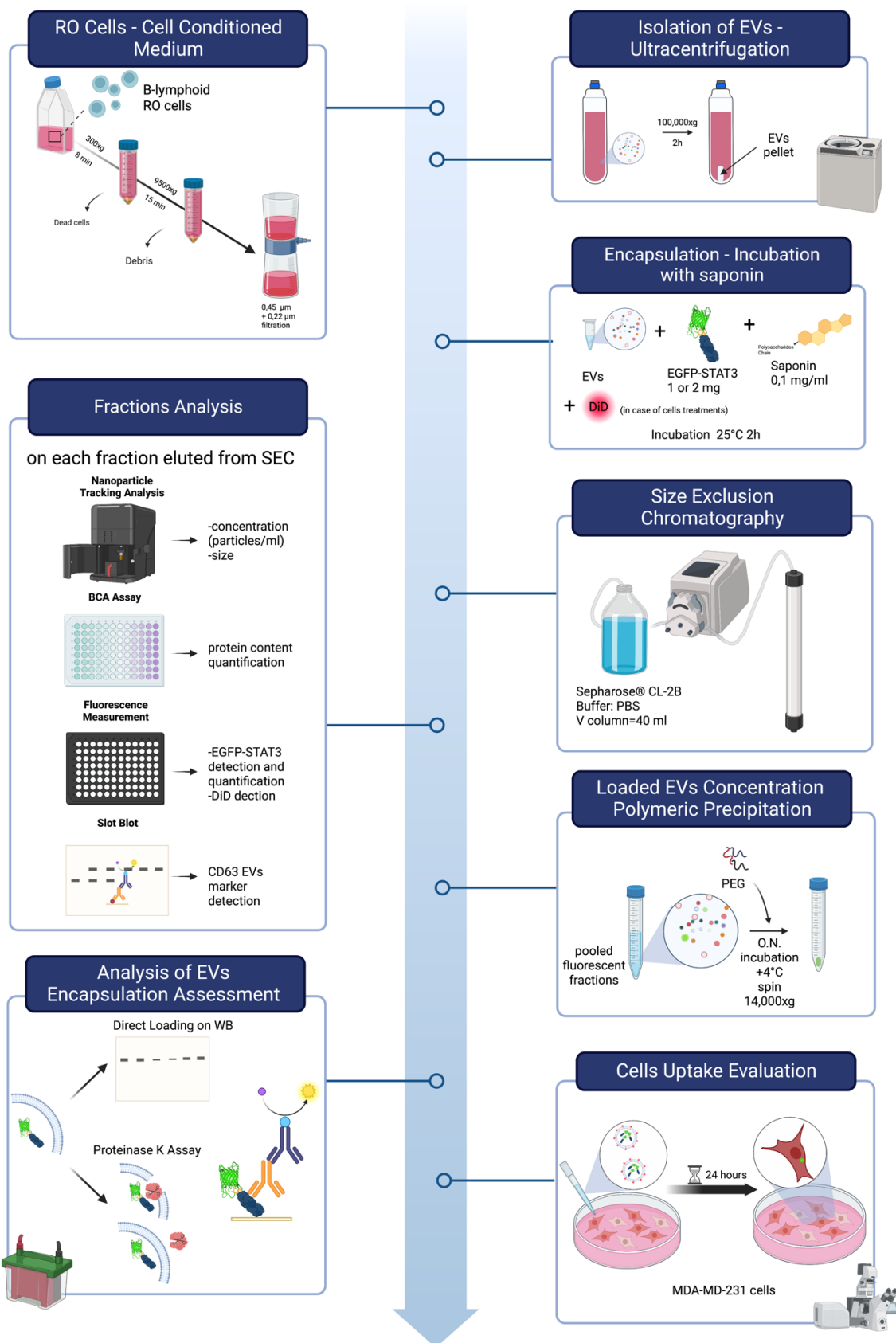


Fig.17. Schematic representation of the workflow for the described experiment. Created with Biorender.com.

Results and Discussion

1. Purification of EGFP-STAT3 and STAT3 recombinant proteins

In this work, a novel fusion construct in which recombinant STAT3 is fused with the fluorescent protein EGFP has been proposed. This design allows to exploit the fluorescence properties of EGFP for easy visualization and tracking of the STAT3 protein. In more detail, the human full-length STAT3 gene is linked to the EGFP gene through an aminoacidic linker, which, in turn, can be hydrolysed by the TEV protease. Moreover, a sequence coding for a 10× poly-Histidine has been added to the 5' end of the EGFP gene (Fig. 18) to simplify the purification process.



Fig. 18. Schematic representation of the EGFP-STAT3 fusion protein. In red: poly-Histidine tag. In green: Enhanced Green Fluorescent Protein (EGFP). In yellow: *Tobacco Etch Virus* Cleavage Site (TEV-CS). In light blue: Signal Transducer and Activator of Transcription 3 (STAT3).

EGFP-STAT3 was expressed in ExpiSf9 cells and purified to apparent homogeneity (Fig. 19 A lane 1-4). The purified EGFP-STAT3 was then cleaved with TEV protease and purified by loading the reaction mixture into a Ni²⁺-column to obtain the cleaved target in the flow-through and retain the EGFP tag.

SDS-PAGE of the proteolysis mixture before loading onto Ni²⁺-column confirms that the TEV has not completely cleaved the EGFP-STAT3 in STAT3 and EGFP (Fig. 19 A lane 5). The loading on the Ni²⁺-column allowed the successful removal of EGFP and TEV protease, but not completely of the non-cleaved EGFP-STAT3 (Fig. 19 B, lane 6).

As a final step of purification, STAT3 was fractionated by size exclusion chromatography (SEC). The chromatographic profile reveals the presence of two peaks at 10.03 mL and 14.45 mL elution volume which are not completely resolved and partially overlap (Fig. 19 C). SDS-PAGE analysis of the fractions eluted from 10 to 13 mL shows three main bands with apparent molecular masses corresponding to ~80 kDa (STAT3), ~120 kDa (EGFP-STAT3), and >180 kDa (Fig. 19 B, lanes 7-10). It could be hypothesised that the latter band corresponds to a dimeric form of STAT3, resistant to denaturing and reducing treatments routinely performed for SDS-PAGE gel samples. Moreover, analogous speculations can be made for EGFP-STAT3 regarding the upper band visible in Fig. 19 A, lanes 3-4. These results suggest the need to perform further experiments to fully characterise the dimerization mechanism of STAT3, a topic already under investigation in the Laboratory of Prof. Mariotto (244,245). Nonetheless, this is beyond the scope of this thesis. SDS-PAGE analysis of the fractions at 14 and 16 mL elution volumes shows the highest STAT3:EGFP-STAT3 ratio, suggesting that the peak at 14.45 mL is the peak of cleaved STAT3 (Fig. 19 B, lanes 12 and 13).

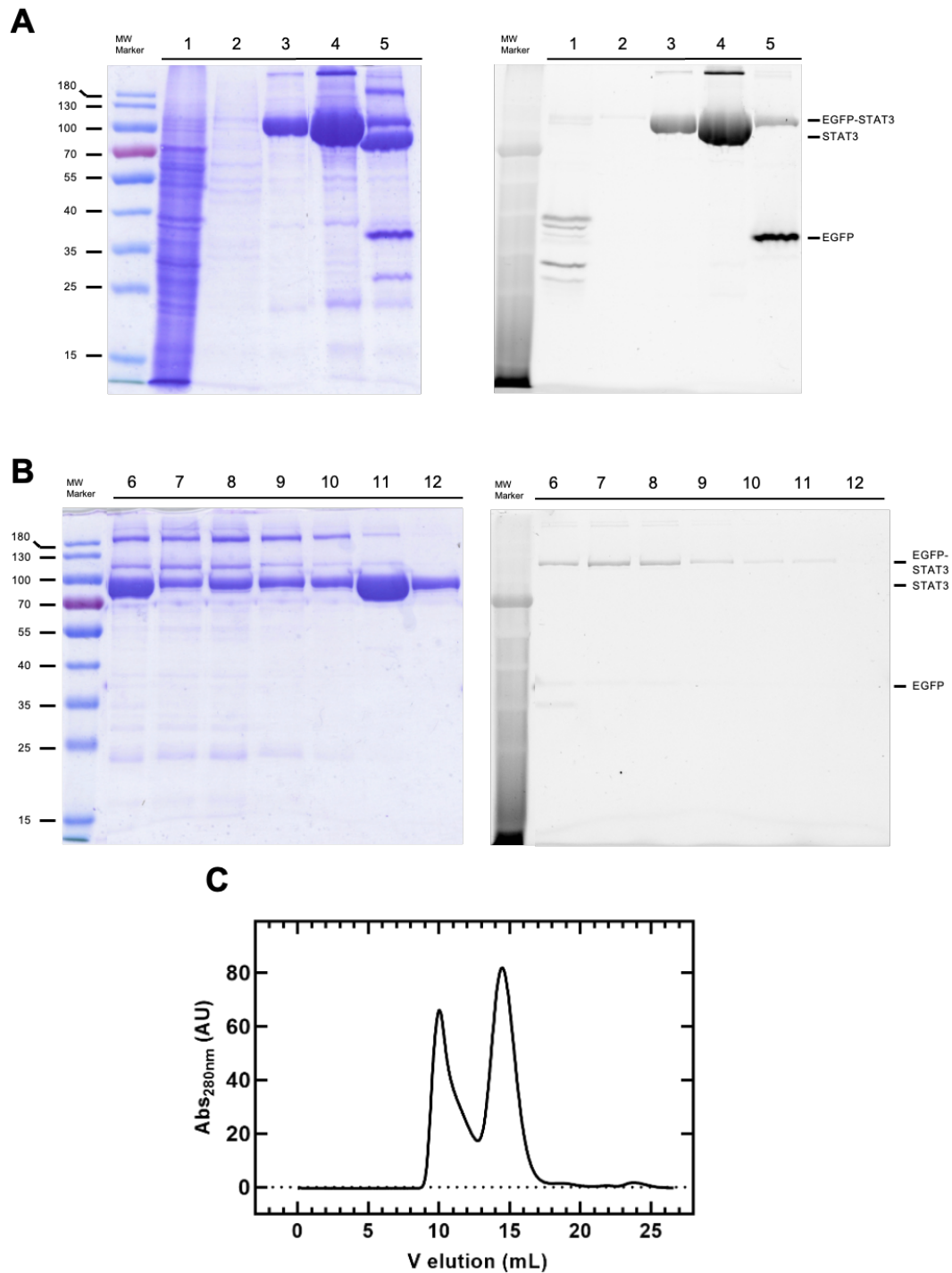


Fig. 19. Purification of recombinant WT STAT3 and EGFP-STAT3. (A-B) SDS-PAGE gel Coomassie-stained and fluorescence detection of the unstained gel. Lane 1: Cell lysate. Lane 2: Flow-through Ni^{2+} -column loading. Lane 3: Eluted (in buffer B+250 mM Imidazole) EGFP-STAT3 ($\sim 5 \mu\text{g}$). Lane 4: EGFP-STAT3 after concentration and buffer exchange with PD10 ($\sim 20 \mu\text{g}$). Lane 5: sample after overnight treatment with TEV ($\sim 18 \mu\text{g}$). Lane 6: isolated STAT3 ($\sim 7 \mu\text{g}$) from Ni^{2+} -column before SEC. Lanes 7 to 12: aliquots ($5 \mu\text{L}$) of fractions eluted at 10, 11, 12, 13, 14, and 16 mL. (C) SEC chromatogram of STAT3 (after TEV treatment).

2. Biophysical and biochemical characterization of EGFP-STAT3 and STAT3 recombinant proteins

The folding states of STAT3 and EGFP-STAT3 were assessed by Circular Dichroism spectroscopy. The Far-UV spectrum of the recombinant purified STAT3 shows the typical dichroic signal of a protein rich in α -helix secondary structure (Fig. 20 A, black line). Precisely, two minima are present at 209 and 220 nm, which are slightly shifted in comparison with the reference spectra of α -helix proteins (240).

However, estimation of the secondary structure content confirms the predominant α -helix composition of the protein and the presence of a small percentage of random coil structure (Table 10). These results are in accordance with the deposited three-dimensional structure (PDB: 1BG1) and previous CD analyses on the recombinant construct of STAT3 core (residues 124-723) (244). The Far-UV spectrum of EGFP-STAT3 presents a flatter shape at approximately 220 nm and a lower signal intensity than the STAT3 spectrum (Fig. 20 A, red line). The minima values are set at 210 and 218 nm, further shifted compared to STAT3 spectrum minima. The secondary structure is remarkably different from that of STAT3, with an estimated percentage of α -helix dropping to 37.7% and an increase in β - and random coil structure to 17% and 45.3%, respectively. These differences could be ascribed to the presence of the EGFP domain, which is mainly composed of β -strands (250).

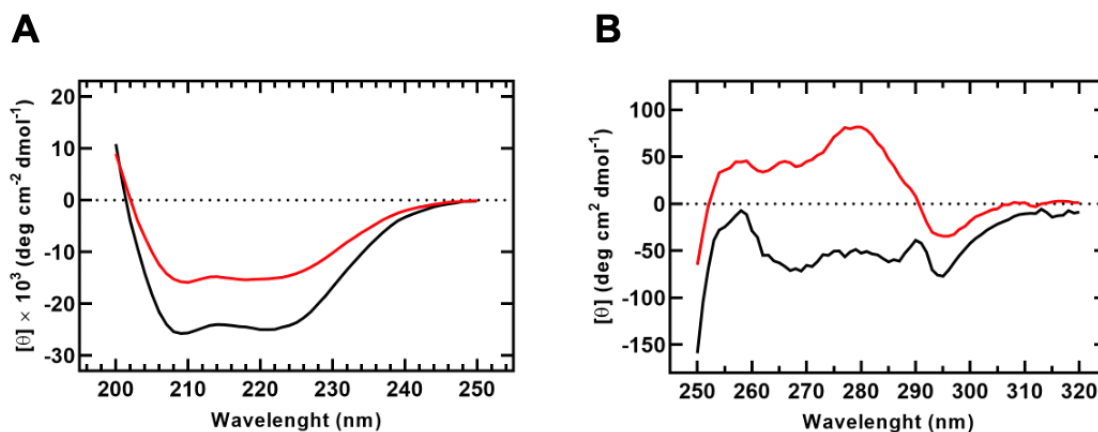


Fig. 20. CD spectra of EGFP-STAT3 and STAT3 in far and near UV regions. (A) Far-UV spectra recorded in the 250-200 nm spectral range. (B) Near-UV spectra recorded in the 320-250 nm spectral range. STAT3 (black line), EGFP-STAT3 (red line).

In the near-UV spectrum, STAT3 presents a negative dichroic band from 250 to 260 nm and from 290 to 300 nm (Fig. 20 B, black line). This CD spectrum is comparable with the near UV spectrum previously obtained for the STAT3 core protein (244,245). The EGFP-STAT3 near-UV spectrum shows a predominant contribution of EGFP in the range from 260 to 290 nm when compared to the near-UV spectrum of GFP (251) (Fig. 20 B, red line).

	α -helix	β -sheet	Random Coil
STAT3 (124-723) ^a	67.4	14.9	17.7
STAT3	67.3	8.9	23.8
EGFP-STAT3	37.7	17	45.3

Table 10. Secondary structure content of STAT3 core (124-723), STAT3, and EGFP-STAT3. Values are expressed in percentages. ^a Values reported from (2).

The thermal stability of both proteins was investigated by monitoring the ellipticity at 208 nm ($\theta_{208\text{nm}}$) between 10 and 96°C (Fig. 21). Both EGFP-STAT3 and STAT3 profiles exhibit a sigmoidal trend compatible with a two-state unfolding process and almost identical melting temperatures, for EGFP-STAT3 $T_m=55^\circ\text{C}$, for STAT3 $T_m=55.34^\circ\text{C}$.

Taken together these data suggests a proper folding of both proteins.

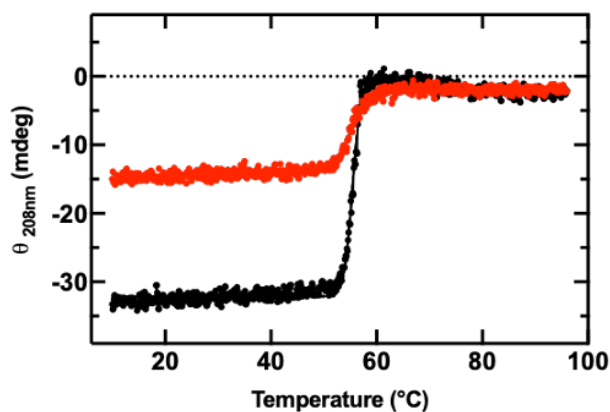


Fig. 21. Thermal denaturation of EGFP-STAT3 and STAT3 monitored by CD spectroscopy. Raw experimental data were interpolated with a sigmoidal 4PL curve providing the melting temperatures (T_m) for both proteins. EGFP-STAT3 (red dots), STAT3 (black dots). Data analysis was performed using GraphPad Prism v 9.0.

According to the canonical model (209, 252), phosphorylation of Tyr residue 705 is fundamental for the recruitment and dimerization of STAT3. Thus, phosphorylation by JAK2 active kinase was investigated for both proteins.

As shown in Fig. 22, both EGFP-STAT3 and STAT3 are successfully phosphorylated providing evidence of the correct folding of the proteins and proper accessibility of Tyr residue 705.

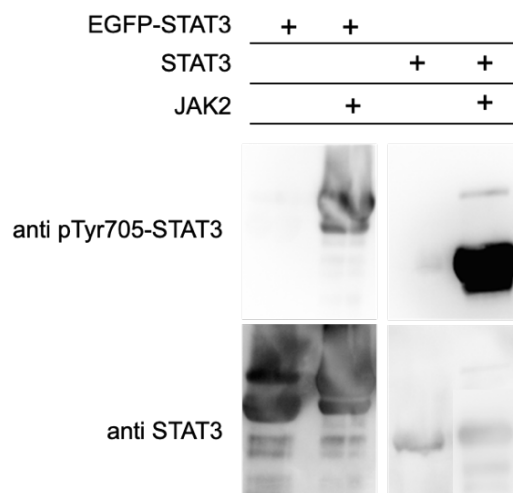


Fig. 22. *In vitro* JAK2 kinase assay with EGFP-STAT3 and STAT3. Both STAT3 and EGFP-STAT3 were subjected to an *in vitro* JAK2 kinase assay, the resulting membrane was probed with anti-pTyr705 STAT3 antibody and, after stripping, with anti-STAT3 antibody.

3. Isolation and characterization of EVs from RO cells

The work presented in these paragraphs was carried out part in the Laboratory of Prof. G. Fuhrmann at the Friedrich Alexander Universität in Erlangen, Germany, and part in the Laboratory of Prof. S. Mariotto in Verona.

EVs were isolated from RO cells conditioned medium (CCM) by ultracentrifugation and purified by SEC. After elution from the SEC column, the protein content of each fraction was quantified using BCA assay, and the SEC elution profile was built (Fig. 23 A). The obtained profile shows a peak centred at 12 mL elution volume due to proteins associated with the EVs and a later and wider peak due to proteins co-precipitated during the ultracentrifugation step. These data confirm that SEC provides an efficient method for separating EVs from protein impurities.

The evaluation of particle size by NTA (NanoSight N300, Malvern) confirms that the first SEC peak contained particles in the size range of EVs (from 100 to 200 nm) (Fig. 23 B, red bars). NTA data shows that fraction 12 presents the highest particle concentration, in the range of 10^{10} particles/mL (Fig. 23 B, black bars). Particle size distribution shows a main peak centred at approximately 130 nm but particles with hydrodynamic diameters from 70 to 300 nm were also detected (Fig. 23 C). Notably, this fraction also presents the highest protein concentration. On the other hand, the size distribution graph relative to fractions 10 to 15, after pooling and concentration, displays a main peak centred at approximately 130 nm, but a broader size distribution compared to fraction 12 before concentration (Fig. 23 D), suggesting the formation of aggregates. It could be hypothesized that the method used for the fraction concentration, that is, polymeric precipitation, might induce EVs aggregation in these experimental settings. Further experiments will be performed using other concentration methods (e.g., ultracentrifugation or

ultrafiltration) to clarify whether polymeric precipitation is the cause of EVs aggregation or if other factors come into play. This evaluation will allow us to determine which would be the more convenient approach in relation to our specific aim.

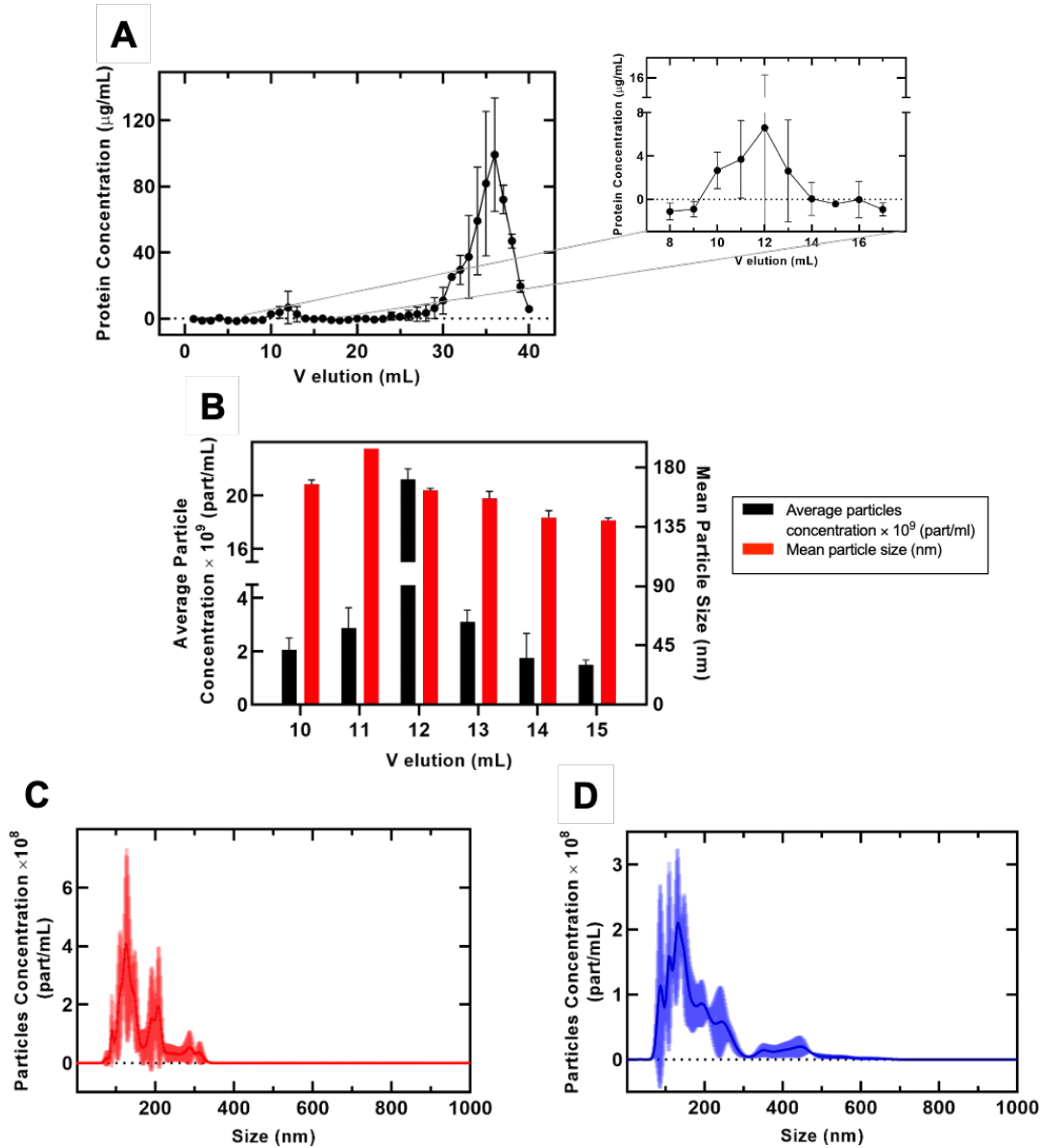


Fig. 23. Characterization of unloaded EVs from RO cells. (A) BCA assay of SEC eluted fractions. Mean \pm SD. (B) Graph representing average particle concentration (part/ml) and mean particle size (nm) for the EVs-rich SEC fractions (9-15) upon NTA measurement using a Nanosight N300 instrument. n=3 technical replicates. mean \pm SEM. (C) Representative particle size distribution of one of the EVs-rich SEC fractions (fraction 12). (D) Representative particle size distribution of the reunited fractions (10-15). n=3 technical replicates. SEM are displayed in a lighter shade. Y axes refers to the concentration of the samples before dilution required for NTA analysis.

To support the hypothesis of the presence of EVs in the isolated peak, aliquots from each fraction of SEC were blotted onto a nitrocellulose membrane by slot blotting and probed using an anti-CD63 antibody. CD63 is a tetraspanin that has been demonstrated to span the lipid bilayer of the

EVs (253). Since no lysis of the EVs had been carried out before blotting, only a surface marker could be considered, leading to the choice of CD63.

Immunoblotting analysis of each fraction shows enrichment of CD63 in fractions 10 to 15, further corroborating the successful separation of EVs from the contaminants (Fig. 24).

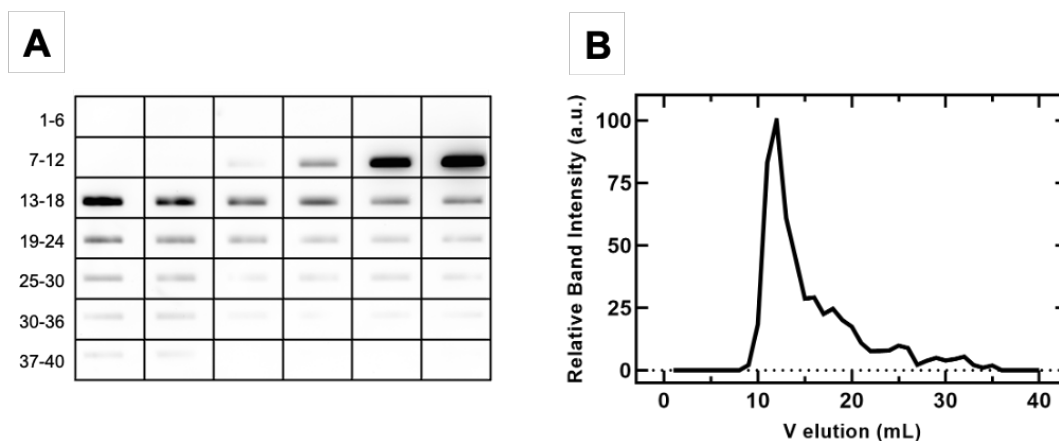


Fig. 24. Characterization of unloaded EVs from RO cells. (A) Slot Blot of SEC eluted fraction probed with anti CD63 antibody. (B) Densitometric analysis of (A).

4. Encapsulation and characterization of EGFP-STAT3 loaded EVs

The encapsulation of recombinant STAT3 into EVs was performed using a membrane permeabilizer-assisted approach by incubation of the mixture of EVs and EGFP-STAT3 with the natural surfactant saponin, following the protocol described in the Material and Methods section (paragraph 2.5). Thereafter, SEC was performed to remove free EGFP-STAT3 and other non-desired components.

BCA analysis (Fig. 25 A) and fluorescence readings (Fig. 25 B) of each eluted fraction allowed the construction of chromatographic profiles that show two different peaks as for the unloaded EVs (Fig. 23 A). Again, this indicates the successful separation of the EVs from the other components.

The peak relative to the EVs is centred around 15 mL while the “contaminants” peak span from 20 mL to the end of the column volume. The presence of EGFP-STAT3 fluorescence emission signal in the fractions corresponding to the EVs suggests the presence of EGFP-STAT3 loaded vesicles, or at least of EGFP-STAT3 molecules associated with the EVs.

NTA analyses were performed on each eluted fraction, as for the unloaded EVs. The obtained data show that the fluorescent positive particles are a fraction of the total number of particles detected by scattering (Fig. 26 A e B). Moreover, no fluorescence-positive particles were detected in fractions 10 and 11, in accordance with the fluorescence emission readings performed with the multiplate reader (Fig. 26 B).

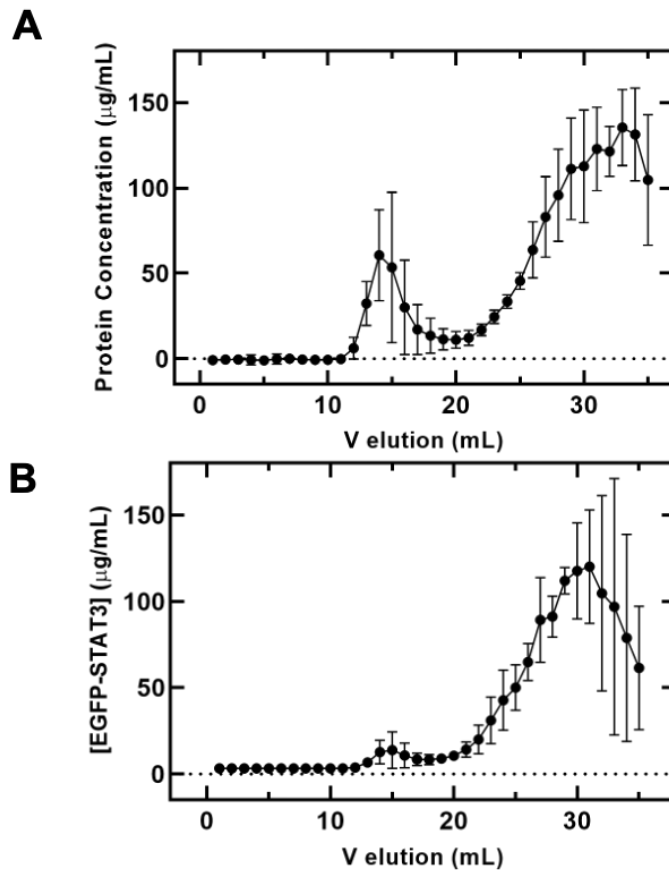


Fig. 25. SEC chromatographic profiles of EGFP-STAT3 EVs. (A) Total protein concentration, determined by BCA assay, has been reported for each fraction. The obtained values were calculated from a BSA calibration curve. (B) EGFP-STAT3 concentration, for each eluted fraction, was determined by recording the emission intensity of the sample at 535 nm upon excitation at 488 nm. The values were calculated using an EGFP-STAT3 calibration curve. For both graphs $n=3$ biological replicates, $\text{mean}\pm\text{SD}$.

The reported NTA analyses for EGFP-STAT3 were performed using the ZetaViewer instrument, which is different from the one available in Verona, the NanoSight N300. Unfortunately, the two instruments, although working following the same principles, use different hardware and software, leading to considerable difficulties in comparing the obtained results (254). Taking this into account, comparisons regarding particle concentration and size between samples analysed with ZetaViewer and NanoSight instruments will not be made.

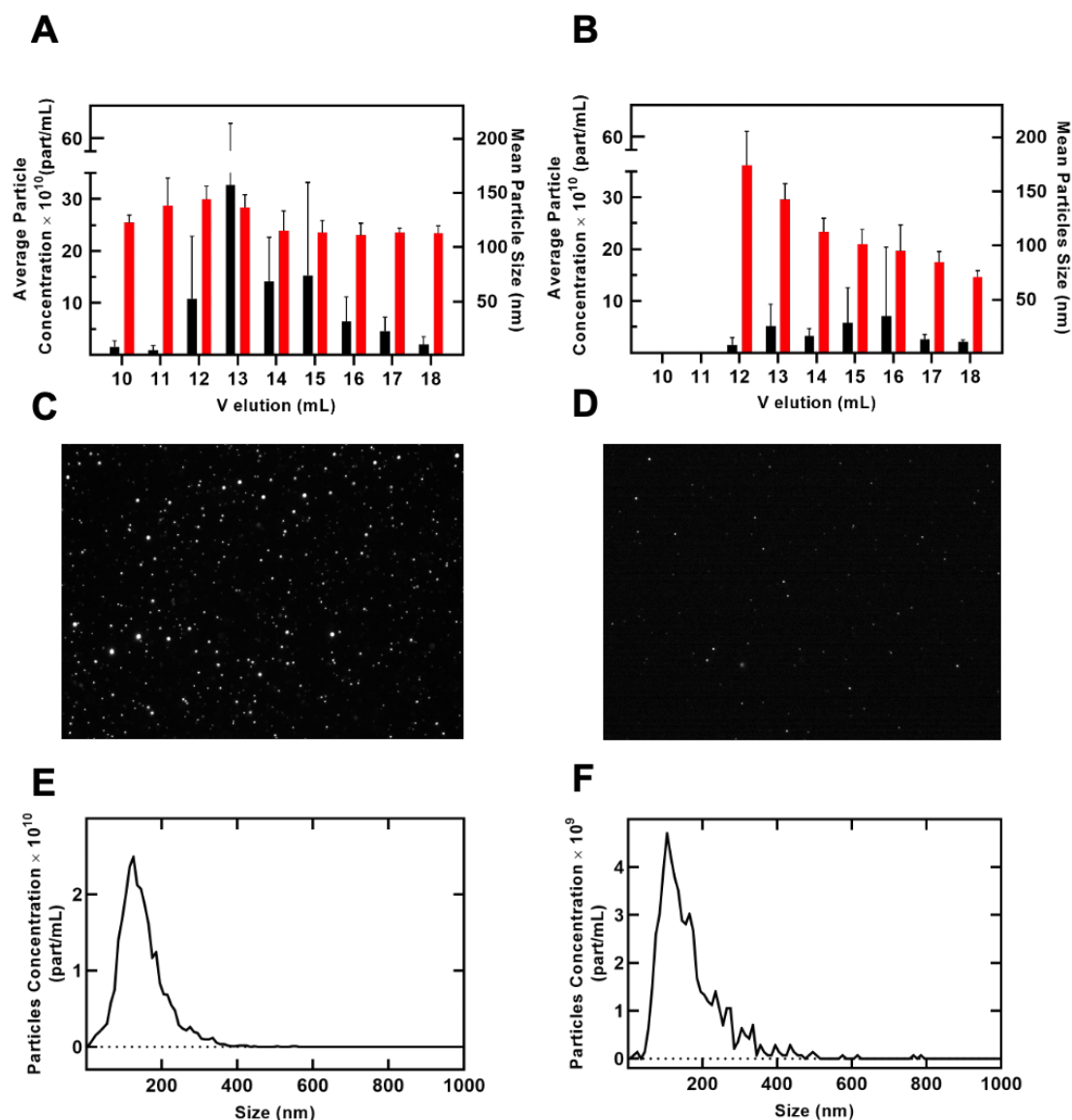


Fig. 26. NTA results for loaded EVs after SEC. (A-B) Graphs representing average particle concentration (part/mL) and mean particle size (nm) for the EVs-rich SEC fractions (10-18), (A) in scattering mode (laser 488 nm and no filter) and (B) in fluorescence mode (laser 488, filter 500 nm). Measurements were carried out with the instrument settings detailed in the Methods section, paragraph 2.6. $n=3$ biological replicates. Mean \pm SD. Y-axes refer to the concentration of the initial sample, before dilution performed for NTA analysis. NTA instrument used was ZetaViewer. (C-D) Representative shots of the videos taken for (C) scattering and (D) fluorescence analysis. (E-F) Particle size distribution of fraction 14 in (E) scattering and (F) fluorescence mode.

To confirm the presence of STAT3 in EVs, WB analysis of concentrated fractions using anti-STAT3 antibody was performed (Fig. 27). It should be noted that WB was performed on two different preparations: encapsulated EVs obtained using 2 mg as EGFP-STAT3 initial protein amount (the condition used for all the other reported experiments) and encapsulated EVs obtained using 1 mg as EGFP-STAT3 initial amount. Different amounts of recombinant EGFP-STAT3 were loaded onto the gel for comparison. The membrane probed with an anti-STAT3 antibody shows the presence of EGFP-STAT3 in both the preparations (Fig. 27).

In summary, the presence of fluorescence-positive particles is confirmed by NTA, and both WB and fluorescence intensity measurements provide evidence of the presence of EGFP-STAT3 as an EV-associated protein.

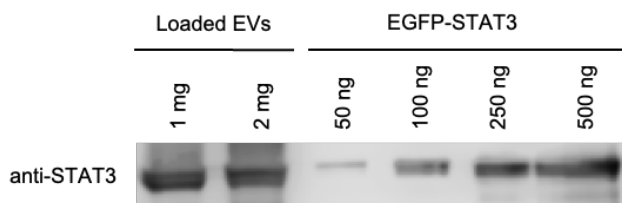


Fig. 27. WB analysis of EGFP-STAT3 loaded EVs. EVs were lysed with reducing Laemmli buffer, heated at 95°C for 5 min, and loaded onto a 10% SDS-PAGE gel. Increasing amounts (50, 100, 250, 500 ng) of EGFP-STAT3 were loaded along on the same gel.

The obvious following question is whether the protein is mainly located inside the lumen of the EVs or merely interacting with the external portion of the membrane lipidic bilayer. Indeed, the need to determine the topology of EV-associated components has been widely discussed and endorsed by the EVs scientific community (48,54). Recently, Rankin-Turner *et al.* underlined the importance of distinguishing whether the therapeutic cargo (e.g., small organic molecule, nucleic acid, or protein) is lumenally incorporated or only associated with EVs (135). This would be of utmost importance for the correct determination of encapsulation efficiency and loading capacity, and therefore, for the definition of the most effective criteria for EVs drug loading. As recommended in (48) and taking into consideration the experiments performed in (255) and (153,168), a protocol has been optimized in the attempt to determine the localization of EGFP-STAT3 in the obtained preparations.

If cargo protein is localised inside the EVs (Fig. 28 A), it should be protected from degradation by proteases since proteases are not likely to penetrate through the lipidic bilayer (54). In contrast, if it only adheres to the membrane, it would be exposed to the protease activity and sensitive to digestion (Fig. 28 B).

In this protocol, Proteinase K (PK) was used as protease given its broad-spectrum enzymatic activity, but other proteases such as trypsin have been used for analogous purposes (256). At the same time, it is important to evaluate the proteolysis upon treatment of EVs with a lysing agent, such as SDS to verify, the effectiveness of the treatment (Fig. 28 C). The detergent determines the exposure of the entire EVs proteinaceous content to the enzymatic action of PK. Evaluation of the results of the assay was performed by Western blot analysis using anti-STAT3 antibody.

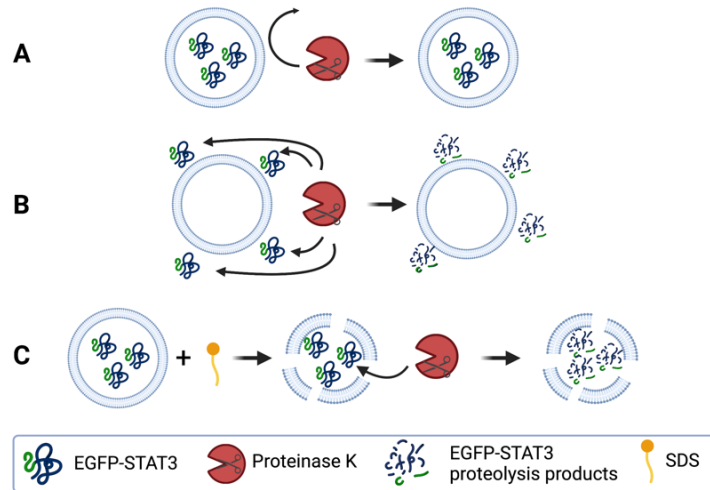


Fig. 28. Schematic representation of treatment of the EGFP-STAT3 EVs with Proteinase K for the assessment of the main localization of the protein. (A) The proteins are in the EV lumen. Proteinase K cannot lyse them. (B) The proteins are outside, adherent to the EV surface. Proteinase K manages to lyse them. (C) The proteins are in the lumen, but treatment with SDS induces the permeabilization of the EV allowing Proteinase K to get in contact with the proteins and lyse them.

As shown in Fig.29, the proteolytic digestion is more extended when the EVs have been previously lysed in comparison to the other treatment conditions. Proteolysis products of untreated EVs are likely due to protein autoproteolysis as previously observed in other WBs and SDS-PAGE gels (data not shown).

These results indicate that the main portion of the EV-associated EGFP-STAT3 is protected by the EVs membrane and is not sensitive to digestion, corroborating the hypothesis of the successful incorporation of EGFP-STAT3 inside the EVs.

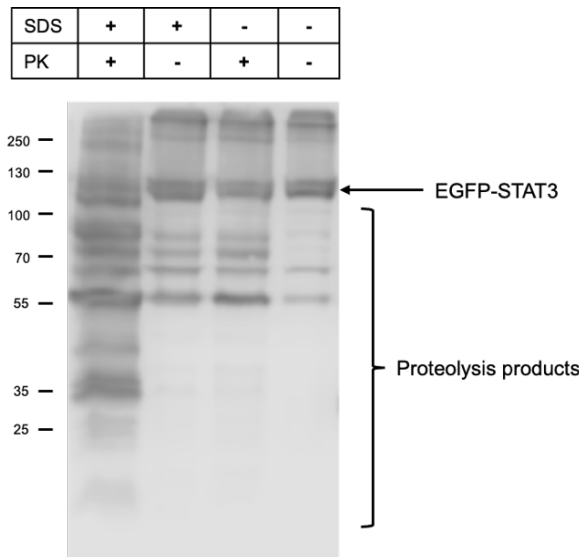


Fig. 29. Western Blot results for the assessment of EGFP-STAT3 encapsulation. Aliquots of loaded EVs were treated as described above, mixed with reducing Laemmli buffer to stop the PK reaction, heated at 95°C for 5 min, and loaded on a 10% SDS-PAGE gel.

It is worth noting that, to the best of the author's knowledge, only a small number of the published papers on EVs as Drug Delivery Systems proposed an exogenous (post-isolation) approach to achieve the protein loading into the EVs (four independent research groups, as reported in Table 3 in the Introduction section). Among these, only a few cases (two out of four groups) clearly expressed the encapsulation efficiency as a percentage of encapsulated protein relative to the total amount of initial protein. In particular, in a study by Haney *et al.*, the amount of encapsulated catalase was retrieved from the enzymatic activity assay performed with the loaded EVs, and it was 18.5% in the case of saponin-assisted encapsulation (153). In another case, the protein amount determined by BCA was considered to be correspondent to the amount of encapsulated therapeutic protein. Indeed, the authors assumed that the loading procedure (electroporation) led to the complete removal of EVs protein content; thus, the amount of the loaded therapeutic protein could be retrieved by BCA. This calculation led to a claimed encapsulation efficiency of 73.5% (170).

Since in our case it is not possible to quantify the amount of encapsulated protein from the protein activity nor it would be suitable to use the BCA assay to determine the amount of encapsulated protein, we mainly focused on the EGFP-STAT3 fluorescence measurement.

EGFP fluorescence intensity detection (Fig. 25 B) shows that a large amount of EGFP-STAT3 is not encapsulated. Indeed, by retrieving the mean amount of EGFP-STAT3 from the area under the curve of the different elution profiles, the encapsulation efficiency is 2.92%.

Even though this might suggest a very poor encapsulation efficiency, it may also suggest that the initial amount of protein is too elevated in comparison with the effective loading capacity of the particles. Indeed, as shown in Fig. 27, no remarkable differences can be appreciated between 1 mg and 2 mg of initial protein. To test this hypothesis, further experiments will be performed using lower amount of initial EGFP-STAT3.

Nonetheless, it might be more appropriate to evaluate not only the plain numbers but also the *in vitro* biological outcome.

5. Evaluation of EGFP-STAT3 EVs uptake by MDA-MD-31 cells

To evaluate whether the EGFP-STAT3 EVs could be internalised by the cells, a pilot experiment was performed using MDA-MD-31 cells as a cellular model.

For this purpose, isolation, encapsulation, and characterization of EGFP-STAT3 EVs were carried out as described above. It is important to note that the elution volume of the enriched EVs fractions is likely to shift slightly with every new EVs preparation. Therefore, for quick evaluation of the EV- enriched fractions, BCA assay (Fig. 30 A), fluorescence measurements (Fig. 30 B) and slot blot analysis (using anti-CD63 antibody) (Fig. 30 C-D) were performed on the first 18 fractions.

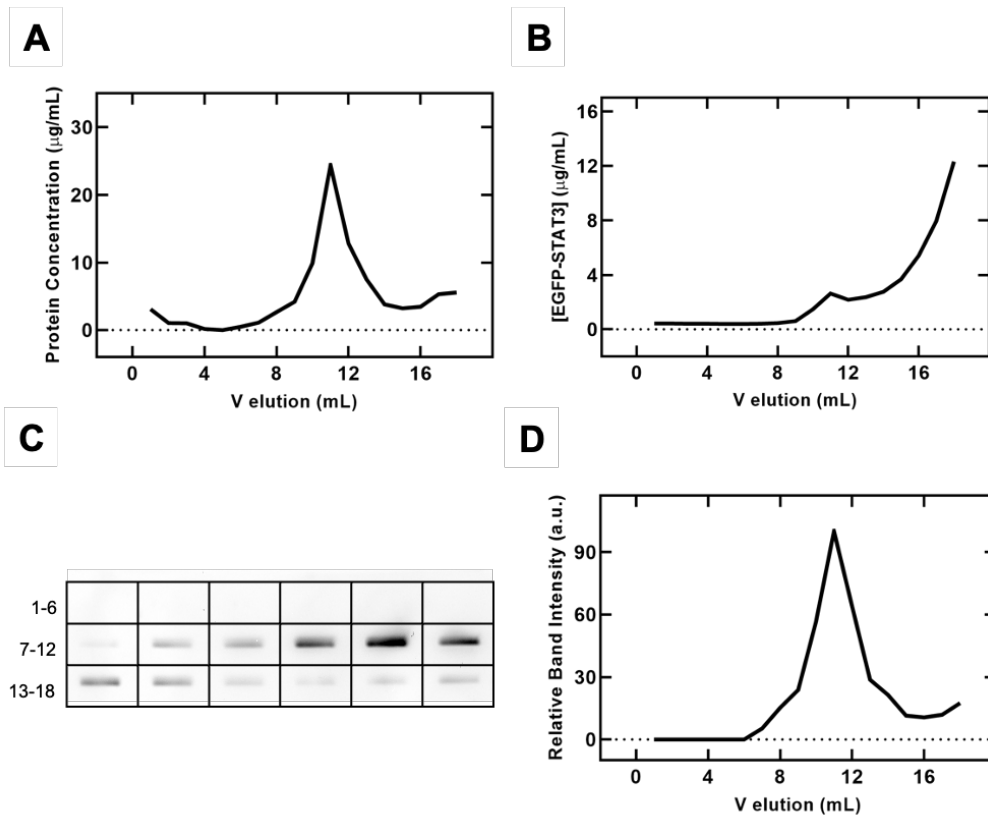


Fig. 30. Quick evaluation of the EVs-enriched fractions. (A) Protein quantification by BCA assay, (B) EGFP-STAT3 concentration by fluorescence detection, (C) anti-CD63 immunoblotting and (D) its densitometric analysis of fractions from 1 to 18.

MDA-MD-231 cells were seeded at 90,000 cells/well and treated with 1.5×10^8 particles, resulting in a 1.6×10^3 particle:cells ratio. An increase in the fluorescence signal was detected over time upon observation of the cells under a fluorescent microscope (Fig. 31), suggesting an interaction between the cells and EGFP-STAT3 EVs.

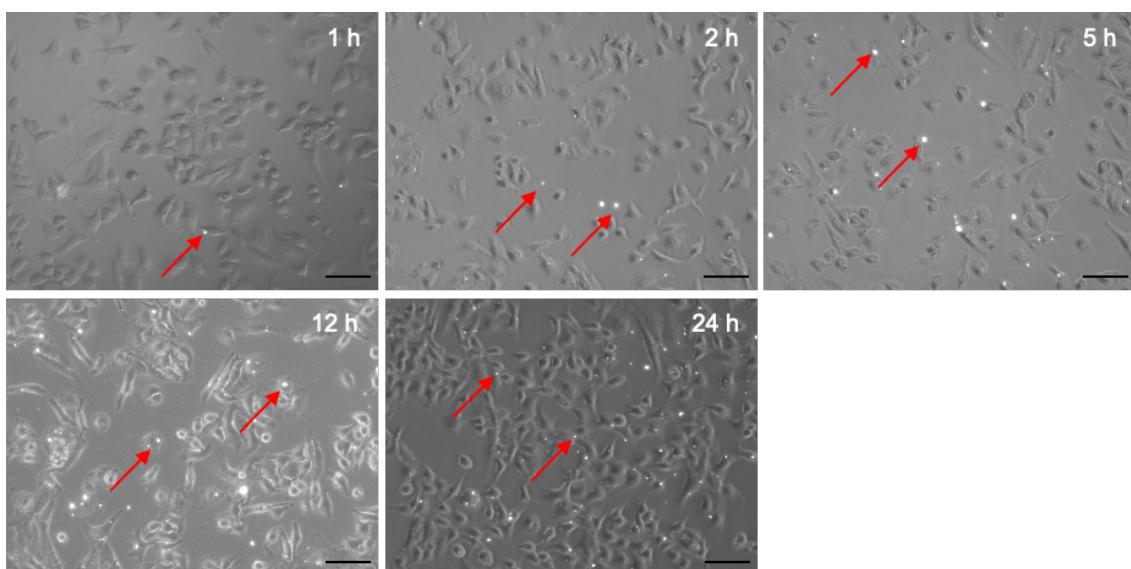


Fig. 31. Uptake of EGFP-STAT3 EVs by MDA-MD-231 cells by fluorescence microscopy. Arrowheads indicate colocalization of MDA-MD-231 cells and EGFP-STAT3. Scale bar: 50 µm.

To further investigate the hypothesis of the cellular uptake of EGFP-STAT3 EVs, confocal microscopy analysis was performed on MDA-MD-231 cells treated with EGFP-STAT3 EVs for 24 h at the particles:cells ratio previously used. The EVs used in this experiment were also stained with a fluorescent membrane dye, that is, DiD. As shown in Fig.14, the DiD-positive fractions corresponded to the EVs-enriched fractions (Fig. 32).

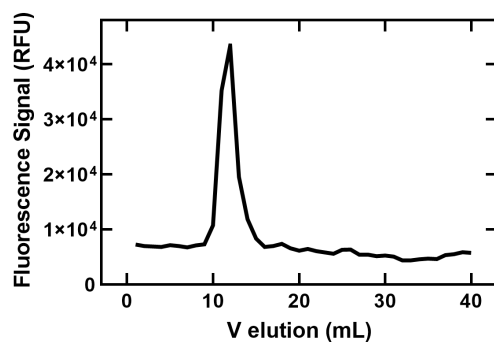


Fig. 32. Evaluation of DiD staining of EVs. DiD fluorescence emission at 670nm upon excitation at 640 nm was measured for each eluted SEC fraction.

Analysis by confocal microscopy confirms that EGFP-STAT3 EVs were internalized after 24 hours of treatment (Fig. 33). Very interestingly, the images highlight a co-localization of EGFP and DiD signals, supporting the hypothesis of the delivery potential of EGFP-STAT3 by EVs.

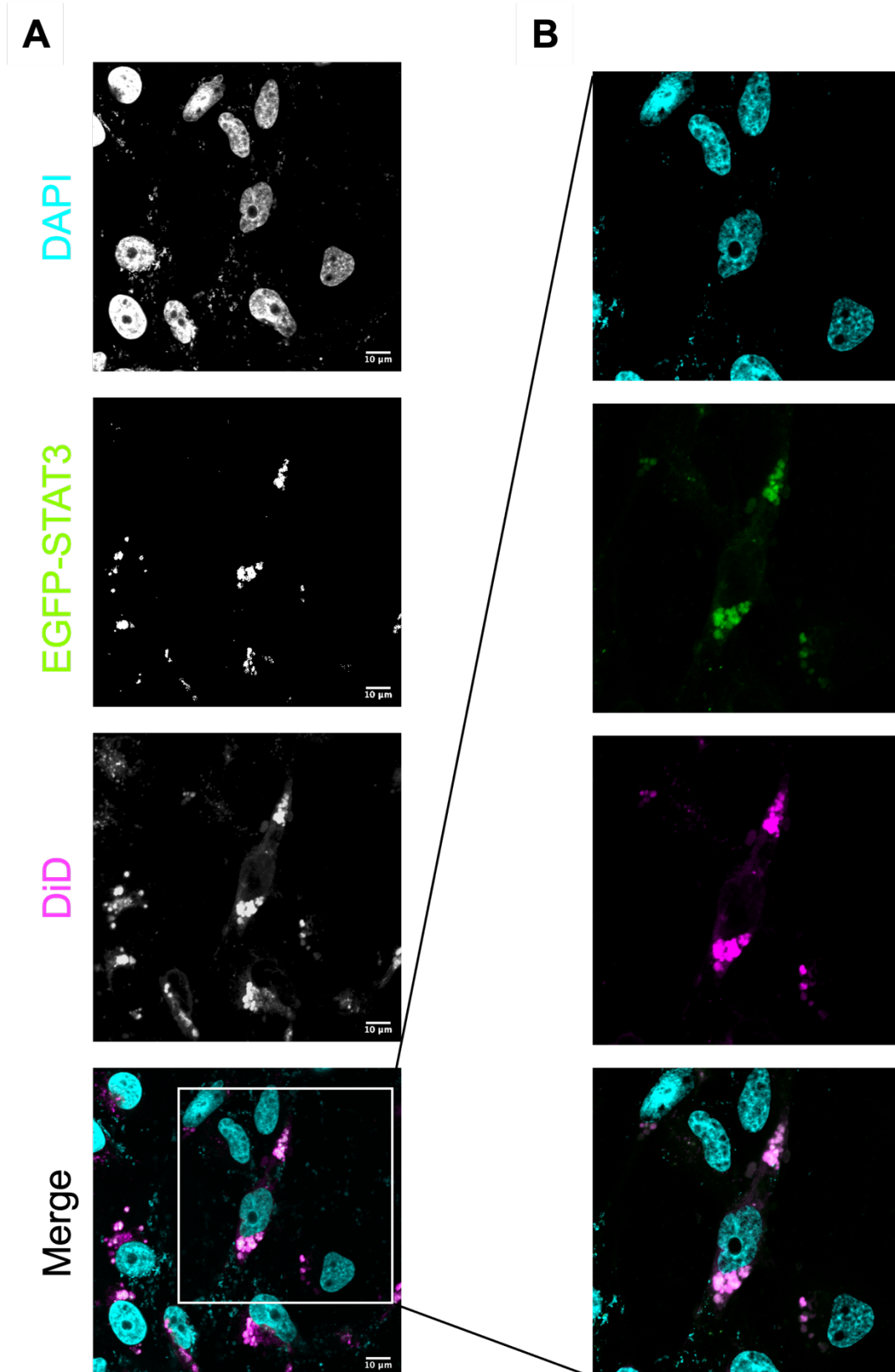


Fig. 33. Uptake of EGFP-STAT3 EVs by MDA-MD-231 cells after 24 hours, confocal microscopy. (A) Confocal analysis performed using a 40× objective lens. (B) 3× magnification of the section. Scale bar in panel A: 10 μm. Images are representative of three different experiments.

Conclusions and Outlook

In this work, a novel biogenic EV-based drug delivery system to restore STAT3 signalling in AD-HIES patients is proposed.

Firstly, an EGFP-STAT3 fusion protein was designed to introduce a tracking moiety for STAT3. EGFP is nowadays routinely used as a fluorescent tag (e.g., for studies on localization and movement of a certain protein) (257). Therefore, we choose EGFP to exploit the fluorescence signal for tracking STAT3 loaded EVs in *in vitro* cell experiments and for the detection and evaluation of STAT3 loading efficiency in the EVs.

Moreover, the designed construct also presents a poly-Histidine tag for an easy purification protocol of the recombinant protein and a protease cleavage site to obtain the untagged full-length STAT3 recombinant protein by a straightforward proteolysis reaction.

This construct was cloned and expressed in a baculovirus expression system, and the recombinant EGFP-STAT3 was successfully purified from the infected insect cells. The average yield of the performed purifications was 7.3 mg/100mL of insect cell culture. The establishment of this system allows us to obtain the full-length STAT3, which has never been previously obtained in our laboratory in the classical *E. coli* expression system.

The biochemical and biophysical analysis of the EGFP-STAT3 confirmed the proper folding and functionality of the fusion construct when compared with the untagged STAT3. These results suggested that, despite its steric hindrance, the EGFP tag might not affect the overall STAT3 *in vitro* activity.

Moreover, a protocol for the encapsulation of the EGFP-STAT3 protein in cells derived EVs has been established. A commercially available cell line was used for this purpose. Indeed, even though the limited ethical concerns regarding the use of PBMC (258), we considered more appropriate not to use EVs from PBMC in these first steps. Specifically, we used RO cells, a B-lymphoblastoid cell line. Importantly, RO cells present some major advantages which are remarkably favourable for our experimental settings (possibility of a serum-free culture condition, high conditioned media yield and potential low immunogenicity (247,248)).

Overall Nanoparticle Tracking Analysis results, fluorescence detection, and Western Blot analysis confirmed the presence of EGFP-STAT3 as an EV-associated protein. Very importantly, Proteinase K assay suggested successful encapsulation of the target protein in the EVs lumen. Future experiments will try to define a more suitable method for the determination of encapsulation efficiency, with close attention to the stability and aggregation propensity of the EVs.

Very encouragingly, the experiments performed on the model cell system (MDA-MD-231 cells) showed a degree of cellular uptake of the encapsulated EVs.

In the next steps EGFP-STAT3 EVs will be administered to PBMC from healthy donor to evaluate the EVs cellular uptake and, eventually, to determine if the delivered EGFP-STAT3 could be phosphorylated. EGFP-STAT3 phosphorylation will be evaluated using different techniques (e.g., immunoblotting, confocal microscopy, and flow activated cell sorting (FACS)), upon treatment with an appropriate cytokine cocktail. Subsequently, the cellular localization and the transcription of STAT3-related genes will be assessed. As following step, the delivery system will be evaluated and validated in a pathological model isolating the CD4⁺ naïve T cells from AD-HIES patients to test the efficacy and feasibility of our systems. Indeed, the crucial point will be to determine if this treatment would be successful in inducing the differentiation of the CD4⁺ T cells in T_H17 cells upon proper stimuli.

In conclusion, the data obtained thus far pave the way for the development of a new personalized therapy based on the use of EGFP-STAT3 EVs for the treatment of AD-HIES. Indeed, the use of EVs isolated in autologous manner for re-administration to the patient, after loading of the therapeutic cargo, might represent an alternative approach to the current conventional treatments.

Appendixes

Appendix I

During my 2nd and 3rd years as PhD student in the Biomolecular Medicine Program, I was involved in a second project in the laboratory of Prof. S. Mariotto.

Precisely this project was aimed to elucidate the role of STAT1 in EVs released by activated microglial cells in the context of neuroinflammation. This project was presented in the poster session of two congresses, FEBS 2021 (3-8 July 2021), and SIB 2021 (23-24 September 2021). Hereafter the research output of this project is presented.

Microglial cells release STAT1-containing EVs: possible implications in M1 activated microglia-neurons communication

Background

Extracellular Vesicles (EVs) play a paramount role in the central nervous system (CNS), which is built on connectivity and fine-tuned cell-to-cell interactions. Indeed, it has been observed that all major cell types in the CNS are able to send and receive messages through EVs (259). In particular, microglia, the resident macrophages of the CNS, have been suggested to largely rely on EVs as a means to propagate cytokine-mediated inflammatory responses across the CNS (260). As key players in immune regulation in the CNS, microglial cells are very dynamic cells, constantly expanding and retracting their pseudopods, patrolling the surrounding environment (261). Under physiological conditions, microglia are in a resting state but these cells may undergo a morphological and phenotypical shift in a process called M1 polarization in response to any stimuli that could compromise brain homeostasis, like in case of pathogen invasion (262), presence of misfolded proteins (263), or hypoxic conditions (264). M1 activated microglia react through phagocytic activity, releasing inflammatory cytokines such as IFN- γ , IL-6, IL-1 β and TNF- α , and producing neurotoxic mediators, such as reactive oxygen species (264). In spite of this, it has been demonstrated that the overactivation of microglia can sustain the inflammatory response, leading to a vicious cycle of neurotoxicity (265,266). Indeed, hyperactivation of microglia is one of the hallmarks of neuroinflammation (267) (Fig.34).

Within this framework, during the last few years, Prof. Mariotto's group carried out investigations aimed to elucidate the molecular mechanisms underlying microglial activation in hypoxic environment. Specifically, studies have been focused on the role of the nuclear transcription factor STAT1, one of the key players in the regulation of inflammatory response and cell death (268). The obtained data demonstrate that hypoxia induces oxidative stress, leading to the activation of STAT1 through its phosphorylation and S-glutathionylation in the microglia BV2 cell line.

Indeed, aberrant activation of STAT1 drives microglia towards pro-inflammatory M1 phenotype modulating the expression of downstream targets inducible nitric oxide synthase (iNOS) and cyclooxygenase-2 (COX2) (269,270). Very interestingly, pre-treatment of microglial cells with the anti-STAT1 polyphenol myricetin counteracted hypoxia M1 activation and led to a neuroprotective effect in an *in vitro* model of neurotoxicity (271).

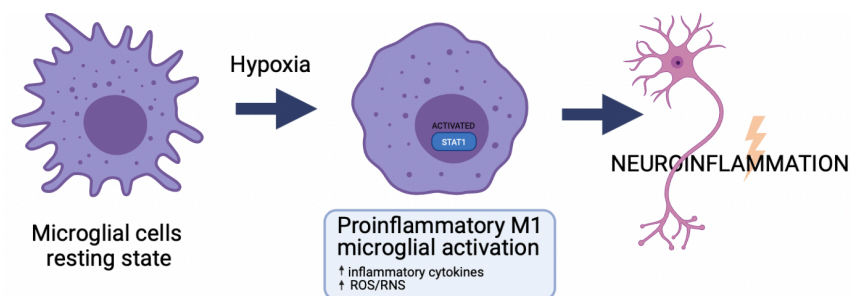


Fig. 34. Schematic representation of microglial activation in hypoxic conditions. Image created with BioRender.com.

These results demand further investigations on the involvement of activated STAT1 in the crosstalk between M1 polarized microglia and neurons. Given the crucial role of EVs in cell-to-cell communication, their involvement as actors in the trafficking of oxidative stress-activated STAT1 from M1 microglia to neurons has been hypothesized.

Materials and Methods

Materials

All chemicals used were of the highest analytical grade, purchased from Sigma, unless otherwise specified. Dulbecco's modified Eagle's medium (DMEM), penicillin, streptomycin, gentamycin, and fetal bovine serum (FBS) were obtained from Thermo Fisher Scientific.

Cell culture

Murine microglial BV2 cells (a kind gift from Prof. Persichini, University of Roma Tre) were cultured in DMEM supplemented with 5% FBS, 100 UI/mL penicillin, 100 µg/mL streptomycin and 40 µg/mL gentamycin. Normoxic culture conditions were obtained in 5% CO₂ humidified atmosphere at 37 °C, whereas hypoxic culture conditions were achieved by culturing the cells in a multigas incubator containing a gas mixture composed of 94% N₂, 5% CO₂, and 1% O₂ (RUSKINN C300 *in vivo*, RUSKINN Technology Ltd).

EVs Isolation and Purification

BV2 cells (2×10^6 cells) were seeded in T175 flask in DMEM complete medium and let adhere overnight. The day after, the medium was replaced with serum-free media and the cells were grown for 18 hours under hypoxic or normoxic conditions. Cell conditioned media were then collected and centrifuged at $500 \times g$ for 5 min and $2000 \times g$ for 30 min to remove any cellular

components and debris. The resulting suspensions were filtered through a 0.22 µm sterile syringe filter and concentrated using a 30 kDa cut-off Amicon ultracentrifuge filter unit (Millipore). Isolation of EVs was performed by polymeric precipitation using the Total Exosome Isolation reagent (Invitrogen) following the manufacturer's instructions. The obtained pellets were resuspended in sterile DPBS previously filtered using a 0.22 µm sterile syringe filter.

Transmission Electron Microscopy and Nanoparticle Tracking Analysis

Both EVs derived from BV2 cells subjected to acute hypoxic conditions (HEVs) and from BV2 cells cultured in normoxic conditions (NEVs) were analysed with Transmission Electron Microscopy (TEM) using a Morgagni 268D electron microscope (Philips) operating at 80 kV. Briefly, 10 µl of EVs suspension were placed on a formvar/carbon-coated grid, fixed with a 4% paraformaldehyde solution until completely dried, and negatively stained with UranylLess contrast solution (Electron Microscopy Sciences).

NS300 NanoSight (Malvern Panalytical) was used to perform Nanoparticle Tracking Analysis. Serial dilutions (ranging from 1:1000 to 1:5000) were prepared in 0.22 µm filtered DPBS from both HEVs and NEVs to achieve a final particle count between 20 and 120 per frame. Each measurement was performed in technical replicates (three videos of 60 seconds each), the capture parameters were set in order to obtain a sharp image of the particles and the acquired videos were processed using the instrument's software (81).

Western Blot

BCA assay on isolated HEVs and NEVs was used to quantify the protein amount in the isolated samples using the Pierce™ BCA Protein Assay Kit (ThermoFisher) following the manufacturer's instructions. Before the BCA assay, EVs were lysed by the addition of SDS to a final concentration of 1% (v/v) for 30 min at 25°C under mixing. For this assay, a calibration curve (500, 250, 125, 62.5, 31.25, 15.62 and 0 µg/mL) was constructed using standard Bovine Serum Albumin (BSA), in triplicate. Each sample was measured in duplicate. All the measurements were performed using a Multiplex M Nano microplate reader (Tecan).

Aliquots containing 12 µg of both HEVs and NEVs were mixed with 4x reducing Laemmli Buffer, heated at 95°C for 5 minutes, resolved by SDS-PAGE, and transferred to a PVDF membrane (Immobilon P, Millipore) by wet tank blotting. The membrane was blocked with a solution of 5% (w/v) BSA in Tris-buffer saline supplemented with 0.1% (v/v) Tween 20 (TBS-T) at RT for 1h under gentle agitation. Immunoblotting was performed by probing the membrane with anti-Hsp70 (Santa Cruz Biotechnology, sc-1060, 1:500), anti-Alix (Santa Cruz Biotechnology, sc-49268, 1:50), anti-Flotillin 1 (BD Bioscience, 610820, 1:500), and anti-STAT1 (Santa Cruz Biotechnology, sc-346, 1:1000) antibodies. After washing, membranes were developed using anti-rabbit, anti-mouse (Cell Signaling Technology, 7074S rabbit, 7076S mouse,

1:2000), or anti-goat IgG peroxidase-conjugated antibody (Santa Cruz Biotechnology, sc-2354, 1:2000) and chemiluminescent detection system (Immobilon® ECL Ultra Western HRP Substrate, Millipore). Immunoreactive proteins were detected using a ChemiDoc XRS Imaging System (BioRad).

Confocal Microscopy

Samples from both NEVs and HEVs were fixed on glass slides with 4% paraformaldehyde for 30 minutes, permeabilized with 0,1% Triton X-100 in PBS for 10 min and blocked with 5% BSA, 0,05% Triton X-100 in PBS for 1h at RT. The samples were then incubated overnight with anti-STAT1 antibody (sc-364, Santa Cruz Biotechnology, 1:50) at 4°C, washed with PBS, and incubated with Alexa Fluor™ 488 anti-rabbit secondary antibody (A-11008, Invitrogen, 1:1000) for 1h at room temperature. Finally, samples were stained with Concanavalin A Alexa Fluor™ 633 Conjugate (Thermo Fisher Scientific). Images were captured using a confocal laser-scanning fluorescence microscope Leica SP5 (Leica Microsystems) with a 63x objective. Adobe Photoshop and ImageJ software (Rasband, W.S., ImageJ, U. S. National Institute of Health, Bethesda, Maryland, <http://rsb.info.nih.gov/ij/>, 1997–2008) were used for image processing.

Results

Characterization of Normoxia and Hypoxia Extracellular Vesicles

To assess the quantity, size, and morphology of the isolated extracellular vesicles (NEVs and HEVs) Transmission Electron Microscopy (TEM) and Nanoparticle Tracking Analysis (NTA) analyses were carried out.

TEM imaging of both isolated HEVs and NEVs (Fig. 35 A and B) shows several spheroidal structures, some displaying a central depression, which is consistent with the EVs characteristic morphology in TEM images (48,93). Moreover, the visualized particles presented size of around 100-200 nm.

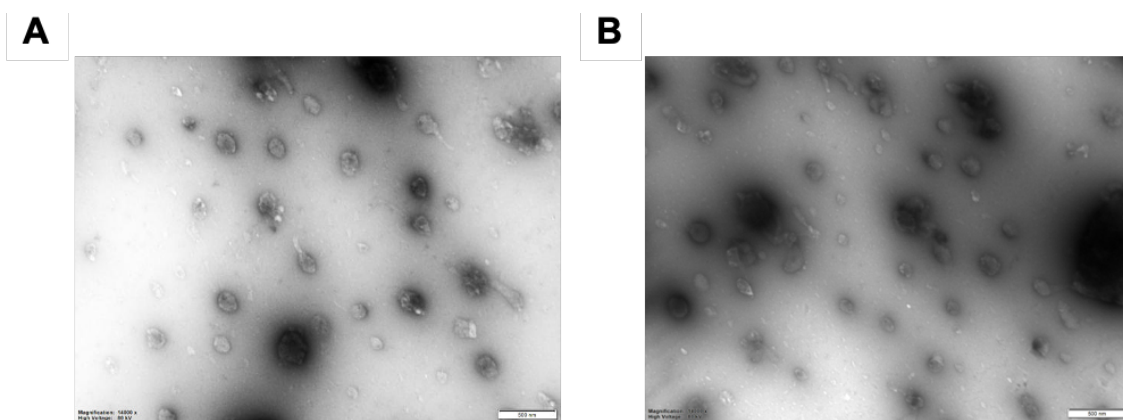


Fig. 35. Characterization of HEVs and NEVs by TEM. Characterization of vesicle size and morphology (A) NEVs and (B) HEVs. Scale bar corresponds to 500 nm.

NTA analysis allowed the quantification of the number and size distribution determination of the vesicular population. NTA analyses of both NEVs and HEVs (Fig. 36 A) show a size distribution typical of EVs with a peak at approximately 120 nm, in accordance with the TEM results.

Immunoblotting allowed the detection of EVs protein markers Hsp70, Alix and Flotillin 1 in both the NEVs and HEVs samples (Fig. 37 B). Importantly, STAT1 is also detected in both types of EVs.

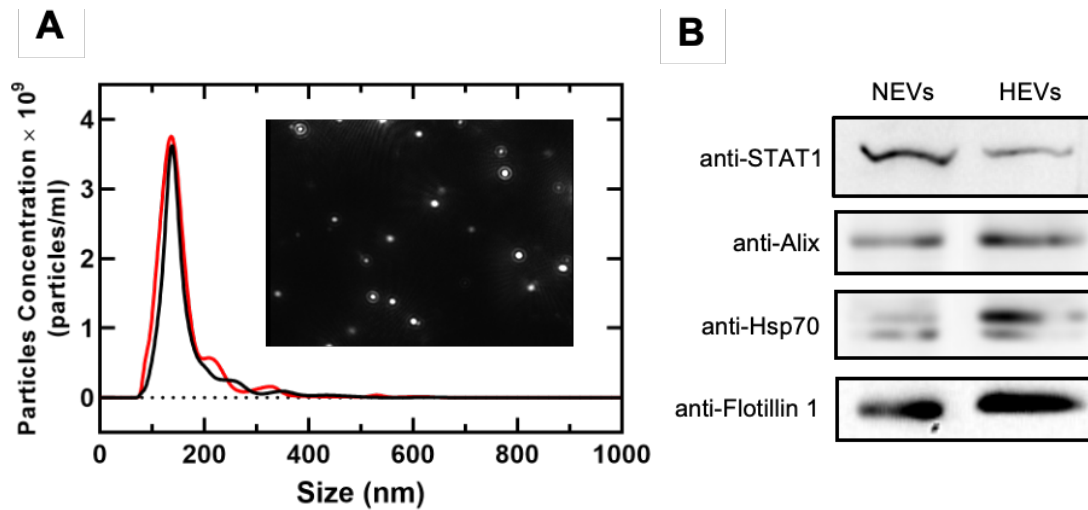


Fig. 36. Characterization of HEVs and NEVs by NTA and WB. (A) NTA of the HNEVs (–) and NEVs (–) extracellular vesicles: typical particles size distribution and concentration graph of the isolated particles, enclosed a representative video frame. n=3 technical replicates. SEM was omitted to obtain a clear representation of the data. Y axis refers to the concentration before dilution required for NTA analysis. (B) Detection of STAT1 and three EVs markers (Alix, Hsp70 and Flotillin 1). The images are representative of two independent experiments.

To further investigate the association of STAT1 with the EVs secreted from BV2 microglia, immunofluorescence experiments were carried out. Concanavalin A Alexa Fluor™ 633 Conjugate was used as dye for the surface of EVs. Confocal microscopy images show the colocalization of STAT1 and Concanavalin A signals, in both NEVs and HEVs samples, corroborating the previous evidence on the presence of STAT1 in the EVs (Fig. 37). Orthogonal-view images confirm the presence of STAT1 within the vesicular compartment (data not shown). Overall, the obtained data support the hypothesis of the role of EVs as actors in the trafficking of STAT1 from microglial cells and provide strong bases for the hypothesis of the involvement of STAT1 in cell-to-cell communication in the CNS.

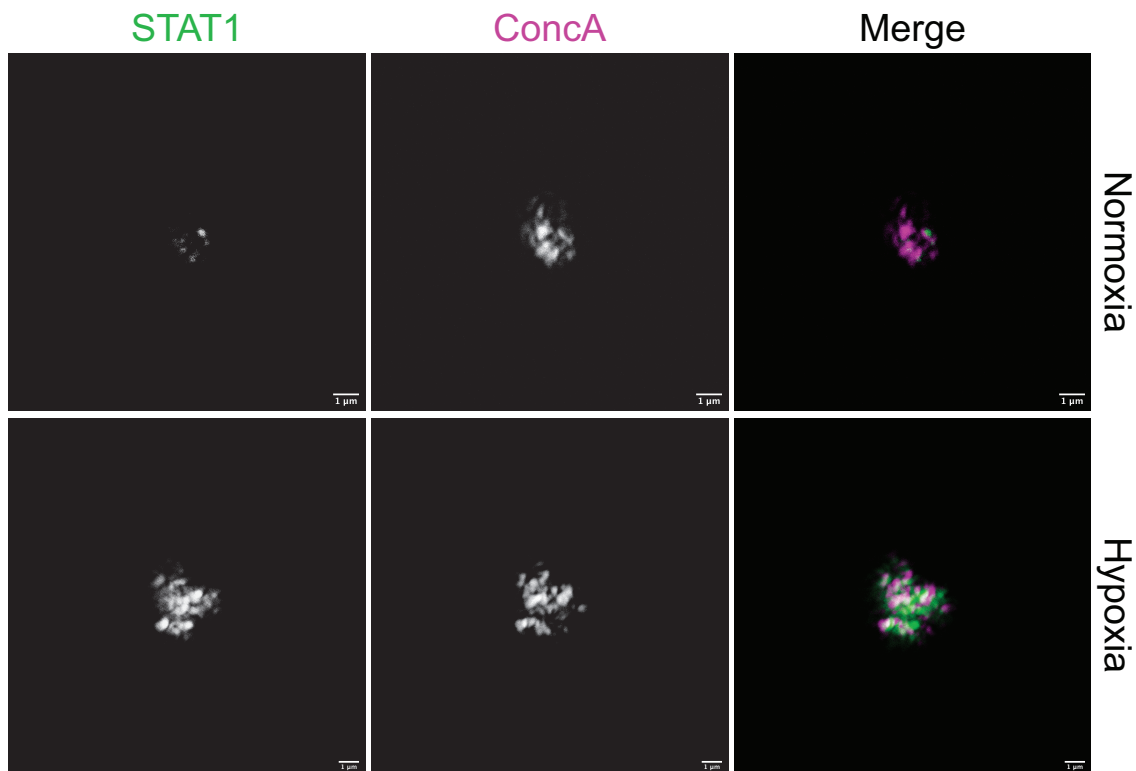


Fig. 37. Characterization of HEVs and NEVs by confocal microscopy. NEVs and HEVs were immunostained for STAT1 (green). EVs' membranes were stained with Concanavalin A (ConcA) 633 Alexa Fluor Conjugate (magenta). Objective lens 63x. Scale bar: 1 μm. Images are representative of three different experiments.

Future Perspectives

Further experiments will be performed using an *in vitro* model of neurotoxicity as previously described (271). Viability and modification in metabolic activity of human neuroblast-like SH-SY5Y cells will be evaluated upon administration of the HNEVs and NEVs. Moreover, EVs uptake by SH-SY5Y cells will be assessed by confocal microscopy.

Hopefully, the data obtained from these experiments will shed light on the role of STAT1 in microglia-neuron communication, especially in the context of neuroinflammation.

Appendix II

During my 1st year as PhD student, I was involved in different projects in the Laboratory of Prof. G. Gotte focused on the structural and enzymatic characterization of dimeric forms of “pancreatic-type” ribonucleases.

In particular, the first project aimed to unveil the dimerization mechanism of the “pancreatic-type” ribonuclease Angiogenin (ANG) and of three of its pathogenic variants (H13A, S28N and R121C). In this work, it was demonstrated that wild type ANG, as well as S28N and R121C variants, can form enzymatically active dimers through the three-dimensional domain swapping (3D-DS) mechanism. Moreover, molecular modelling was used to predict the structure of the N-termini domain-swapped dimer, starting from the crystal structure of the domain-swapped dimers of Ribonuclease A (RNase A).

In a second project, RNase A large aggregates, slowly formed from not highly concentrated RNase A oligomeric precursors, were investigated. The obtained results showed that these large aggregates did not present the typical linear structure of fibrils or annular structures but could be regarded as amorphous protein aggregates. Interestingly, the aggregates could be obtained only from oligomers containing at least two subunits undergoing N-termini swapping.

I also contributed to a third project whose purpose was to obtain and resolve the crystallographic structure of the dimeric form of Onconase (ONC), another “pancreatic-type” ribonuclease, and to compare its catalytic and antitumoral activity to the monomeric form. The resolved crystal structures demonstrated that these dimers are formed through swapping of the N-terminal helices. Moreover, comparable catalytic activity was detected for the dimer in comparison with the monomer, suggesting that the dimerization do not alter the global and local structural features of the active site residues. Finally, a reduction in the viability of two different melanoma cell lines was observed upon treatment with the ONC dimers, although to a lesser extent than the ONC monomer.

The results obtained from these projects have been published in three peer-reviewed papers.

- Fasoli S*, **Bettin I***, Montioli R, Fagagnini A, Peterle D, Laurents DV, Gotte G. Dimerization of Human Angiogenin and of Variants Involved in Neurodegenerative Diseases. *International Journal of Molecular Sciences*. 2021; 22(18):10068. <https://doi.org/10.3390/ijms221810068>
*Co-first authors
- Gotte G, Butturini E, **Bettin I**, Noro I, Mahmoud Helmy A, Fagagnini A, Cisterna B, Malatesta M. Slow Evolution toward “Super-Aggregation” of the Oligomers Formed through the Swapping of RNase A N-Termini: A Wish for Amyloidosis? *International Journal of Molecular Sciences*. 2022; 23(19):11192. <https://doi.org/10.3390/ijms231911192>
- Gotte G, Campagnari R, Loreto D, **Bettin I**, Calzetti F, Menegazzi M, Merlino A. The crystal structure of the domain-swapped dimer of onconase highlights some catalytic and antitumor activity features of the enzyme. *International Journal of Biological Macromolecules*. 2021; 191:560-571. <https://doi.org/10.1016/j.ijbiomac.2021.09.095>

Bibliography

1. Wolf P. The Nature and Significance of Platelet Products in Human Plasma. *British Journal of Haematology*. 1967;13(3):269–88.
2. Dalton AJ. Microvesicles and vesicles of multivesicular bodies versus ‘virus-like’ particles. *J Natl Cancer Inst*. 1975 May 1;54(5):1137–48.
3. Couch Y, Buzàs EI, Di Vizio D, Gho YS, Harrison P, Hill AF, et al. A brief history of nearly EV-erything – The rise and rise of extracellular vesicles. *Journal of Extracellular Vesicles*. 2021;10(14):e12144.
4. Raposo G, Nijman HW, Stoorvogel W, Liejendekker R, Harding CV, Melief CJ, et al. B lymphocytes secrete antigen-presenting vesicles. *The Journal of experimental medicine*. 1996 Mar;183(3):1161–72.
5. Bazzan E, Tinè M, Casara A, Biondini D, Semenzato U, Cocconcelli E, et al. Critical Review of the Evolution of Extracellular Vesicles’ Knowledge: From 1946 to Today. *International Journal of Molecular Sciences*. 2021 Jan;22(12):6417.
6. Buzas EI. The roles of extracellular vesicles in the immune system. *Nat Rev Immunol*. 2022 Aug 4;1–15.
7. El Andaloussi S, Mäger I, Breakefield XO, Wood MJA. Extracellular vesicles: Biology and emerging therapeutic opportunities. *Nature Reviews Drug Discovery*. 2013;12(5):347–57.
8. Jeppesen DK, Fenix AM, Franklin JL, Higginbotham JN, Zhang Q, Zimmerman LJ, et al. Reassessment of Exosome Composition. *Cell*. 2019;177(2):428–445.e18.
9. Dixon AC, Dawson TR, Di Vizio D, Weaver AM. Context-specific regulation of extracellular vesicle biogenesis and cargo selection. *Nat Rev Mol Cell Biol*. 2023 Feb 10;1–23.
10. Ma L, Li Y, Peng J, Wu D, Zhao X, Cui Y, et al. Discovery of the migrasome, an organelle mediating release of cytoplasmic contents during cell migration. *Cell Res*. 2015 Jan;25(1):24–38.
11. Gan X, Gould SJ. Identification of an inhibitory budding signal that blocks the release of HIV particles and exosome/microvesicle proteins. *MBoC*. 2011 Mar 15;22(6):817–30.
12. Nabhan JF, Hu R, Oh RS, Cohen SN, Lu Q. Formation and release of arrestin domain-containing protein 1-mediated microvesicles (ARMMs) at plasma membrane by recruitment of TSG101 protein. *Proceedings of the National Academy of Sciences*. 2012 Mar 13;109(11):4146–51.
13. Di Vizio D, Morello M, Dudley AC, Schow PW, Adam RM, Morley S, et al. Large Oncosomes in Human Prostate Cancer Tissues and in the Circulation of Mice with Metastatic Disease. *The American Journal of Pathology*. 2012 Nov 1;181(5):1573–84.
14. Minciacchi VR, Freeman MR, Di Vizio D. Extracellular Vesicles in Cancer: Exosomes, Microvesicles and the Emerging Role of Large Oncosomes. *Seminars in Cell & Developmental Biology*. 2015 Apr 1;40:41–51.
15. Maas SLN, Breakefield XO, Weaver AM. Extracellular Vesicles: Unique Intercellular Delivery Vehicles. *Trends in Cell Biology*. 2017 Mar 1;27(3):172–88.
16. Witwer KW, Soekmadji C, Hill AF, Wauben MH, Buzàs EI, Di Vizio D, et al. Updating the MISEV minimal requirements for extracellular vesicle studies: building bridges to reproducibility. *Journal of Extracellular Vesicles*. 2017;6(1).

17. Mathieu M, Martin-Jaular L, Lavieu G, Théry C. Specificities of secretion and uptake of exosomes and other extracellular vesicles for cell-to-cell communication. *Nature Cell Biology*. 2019;21(1):9–17.
18. Kowal J, Arras G, Colombo M, Jouve M, Morath JP, Primdal-Bengtson B, et al. Proteomic comparison defines novel markers to characterize heterogeneous populations of extracellular vesicle subtypes. *Proceedings of the National Academy of Sciences*. 2016 Feb 23;113(8):E968–77.
19. Raposo G, Stoorvogel W. Extracellular vesicles: Exosomes, microvesicles, and friends. *Journal of Cell Biology*. 2013;200(4):373–83.
20. Klumperman J, Raposo G. The Complex Ultrastructure of the Endolysosomal System. *Cold Spring Harb Perspect Biol*. 2014 Jan 10;6(10):a016857.
21. van Niel G, D’Angelo G, Raposo G. Shedding light on the cell biology of extracellular vesicles. *Nat Rev Mol Cell Biol*. 2018 Apr;19(4):213–28.
22. Teng F, Fussenegger M. Shedding Light on Extracellular Vesicle Biogenesis and Bioengineering. *Advanced Science*. 2021;8(1):2003505.
23. Granger E, McNee G, Allan V, Woodman P. The role of the cytoskeleton and molecular motors in endosomal dynamics. *Seminars in Cell & Developmental Biology*. 2014 Jul 1;31:20–9.
24. Sinha S, Hoshino D, Hong NH, Kirkbride KC, Grega-Larson NE, Seiki M, et al. Cortactin promotes exosome secretion by controlling branched actin dynamics. *Journal of Cell Biology*. 2016 Jul 11;214(2):197–213.
25. Jahn R, Scheller RH. SNAREs — engines for membrane fusion. *Nat Rev Mol Cell Biol*. 2006 Sep;7(9):631–43.
26. Hurley JH. ESCRT complexes and the biogenesis of multivesicular bodies. *Current Opinion in Cell Biology*. 2008 Feb 1;20(1):4–11.
27. Hurley JH, Hanson PI. Membrane budding and scission by the ESCRT machinery: it’s all in the neck. *Nat Rev Mol Cell Biol*. 2010 Aug;11(8):556–66.
28. Yang JM, Gould SJ. The cis-acting signals that target proteins to exosomes and microvesicles. *Biochemical Society Transactions*. 2013 Jan 29;41(1):277–82.
29. Tricarico C, Clancy J, D’Souza-Schorey C. Biology and biogenesis of shed microvesicles. *Small GTPases*. 2017 Oct 2;8(4):220–32.
30. Hugel B, Martínez MC, Kunzelmann C, Freyssinet JM. Membrane Microparticles: Two Sides of the Coin. *Physiology*. 2005 Feb;20(1):22–7.
31. Mulcahy LA, Pink RC, Carter DRF. Routes and mechanisms of extracellular vesicle uptake. *Journal of Extracellular Vesicles*. 2014 Jan 1;3(1):24641.
32. Théry C, Boussac M, Véron P, Ricciardi-Castagnoli P, Raposo G, Garin J, et al. Proteomic Analysis of Dendritic Cell-Derived Exosomes: A Secreted Subcellular Compartment Distinct from Apoptotic Vesicles1. *The Journal of Immunology*. 2001 Jun 15;166(12):7309–18.
33. Buschow SI, Liefhebber JMP, Wubbolts R, Stoorvogel W. Exosomes contain ubiquitinated proteins. *Blood Cells, Molecules, and Diseases*. 2005 Nov 1;35(3):398–403.

34. Valadi H, Ekström K, Bossios A, Sjöstrand M, Lee JJ, Lötvall JO. Exosome-mediated transfer of mRNAs and microRNAs is a novel mechanism of genetic exchange between cells. *Nat Cell Biol.* 2007 Jun;9(6):654–9.
35. Gurung S, Perocheau D, Touramanidou L, Baruteau J. The exosome journey: from biogenesis to uptake and intracellular signalling. *Cell Communication and Signaling.* 2021 Apr 23;19(1):47.
36. Morelli AE, Larregina AT, Shufesky WJ, Sullivan MLG, Stolz DB, Papworth GD, et al. Endocytosis, intracellular sorting, and processing of exosomes by dendritic cells. *Blood.* 2004 Nov 15;104(10):3257–66.
37. Sung BH, Ketova T, Hoshino D, Zijlstra A, Weaver AM. Directional cell movement through tissues is controlled by exosome secretion. *Nat Commun.* 2015 May 13;6(1):7164.
38. Miyanishi M, Tada K, Koike M, Uchiyama Y, Kitamura T, Nagata S. Identification of Tim4 as a phosphatidylserine receptor. *Nature.* 2007 Nov 15;450(7168):435–9.
39. Abels ER, Breakefield XO. Introduction to Extracellular Vesicles: Biogenesis, RNA Cargo Selection, Content, Release, and Uptake. *Cell Mol Neurobiol.* 2016 Apr;36(3):301–12.
40. Montecalvo A, Larregina AT, Shufesky WJ, Beer Stolz D, Sullivan MLG, Karlsson JM, et al. Mechanism of transfer of functional microRNAs between mouse dendritic cells via exosomes. *Blood.* 2012 Jan 19;119(3):756–66.
41. Ginini L, Billan S, Fridman E, Gil Z. Insight into Extracellular Vesicle-Cell Communication: From Cell Recognition to Intracellular Fate. *Cells.* 2022 Jan;11(9):1375.
42. Roberts-Dalton HD, Cocks A, Falcon-Perez JM, Sayers EJ, Webber JP, Watson P, et al. Fluorescence labelling of extracellular vesicles using a novel thiol-based strategy for quantitative analysis of cellular delivery and intracellular traffic. *Nanoscale.* 2017 Sep 21;9(36):13693–706.
43. Tian T, Zhu YL, Hu FH, Wang YY, Huang NP, Xiao ZD. Dynamics of exosome internalization and trafficking. *Journal of Cellular Physiology.* 2013;228(7):1487–95.
44. van Niel G, Carter DRF, Clayton A, Lambert DW, Raposo G, Vader P. Challenges and directions in studying cell–cell communication by extracellular vesicles. *Nat Rev Mol Cell Biol.* 2022 May;23(5):369–82.
45. Kalluri R, LeBleu VS. The biology, function, and biomedical applications of exosomes. *Science.* 2020;367(6478).
46. Herrmann IK, Wood MJA, Fuhrmann G. Extracellular vesicles as a next-generation drug delivery platform. *Nature Nanotechnology.* 2021;16(7):748–59.
47. Théry C, Amigorena S, Raposo G, Clayton A. Isolation and Characterization of Exosomes from Cell Culture Supernatants and Biological Fluids. *Current Protocols in Cell Biology.* 2006;30(1):3.22.1-3.22.29.
48. Théry C, Witwer KW, Aikawa E, Alcaraz MJ, Anderson JD, Andriantsitohaina R, et al. Minimal information for studies of extracellular vesicles 2018 (MISEV2018): a position statement of the International Society for Extracellular Vesicles and update of the MISEV2014 guidelines. *Journal of Extracellular Vesicles.* 2018;7(1).
49. Urzi O, Bagge RO, Crescitelli R. The dark side of foetal bovine serum in extracellular vesicle studies. *Journal of Extracellular Vesicles.* 2022;11(10).

50. Lehrich BM, Liang Y, Fiandaca MS. Foetal bovine serum influence on in vitro extracellular vesicle analyses. *Journal of Extracellular Vesicles*. 2021 Jan 1;10(3).
51. Lee YXF, Johansson H, Wood MJA, El Andaloussi S. Considerations and Implications in the Purification of Extracellular Vesicles – A Cautionary Tale. *Frontiers in Neuroscience*. 2019;13.
52. Lobb RJ, Becker M, Wen SW, Wong CSF, Wiegman AP, Leimgruber A, et al. Optimized exosome isolation protocol for cell culture supernatant and human plasma. *Journal of Extracellular Vesicles*. 2015;4(1).
53. Royo F, Théry C, Falcón-Pérez JM, Nieuwland R, Witwer KW. Nanoparticle Tracking Analysis for the Multiparameter Characterization and Counting of Nanoparticle Suspension. *Cells*. 2020;9(9).
54. Cvjetkovic A, Lötvall J, Lässer C. The influence of rotor type and centrifugation time on the yield and purity of extracellular vesicles. *Journal of Extracellular Vesicles*. 2014;3(1).
55. El Harane N, Kervadec A, Bellamy V, Pidial L, Neametalla HJ, Perier MC, et al. Acellular therapeutic approach for heart failure: in vitro production of extracellular vesicles from human cardiovascular progenitors. *European Heart Journal*. 2018 May 21;39(20):1835–47.
56. Livshits MA, Khomyakova E, Evtushenko EG, Laz VN. Isolation of exosomes by differential centrifugation: Theoretical analysis of a commonly used protocol. *Nature Publishing Group*. 2015;(October):1–14.
57. Pavani KC, Lin X, Hamacher J, Broeck W Van Den, Couck L, Peelman L, et al. The Separation and Characterization of Extracellular Vesicles from Medium Conditioned by Bovine Embryos. *International journal of molecular sciences*. 2020 Apr;21(8).
58. Arab T, Raffo-Romero A, Van Camp C, Lemaire Q, Le Marrec-Croq F, Drago F, et al. Proteomic characterisation of leech microglia extracellular vesicles (EVs): comparison between differential ultracentrifugation and Optiprep™ density gradient isolation. *Journal of Extracellular Vesicles*. 2019;8(1).
59. Brakke MK. Density Gradient Centrifugation: A New Separation Technique¹. *Journal of the American Chemical Society*. 1951 Apr 1;73(4):1847–8.
60. Yang D, Zhang W, Zhang H, Zhang F, Chen L, Ma L, et al. Progress, opportunity, and perspective on exosome isolation - Efforts for efficient exosome-based theranostics. *Theranostics*. 2020;10(8):3684–707.
61. Palma J, Yaddanapudi SC, Pigati L, Havens MA, Jeong S, Weiner GA, et al. MicroRNAs are exported from malignant cells in customized particles. *Nucleic Acids Research*. 2012 Oct 1;40(18):9125–38.
62. Yang D, Zhang W, Zhang H, Zhang F, Chen L, Ma L, et al. Progress, opportunity, and perspective on exosome isolation - efforts for efficient exosome-based theranostics. *Theranostics*. 2020 Feb 19;10(8):3684–707.
63. Taylor DD, Shah S. Methods of isolating extracellular vesicles impact down-stream analyses of their cargoes. *Methods*. 2015;87:3–10.
64. Monguió-Tortajada M, Gálvez-Montón C, Bayes-Genis A, Roura S, Borràs FE. Extracellular vesicle isolation methods: rising impact of size-exclusion chromatography. *Cellular and Molecular Life Sciences*. 2019;76(12):2369–82.
65. Liangsupree T, Multia E, Riekkola ML. Modern isolation and separation techniques for extracellular vesicles. *Journal of Chromatography A*. 2021;1636:461773.

66. Visan KS, Lobb RJ, Ham S, Lima LG, Palma C, Edna CPZ, et al. Comparative analysis of tangential flow filtration and ultracentrifugation, both combined with subsequent size exclusion chromatography, for the isolation of small extracellular vesicles. *Journal of Extracellular Vesicles*. 2022;11(9).
67. Heinemann ML, Ilmer M, Silva LP, Hawke DH, Recio A, Vorontsova MA, et al. Benchtop isolation and characterization of functional exosomes by sequential filtration. *Journal of Chromatography A*. 2014;1371:125–35.
68. Atha DH, Ingham KC. Mechanism of precipitation of proteins by polyethylene glycols. Analysis in terms of excluded volume. *Journal of Biological Chemistry*. 1981;256(23):12108–17.
69. Stam J, Bartel S, Bischoff R, Wolters JC. Isolation of extracellular vesicles with combined enrichment methods. *Journal of Chromatography B: Analytical Technologies in the Biomedical and Life Sciences*. 2021;1169(February):122604.
70. Brett SI, Lucien F, Guo C, Williams KC, Kim Y, Durfee PN, et al. Immunoaffinity based methods are superior to kits for purification of prostate derived extracellular vesicles from plasma samples. *The Prostate*. 2017 May 1;77(13):1335–43.
71. Brennan K, Martin K, FitzGerald SP, O’Sullivan J, Wu Y, Blanco A, et al. A comparison of methods for the isolation and separation of extracellular vesicles from protein and lipid particles in human serum. *Scientific Reports*. 2020;10(1):1–13.
72. Linares R, Tan S, Gounou C, Arraud N, Brisson AR. High-speed centrifugation induces aggregation of extracellular vesicles. *Journal of Extracellular Vesicles*. 2015;4(1):1–7.
73. Konoshenko MY, Lekchnov EA, Vlassov AV, Laktionov PP. Isolation of Extracellular Vesicles: General Methodologies and Latest Trends. *BioMed Research International*. 2018 Jan 30;2018:e8545347.
74. Li X, Donowitz M. Fractionation of Subcellular Membrane Vesicles of Epithelial and Non-epithelial Cells by OptiPrep™ Density Gradient Ultracentrifugation. Ivanov AI, editor. *Exocytosis and Endocytosis*. New York, NY: Springer New York; 2014. 85–99 p.
75. Benedikter BJ, Bouwman FG, Vajen T, Heinzmann ACA, Grauls G, Mariman EC, et al. Ultrafiltration combined with size exclusion chromatography efficiently isolates extracellular vesicles from cell culture media for compositional and functional studies. *Scientific Reports*. 2017;7(1):1–13.
76. Busatto S, Vilanilam G, Ticer T, Lin WL, Dickson DW, Shapiro S, et al. Tangential flow filtration for highly efficient concentration of extracellular vesicles from large volumes of fluid. *Cells*. 2018;7(12).
77. Arab T, Mallick ER, Huang Y, Dong L, Liao Z, Zhao Z, et al. Characterization of extracellular vesicles and synthetic nanoparticles with four orthogonal single-particle analysis platforms. *Journal of Extracellular Vesicles*. 2021 Apr 1;10(6).
78. Hassan PA, Rana S, Verma G. Making Sense of Brownian Motion: Colloid Characterization by Dynamic Light Scattering. *Langmuir*. 2015 Jan 13;31(1):3–12.
79. Stetefeld J, McKenna SA, Patel TR. Dynamic light scattering: a practical guide and applications in biomedical sciences. *Biophys Rev*. 2016 Dec 1;8(4):409–27.
80. Mourdikoudis S, Pallares RM, Thanh NTK. Characterization techniques for nanoparticles: comparison and complementarity upon studying nanoparticle properties. *Nanoscale*. 2018 Jul 13;10(27):12871–934.

81. Gardiner C, Ferreira YJ, Dragovic RA, Redman CWG, Sargent IL. Extracellular vesicle sizing and enumeration by nanoparticle tracking analysis. *Journal of Extracellular Vesicles*. 2013;2(1).
82. Gross J, Sayle S, Karow AR, Bakowsky U, Garidel P. Nanoparticle tracking analysis of particle size and concentration detection in suspensions of polymer and protein samples: Influence of experimental and data evaluation parameters. *European Journal of Pharmaceutics and Biopharmaceutics*. 2016 Jul 1;104:30–41.
83. Wright M. Nanoparticle Tracking Analysis for the Multiparameter Characterization and Counting of Nanoparticle Suspensions. In: Soloviev M, editor. *Nanoparticles in Biology and Medicine*. Totowa, NJ: Humana Press; 2012. p. 511–24.
84. Midekessa G, Godakumara K, Dissanayake K, Hasan MM, Reshi QUA, Rincken T, et al. Characterization of Extracellular Vesicles Labelled with a Lipophilic Dye Using Fluorescence Nanoparticle Tracking Analysis. *Membranes*. 2021 Oct;11(10):779.
85. Desgeorges A, Hollerweger J, Lassacher T, Rohde E, Helmbrecht C, Gimona M. Differential fluorescence nanoparticle tracking analysis for enumeration of the extracellular vesicle content in mixed particulate solutions. *Methods*. 2020 May 1;177:67–73.
86. Corso G, Heusermann W, Trojer D, Görgens A, Steib E, Voshol J, et al. Systematic characterization of extracellular vesicles sorting domains and quantification at the single molecule–single vesicle level by fluorescence correlation spectroscopy and single particle imaging. *Journal of Extracellular Vesicles*. 2019;8(1).
87. Woo CH, Kim HK, Jung GY, Jung YJ, Lee KS, Yun YE, et al. Small extracellular vesicles from human adipose-derived stem cells attenuate cartilage degeneration. *Journal of Extracellular Vesicles*. 2020;9(1):1735249.
88. Shao H, Chung J, Balaj L, Charest A, Bigner DD, Carter BS, et al. Protein typing of circulating microvesicles allows real-time monitoring of glioblastoma therapy. *Nat Med*. 2012 Dec;18(12):1835–40.
89. Imanbekova M, Suarasan S, Lu Y, Jurchuk S, Wachsmann-Hogiu S. Recent advances in optical label-free characterization of extracellular vesicles. *Nanophotonics*. 2022 Jun 1;11(12):2827–63.
90. Pascucci L, Scattini G. Imaging extracellular vesicles by transmission electron microscopy: Coping with technical hurdles and morphological interpretation. *Biochimica et Biophysica Acta (BBA) - General Subjects*. 2021 Apr 1;1865(4):129648.
91. Malenica M, Vukomanović M, Kurtjak M, Masciotti V, dal Zilio S, Greco S, et al. Perspectives of Microscopy Methods for Morphology Characterisation of Extracellular Vesicles from Human Biofluids. *Biomedicines*. 2021 Jun;9(6):603.
92. Cizmar P, Yuana Y. Detection and Characterization of Extracellular Vesicles by Transmission and Cryo-Transmission Electron Microscopy. In: Kuo WP, Jia S, editors. *Extracellular Vesicles*. New York, NY: Springer New York; 2017. p. 221–32. (Methods in Molecular Biology; vol. 1660).
93. van der Pol E, de Rond L, Coumans FAW, Gool EL, Böing AN, Sturk A, et al. Absolute sizing and label-free identification of extracellular vesicles by flow cytometry. *Nanomedicine: Nanotechnology, Biology and Medicine*. 2018 Apr 1;14(3):801–10.
94. Parisse P, Rago I, Ulloa Severino L, Perissinotto F, Ambrosetti E, Paoletti P, et al. Atomic force microscopy analysis of extracellular vesicles. *Eur Biophys J*. 2017 Dec 1;46(8):813–20.

95. Tian T, Wang Y, Wang H, Zhu Z, Xiao Z. Visualizing of the cellular uptake and intracellular trafficking of exosomes by live-cell microscopy. *Journal of Cellular Biochemistry*. 2010;111(2):488–96.
96. Vogel R, Coumans FAW, Maltesen RG, Böing AN, Bonnington KE, Broekman ML, et al. A standardized method to determine the concentration of extracellular vesicles using tunable resistive pulse sensing. *Journal of Extracellular Vesicles*. 2016 Jan 1;5(1):31242.
97. Gardiner C, Vizio DD, Sahoo S, Théry C, Witwer KW, Wauben M, et al. Techniques used for the isolation and characterization of extracellular vesicles: results of a worldwide survey. *Journal of Extracellular Vesicles*. 2016 Jan 1;5(1):32945.
98. Coumans FAW, Brisson AR, Buzas EI, Dignat-George F, Drees EEE, El-Andaloussi S, et al. Methodological Guidelines to Study Extracellular Vesicles. *Circulation Research*. 2017 May 12;120(10):1632–48.
99. Vergauwen G, Dhondt B, Van Deun J, De Smedt E, Berox G, Timmerman E, et al. Confounding factors of ultrafiltration and protein analysis in extracellular vesicle research. *Sci Rep*. 2017 Jun 2;7(1):2704.
100. Subedi P, Schneider M, Philipp J, Azimzadeh O, Metzger F, Moertl S, et al. Comparison of methods to isolate proteins from extracellular vesicles for mass spectrometry-based proteomic analyses. *Analytical Biochemistry*. 2019 Nov;584:113390.
101. Coumans FAW, Brisson AR, Buzas EI, Dignat-George F, Drees EEE, El-Andaloussi S, et al. Methodological guidelines to study extracellular vesicles. *Circulation Research*. 2017;120(10):1632–48.
102. Suárez H, Gámez-Valero A, Reyes R, López-Martín S, Rodríguez MJ, Carrascosa JL, et al. A bead-assisted flow cytometry method for the semi-quantitative analysis of Extracellular Vesicles. *Sci Rep*. 2017 Sep 12;7(1):11271.
103. Stoner SA, Duggan E, Condello D, Guerrero A, Turk JR, Narayanan PK, et al. High sensitivity flow cytometry of membrane vesicles. *Cytometry Part A*. 2016;89(2):196–206.
104. Görgens A, Bremer M, Ferrer-Tur R, Murke F, Tertel T, Horn PA, et al. Optimisation of imaging flow cytometry for the analysis of single extracellular vesicles by using fluorescence-tagged vesicles as biological reference material. *Journal of Extracellular Vesicles*. 2019;8(1):1587567.
105. Jalaludin I, Lubman DM, Kim J. A guide to mass spectrometric analysis of extracellular vesicle proteins for biomarker discovery. *Mass Spectrom Rev*. 2023 Mar;42(2):844–72.
106. Hill AF, Pegtel DM, Lambert U, Leonardi T, O’Driscoll L, Pluchino S, et al. ISEV position paper: extracellular vesicle RNA analysis and bioinformatics. *Journal of Extracellular Vesicles*. 2013;2(1):22859.
107. Gandham S, Su X, Wood J, Nocera AL, Alli SC, Milane L, et al. Technologies and Standardization in Research on Extracellular Vesicles. *Trends in Biotechnology*. 2020;38(10):1066–98.
108. Skotland T, Sagini K, Sandvig K, Llorente A. An emerging focus on lipids in extracellular vesicles. *Advanced Drug Delivery Reviews*. 2020 Jan 1;159:308–21.
109. Haraszti RA, Didiot MC, Sapp E, Leszyk J, Shaffer SA, Rockwell HE, et al. High-resolution proteomic and lipidomic analysis of exosomes and microvesicles from different cell sources. *Journal of Extracellular Vesicles*. 2016;5(1):32570.

110. Sun Y, Saito K, Saito Y. Lipidomic Analysis of Extracellular Vesicles Isolated from Human Plasma and Serum. *Methods Mol Biol.* 2022;2504:157–73.
111. Vader P, Mol EA, Pasterkamp G, Schiffelers RM. Extracellular vesicles for drug delivery. *Advanced Drug Delivery Reviews.* 2016;106:148–56.
112. Zipkin M. Big pharma buys into exosomes for drug delivery. *Nature Biotechnology.* 2020 Nov 1;38(11):1226–8.
113. Escudé Martínez de Castilla P, Tong L, Huang C, Sofias AM, Pastorin G, Chen X, et al. Extracellular vesicles as a drug delivery system: A systematic review of preclinical studies. *Advanced Drug Delivery Reviews.* 2021 Aug 1;175:113801.
114. Yáñez-Mó M, Siljander PRM, Andreu Z, Zavec AB, Borràs FE, Buzas EI, et al. Biological properties of extracellular vesicles and their physiological functions. *Journal of Extracellular Vesicles.* 2015;4(2015):1–60.
115. Beetler DJ, Di Florio DN, Bruno KA, Ikezu T, March KL, Cooper LT, et al. Extracellular vesicles as personalized medicine. *Molecular Aspects of Medicine.* 2023 Jun 1;91:101155.
116. Zhou E, Li Y, Wu F, Guo M, Xu J, Wang S, et al. Circulating extracellular vesicles are effective biomarkers for predicting response to cancer therapy. *EBioMedicine.* 2021 May 7;67:103365.
117. van der Meel R, Fens MHAM, Vader P, van Solinge WW, Eniola-Adefeso O, Schiffelers RM. Extracellular vesicles as drug delivery systems: Lessons from the liposome field. *Journal of Controlled Release.* 2014 Dec 10;195:72–85.
118. van der Koog L, Gandek TB, Nagelkerke A. Liposomes and Extracellular Vesicles as Drug Delivery Systems: A Comparison of Composition, Pharmacokinetics, and Functionalization. *Advanced Healthcare Materials.* 2022;11(5):2100639.
119. Elsharkasy OM, Nordin JZ, Hagey DW, de Jong OG, Schiffelers RM, Andaloussi SE, et al. Extracellular vesicles as drug delivery systems: Why and how? *Advanced Drug Delivery Reviews.* 2020;159:332–43.
120. Witwer KW, Wolfram J. Extracellular vesicles versus synthetic nanoparticles for drug delivery. *Nat Rev Mater.* 2021 Feb;6(2):103–6.
121. Colombo M, Raposo G, Théry C. Biogenesis, secretion, and intercellular interactions of exosomes and other extracellular vesicles. *Annual review of cell and developmental biology.* 2014;30:255–89.
122. Ratajczak J, Miekus K, Kucia M, Zhang J, Reca R, Dvorak P, et al. Embryonic stem cell-derived microvesicles reprogram hematopoietic progenitors: evidence for horizontal transfer of mRNA and protein delivery. *Leukemia.* 2006 May;20(5):847–56.
123. Wiklander OPB, Brennan MÁ, Lötvall J, Breakefield XO, EL Andaloussi S. Advances in therapeutic applications of extracellular vesicles. *Science Translational Medicine.* 2019 May 15;11(492):eaav8521.
124. Noren Hooten N, Yáñez-Mó M, DeRita R, Russell A, Quesenberry P, Ramratnam B, et al. Hitting the Bullseye: Are extracellular vesicles on target? *Journal of Extracellular Vesicles.* 2020;10(1):e12032.
125. Wortzel I, Dror S, Kenific CM, Lyden D. Exosome-Mediated Metastasis: Communication from a Distance. *Developmental Cell.* 2019 May 6;49(3):347–60.

126. Zhu X, Badawi M, Pomeroy S, Sutaria DS, Xie Z, Baek A, et al. Comprehensive toxicity and immunogenicity studies reveal minimal effects in mice following sustained dosing of extracellular vesicles derived from HEK293T cells. *Journal of Extracellular Vesicles*. 2017;6(1).
127. Saleh AF, Lázaro-Ibáñez E, Forsgard MAM, Shatnyeva O, Osteikoetxea X, Karlsson F, et al. Extracellular vesicles induce minimal hepatotoxicity and immunogenicity. *Nanoscale*. 2019;11(14):6990–7001.
128. Ikeda G, Santoso MR, Tada Y, Li AM, Vaskova E, Jung JH, et al. Mitochondria-Rich Extracellular Vesicles From Autologous Stem Cell-Derived Cardiomyocytes Restore Energetics of Ischemic Myocardium. *Journal of the American College of Cardiology*. 2021 Mar 2;77(8):1073–88.
129. Villa A, Garofalo M, Crescenti D, Rizzi N, Brunialti E, Vingiani A, et al. Transplantation of autologous extracellular vesicles for cancer-specific targeting. *Theranostics*. 2021;11(5):2034–47.
130. Li YJ, Wu JY, Hu XB, Wang JM, Xiang DX. Autologous cancer cell-derived extracellular vesicles as drug-delivery systems: a systematic review of preclinical and clinical findings and translational implications. *Nanomedicine*. 2019 Feb;14(4):493–509.
131. Kamerkar S, LeBleu VS, Sugimoto H, Yang S, Ruivo CF, Melo SA, et al. Exosomes facilitate therapeutic targeting of oncogenic KRAS in pancreatic cancer. *Nature*. 2017 Jun;546(7659):498–503.
132. Elliott RO, He M. Unlocking the Power of Exosomes for Crossing Biological Barriers in Drug Delivery. *Pharmaceutics*. 2021 Jan 19;13(1):122.
133. Ramos-Zaldívar HM, Polakovicova I, Salas-Huenuleo E, Corvalán AH, Kogan MJ, Yefi CP, et al. Extracellular vesicles through the blood–brain barrier: a review. *Fluids and Barriers of the CNS*. 2022 Jul 25;19(1):60.
134. Armstrong JPK, Stevens MM. Strategic design of extracellular vesicle drug delivery systems. *Advanced Drug Delivery Reviews*. 2018 May 1;130:12–6.
135. Rankin-Turner S, Vader P, O’Driscoll L, Giebel B, Heaney LM, Davies OG. A call for the standardised reporting of factors affecting the exogenous loading of extracellular vesicles with therapeutic cargos. *Advanced Drug Delivery Reviews*. 2021;173:479–91.
136. Seras-franzoso J, González P, Díaz-riascos ZV, Corchero JL, Riera R, García-aranda N, et al. Extracellular vesicles from recombinant cell factories improve the activity and efficacy of enzymes defective in lysosomal storage. 2021;(December 2020).
137. Sterzenbach U, Putz U, Low LH, Silke J, Tan SS, Howitt J. Engineered Exosomes as Vehicles for Biologically Active Proteins. *Molecular Therapy*. 2017;25(6):1269–78.
138. Wang Q, Lu Q. Plasma membrane-derived extracellular microvesicles mediate non-canonical intercellular NOTCH signaling. *Nat Commun*. 2017 Sep 27;8(1):709.
139. Wang Q, Yu J, Kadungure T, Beyene J, Zhang H, Lu Q. ARMMs as a versatile platform for intracellular delivery of macromolecules. *Nat Commun*. 2018 Mar 6;9(1):960.
140. Yim N, Ryu SW, Choi K, Lee KR, Lee S, Choi H, et al. Exosome engineering for efficient intracellular delivery of soluble proteins using optically reversible protein–protein interaction module. *Nat Commun*. 2016 Jul 22;7(1):12277.
141. Sutaria DS, Jiang J, Elgamal OA, Pomeroy SM, Badawi M, Zhu X, et al. Low active loading of cargo into engineered extracellular vesicles results in inefficient miRNA mimic delivery. *Journal of Extracellular Vesicles*. 2017 Dec 1;6(1):1333882.

142. Hung ME, Leonard JN. A platform for actively loading cargo RNA to elucidate limiting steps in EV-mediated delivery. *Journal of Extracellular Vesicles*. 2016 Jan 1;5(1):31027.
143. Ilahibaks NF, Ardisasmita AI, Xie S, Gunnarsson A, Brealey J, Vader P, et al. TOP-EVs: Technology of Protein delivery through Extracellular Vesicles is a versatile platform for intracellular protein delivery. *Journal of Controlled Release*. 2023 Mar 1;355:579–92.
144. Antimisiaris SG, Mourtas S, Marazioti A. Exosomes and exosome-inspired vesicles for targeted drug delivery. *Pharmaceutics*. 2018;10(4).
145. Sun D, Zhuang X, Xiang X, Liu Y, Zhang S, Liu C, et al. A Novel Nanoparticle Drug Delivery System: The Anti-inflammatory Activity of Curcumin Is Enhanced When Encapsulated in Exosomes. *Molecular Therapy*. 2010 Sep 1;18(9):1606–14.
146. Fuhrmann G, Herrmann IK, Stevens MM. Cell-derived vesicles for drug therapy and diagnostics: Opportunities and challenges. *Nano Today*. 2015;10(3):397–409.
147. De Jong OG, Kooijmans SAA, Murphy DE, Jiang L, Evers MJW, Sluijter JPG, et al. Drug Delivery with Extracellular Vesicles: From Imagination to Innovation. *Accounts of Chemical Research*. 2019;52(7):1761–70.
148. Walker S, Busatto S, Pham A, Tian M, Suh A, Carson K, et al. Extracellular vesicle-based drug delivery systems for cancer treatment. *Theranostics*. 2019;9(26):8001–17.
149. Heiser WC. Optimizing Electroporation Conditions for the Transformation of Mammalian Cells. In: *Transcription Factor Protocols* [Internet]. New Jersey: Humana Press; 1999 [cited 2023 Feb 17]. p. 117–34. Available from: <http://link.springer.com/10.1385/1-59259-686-X:117>
150. Kim MS, Haney MJ, Zhao Y, Mahajan V, Deygen I, Klyachko NL, et al. Development of exosome-encapsulated paclitaxel to overcome MDR in cancer cells. *Nanomedicine: Nanotechnology, Biology and Medicine*. 2016 Apr 1;12(3):655–64.
151. Bosch S, de Beaupaire L, Allard M, Mosser M, Heichette C, Chrétien D, et al. Trehalose prevents aggregation of exosomes and cryodamage. *Sci Rep*. 2016 Nov 8;6(1):36162.
152. Jamur MC, Oliver C. Permeabilization of Cell Membranes. In: Oliver C, Jamur MC, editors. *Immunocytochemical Methods and Protocols*. Totowa, NJ: Humana Press; 2010. p. 63–6. (Methods in Molecular Biology).
153. Haney MJ, Klyachko NL, Zhao Y, Gupta R, Plotnikova EG, He Z, et al. Exosomes as drug delivery vehicles for Parkinson's disease therapy. *Journal of Controlled Release*. 2015 Jun;207:18–30.
154. Frank J, Richter M, de Rossi C, Lehr CM, Fuhrmann K, Fuhrmann G. Extracellular vesicles protect glucuronidase model enzymes during freeze-drying. *Scientific Reports*. 2018;8(1):1–8.
155. Richter M, Fuhrmann K, Fuhrmann G. Evaluation of the storage stability of extracellular vesicles. *Journal of Visualized Experiments*. 2019;2019(147):1–9.
156. Goh WJ, Woon ECY, Czarny B, Pastorin G. Doxorubicin-loaded cell-derived nanovesicles: an alternative targeted approach for anti-tumor therapy. *International Journal of Nanomedicine*. 2017;2759–67.
157. Fuhrmann G, Serio A, Mazo M, Nair R, Stevens MM. Active loading into extracellular vesicles significantly improves the cellular uptake and photodynamic effect of porphyrins. *Journal of Controlled Release*. 2015;205:35–44.

158. Pisano S, Pierini I, Gu J, Gazze A, Francis LW, Gonzalez D, et al. Immune (Cell) Derived Exosome Mimetics (IDEM) as a Treatment for Ovarian Cancer. 2020;8(September):1–14.
159. Aqil F, Munagala R, Jeyabalan J, Agrawal AK, Kyakulaga AH, Wilcher SA, et al. Milk exosomes - Natural nanoparticles for siRNA delivery. *Cancer Letters*. 2019 May 1;449:186–95.
160. Zhang X, Liu L, Tang M, Li H, Guo X, Yang X. The effects of umbilical cord-derived macrophage exosomes loaded with cisplatin on the growth and drug resistance of ovarian cancer cells. *Drug Development and Industrial Pharmacy*. 2020 Jul 2;46(7):1150–62.
161. Yang X, Shi G, Guo J, Wang C, He Y. Exosome-encapsulated antibiotic against intracellular infections of methicillin-resistant *Staphylococcus aureus*. *IJN*. 2018 Nov 29;13:8095–104.
162. Nooshabadi VT, Khanmohammadi M, Shafei S, Banafshe HR, Malekshahi ZV, Ebrahimi-Barough S, et al. Impact of atorvastatin loaded exosome as an anti-glioblastoma carrier to induce apoptosis of U87 cancer cells in 3D culture model. *Biochemistry and Biophysics Reports*. 2020 Sep 1;23:100792.
163. Usman WM, Pham TC, Kwok YY, Vu LT, Ma V, Peng B, et al. Efficient RNA drug delivery using red blood cell extracellular vesicles. *Nat Commun*. 2018 Jun 15;9(1):2359.
164. Liang Y, Xu X, Li X, Xiong J, Li B, Duan L, et al. Chondrocyte-Targeted MicroRNA Delivery by Engineered Exosomes toward a Cell-Free Osteoarthritis Therapy. *ACS Appl Mater Interfaces*. 2020 Aug 19;12(33):36938–47.
165. Yang J, Luo S, Zhang J, Yu T, Fu Z, Zheng Y, et al. Exosome-mediated delivery of antisense oligonucleotides targeting α -synuclein ameliorates the pathology in a mouse model of Parkinson's disease. *Neurobiology of Disease*. 2021 Jan 1;148:105218.
166. Didiot MC, Hall LM, Coles AH, Haraszi RA, Godinho BM, Chase K, et al. Exosome-mediated Delivery of Hydrophobically Modified siRNA for Huntingtin mRNA Silencing. *Molecular Therapy*. 2016 Oct 1;24(10):1836–47.
167. Xu Q, Zhang Z, Zhao L, Qin Y, Cai H, Geng Z, et al. Tropism-facilitated delivery of CRISPR/Cas9 system with chimeric antigen receptor-extracellular vesicles against B-cell malignancies. *Journal of Controlled Release*. 2020 Oct 10;326:455–67.
168. Haney MJ, Klyachko NL, Harrison EB, Zhao Y, Kabanov AV, Batrakova EV. TPP1 Delivery to Lysosomes with Extracellular Vesicles and their Enhanced Brain Distribution in the Animal Model of Batten Disease. *Advanced Healthcare Materials*. 2019;8(11):1801271.
169. Busatto S, Iannotta D, Walker SA, Di Marzio L, Wolfram J. A Simple and Quick Method for Loading Proteins in Extracellular Vesicles. *Pharmaceuticals*. 2021 Apr;14(4):356.
170. Jiao Y, Tang Y, Li Y, Liu C, He J, Zhang LK, et al. Tumor cell-derived extracellular vesicles for breast cancer specific delivery of therapeutic P53. *Journal of Controlled Release*. 2022 Sep 1;349:606–16.
171. Richter M, Vader P, Fuhrmann G. Approaches to surface engineering of extracellular vesicles. *Advanced Drug Delivery Reviews*. 2021 Jun 1;173:416–26.
172. Alvarez-Erviti L, Seow Y, Yin H, Betts C, Lakhali S, Wood MJA. Delivery of siRNA to the mouse brain by systemic injection of targeted exosomes. *Nat Biotechnol*. 2011 Apr;29(4):341–5.
173. Mentkowski KI, Lang JK. Exosomes Engineered to Express a Cardiomyocyte Binding Peptide Demonstrate Improved Cardiac Retention in Vivo. *Sci Rep*. 2019 Jul 11;9(1):10041.

174. Choi ES, Song J, Kang YY, Mok H. Mannose-Modified Serum Exosomes for the Elevated Uptake to Murine Dendritic Cells and Lymphatic Accumulation. *Macromolecular Bioscience*. 2019;19(7):1900042.
175. Tian T, Zhang HX, He CP, Fan S, Zhu YL, Qi C, et al. Surface functionalized exosomes as targeted drug delivery vehicles for cerebral ischemia therapy. *Biomaterials*. 2018 Jan 1;150:137–49.
176. Le Blanc K. Mesenchymal stromal cells: Tissue repair and immune modulation. *Cytotherapy*. 2006;8(6):559–61.
177. Bazzoni R, Takam Kamga P, Tanasi I, Krampera M. Extracellular Vesicle-Dependent Communication Between Mesenchymal Stromal Cells and Immune Effector Cells. *Front Cell Dev Biol*. 2020;8:596079.
178. Prockop DJ. Repair of Tissues by Adult Stem/Progenitor Cells (MSCs): Controversies, Myths, and Changing Paradigms. *Molecular Therapy*. 2009 Jun 1;17(6):939–46.
179. Murphy DE, de Jong OG, Brouwer M, Wood MJ, Lavieu G, Schiffelers RM, et al. Extracellular vesicle-based therapeutics: natural versus engineered targeting and trafficking. *Exp Mol Med*. 2019 Mar;51(3):1–12.
180. Lee C, Mitsialis SA, Aslam M, Vitali SH, Vergadi E, Konstantinou G, et al. Exosomes Mediate the Cytoprotective Action of Mesenchymal Stromal Cells on Hypoxia-Induced Pulmonary Hypertension. *Circulation*. 2012 Nov 27;126(22):2601–11.
181. Bruno S, Grange C, Deregibus MC, Calogero RA, Saviozzi S, Collino F, et al. Mesenchymal Stem Cell-Derived Microvesicles Protect Against Acute Tubular Injury. *Journal of the American Society of Nephrology*. 2009 May;20(5):1053.
182. Bai L, Shao H, Wang H, Zhang Z, Su C, Dong L, et al. Effects of Mesenchymal Stem Cell-Derived Exosomes on Experimental Autoimmune Uveitis. *Sci Rep*. 2017 Jun 28;7(1):4323.
183. Qi X, Zhang J, Yuan H, Xu Z, Li Q, Niu X, et al. Exosomes Secreted by Human-Induced Pluripotent Stem Cell-Derived Mesenchymal Stem Cells Repair Critical-Sized Bone Defects through Enhanced Angiogenesis and Osteogenesis in Osteoporotic Rats. *International Journal of Biological Sciences*. 2016 May 25;12(7):836–49.
184. Deng M, Xiao H, Zhang H, Peng H, Yuan H, Xu Y, et al. Mesenchymal Stem Cell-Derived Extracellular Vesicles Ameliorates Hippocampal Synaptic Impairment after Transient Global Ischemia. *Frontiers in Cellular Neuroscience*. 2017;11.
185. Kou M, Huang L, Yang J, Chiang Z, Chen S, Liu J, et al. Mesenchymal stem cell-derived extracellular vesicles for immunomodulation and regeneration: a next generation therapeutic tool? *Cell Death Dis*. 2022 Jul 4;13(7):1–16.
186. Wu CH, Li J, Li L, Sun J, Fabbri M, Wayne AS, et al. Extracellular vesicles derived from natural killer cells use multiple cytotoxic proteins and killing mechanisms to target cancer cells. *Journal of Extracellular Vesicles*. 2019 Dec 1;8(1):1588538.
187. Zhao B, Zhang Y, Han S, Zhang W, Zhou Q, Guan H, et al. Exosomes derived from human amniotic epithelial cells accelerate wound healing and inhibit scar formation. *J Mol Hist*. 2017 Apr 1;48(2):121–32.
188. Chen CW, Wang LL, Zaman S, Gordon J, Arisi MF, Venkataraman CM, et al. Sustained release of endothelial progenitor cell-derived extracellular vesicles from shear-thinning hydrogels improves angiogenesis and promotes function after myocardial infarction. *Cardiovascular Research*. 2018 Jun 1;114(7):1029–40.

189. Khan M, Nickoloff E, Abramova T, Johnson J, Verma SK, Krishnamurthy P, et al. Embryonic stem cell-derived exosomes promote endogenous repair mechanisms and enhance cardiac function following myocardial infarction. *Circ Res.* 2015 Jun 19;117(1):52–64.
190. Tong L, Hao H, Zhang Z, Lv Y, Liang X, Liu Q, et al. Milk-derived extracellular vesicles alleviate ulcerative colitis by regulating the gut immunity and reshaping the gut microbiota. *Theranostics.* 2021 Jul 25;11(17):8570–86.
191. Li G, Chen T, Dahlman J, Eniola-Adefeso L, Ghiran IC, Kurre P, et al. Current challenges and future directions for engineering extracellular vesicles for heart, lung, blood and sleep diseases. *Journal of Extracellular Vesicles.* 2023;12(2):12305.
192. Johnston PA, Grandis JR. STAT3 signaling: Anticancer strategies and challenges. *Molecular Interventions.* 2011;11(1):18–26.
193. Qi QR, Yang ZM. Regulation and function of signal transducer and activator of transcription 3. *World J Biol Chem.* 2014 May 26;5(2):231–9.
194. Aigner P, Just V, Stoiber D. STAT3 isoforms: Alternative fates in cancer? *Cytokine.* 2019 Jun 1;118:27–34.
195. Becker S, Groner B, Müller CW. Three-dimensional structure of the Stat3 β homodimer bound to DNA. *Nature.* 1998 Jul;394(6689):145–51.
196. Ren Z, Mao X, Mertens C, Krishnaraj R, Qin J, Mandal PK, et al. Crystal structure of unphosphorylated STAT3 core fragment. *Biochemical and Biophysical Research Communications.* 2008 Sep 12;374(1):1–5.
197. Xu X, Sun YL, Hoey T. Cooperative DNA Binding and Sequence-Selective Recognition Conferred by the STAT Amino-Terminal Domain. *Science.* 1996 Aug 9;273(5276):794–7.
198. Hu T, Yeh JE, Pinello L, Jacob J, Chakravarthy S, Yuan G cheng, et al. Impact of the N-Terminal Domain of STAT3 in STAT3-Dependent Transcriptional Activity. *Molecular and Cellular Biology.* 2015;35(19):3284–300.
199. Vogt M, Domszalai T, Kleshchanok D, Lehmann S, Schmitt A, Poli V, et al. The role of the N-terminal domain in dimerization and nucleocytoplasmic shuttling of latent STAT3. *Journal of Cell Science.* 2011 Mar 15;124(6):900–9.
200. Zhang T, Kee WH, Seow KT, Fung W, Cao X. The Coiled-Coil Domain of Stat3 Is Essential for Its SH2 Domain-Mediated Receptor Binding and Subsequent Activation Induced by Epidermal Growth Factor and Interleukin-6. *Molecular and Cellular Biology.* 2000 Oct;20(19):7132–9.
201. Ma J, Zhang T, Novotny-Diermayr V, Tan ALC, Cao X. A Novel Sequence in the Coiled-coil Domain of Stat3 Essential for Its Nuclear Translocation*. *Journal of Biological Chemistry.* 2003 Aug 1;278(31):29252–60.
202. Horvath CM, Wen Z, Darnell JE. A STAT protein domain that determines DNA sequence recognition suggests a novel DNA-binding domain. *Genes Dev.* 1995 Apr 15;9(8):984–94.
203. Mertens C, Haripal B, Klinge S, Darnell JE. Mutations in the linker domain affect phospho-STAT3 function and suggest targets for interrupting STAT3 activity. *Proceedings of the National Academy of Sciences.* 2015 Dec;112(48):14811–6.
204. Bowman T, Garcia R, Turkson J, Jove R. STATs in oncogenesis. *Oncogene.* 2000 May;19(21):2474–88.

205. Wen Z, Zhong Z, Darnell JE. Maximal activation of transcription by stat1 and stat3 requires both tyrosine and serine phosphorylation. *Cell*. 1995 Jul 28;82(2):241–50.
206. Levy DE, Darnell JE. STATs: Transcriptional control and biological impact. *Nature Reviews Molecular Cell Biology*. 2002;3(9):651–62.
207. Darnell JE. STATs and gene regulation. *Science*. 1997;277(5332):1630–5.
208. Zhong Z, Wen Z, Darnell Jr JE. Stat3: A STAT Family Member Activated by Tyrosine Phosphorylation in Response to. *Science*. 1994;264(5155):95–8.
209. Mertens C, Darnell JE. SnapShot: JAK-STAT Signaling. *Cell*. 2007 Nov 2;131(3):612-612.e1.
210. Shuai K, Liu B. Regulation of JAK-STAT signalling in the immune system. *Nature Reviews Immunology*. 2003;3(11):900–11.
211. Freeman AF, Holland SM. Clinical Manifestations, Etiology, and Pathogenesis of the Hyper-IgE Syndromes. *Pediatr Res*. 2009 May;65(7):32–7.
212. Davis SD, Schaller J, Wedgwood R. JOB'S SYNDROME: Recurrent, " Cold ", Staphylococcal Abscesses. *The Lancet*. 1966 May 7;287(7445):1013–5.
213. Buckley RH, Wray BB, Belmaker EZ. Extreme hyperimmunoglobulinemia E and undue susceptibility to infection. *Pediatrics*. 1972 Jan;49(1):59–70.
214. Sowerwine KJ, Holland SM, Freeman AF. Hyper-IgE syndrome update. *Annals of the New York Academy of Sciences*. 2012;1250(1):25–32.
215. Freeman AF, Avila EM, Shaw PA, Davis J, Hsu AP, Welch P, et al. Coronary Artery Abnormalities in Hyper-IgE Syndrome. *J Clin Immunol*. 2011 Jun 1;31(3):338–45.
216. Scheuerman O, Hoffer V, Cohen AH, Woellner C, Grimbacher B, Garty BZ. Reduced Bone Density in Patients with Autosomal Dominant Hyper-IgE Syndrome. *J Clin Immunol*. 2013 Jul 1;33(5):903–8.
217. Freeman AF, Renner ED, Henderson C, Langenbeck A, Olivier KN, Hsu AP, et al. Lung Parenchyma Surgery in Autosomal Dominant Hyper-IgE Syndrome. *J Clin Immunol*. 2013 Jul 1;33(5):896–902.
218. Wakim M, Alazard M, Yajima A, Speights D, Saxon A, Stiehm ER. High Dose Intravenous Immunoglobulin in Atopic Dermatitis and Hyper-IgE Syndrome. *Annals of Allergy, Asthma & Immunology*. 1998 Aug 1;81(2):153–8.
219. Kimata H. High-dose intravenous γ -globulin treatment for hyperimmunoglobulinemia E syndrome. *Journal of Allergy and Clinical Immunology*. 1995 Mar 1;95(3):771–4.
220. Goussetis E, Peristeri I, Kitra V, Traeger-Synodinos J, Theodosaki M, Psarra K, et al. Successful long-term immunologic reconstitution by allogeneic hematopoietic stem cell transplantation cures patients with autosomal dominant hyper-IgE syndrome. *Journal of Allergy and Clinical Immunology*. 2010 Aug 1;126(2):392–4.
221. Gennery AR, Flood TJ, Abinun M, Cant AJ. Bone marrow transplantation does not correct the hyper IgE syndrome. *Bone Marrow Transplant*. 2000 Jun;25(12):1303–5.
222. Milner JD, Brenchley JM, Laurence A, Freeman AF, Hill BJ, Elias KM, et al. Impaired TH17 cell differentiation in subjects with autosomal dominant hyper-IgE syndrome. *Nature*. 2008;452(7188):773–6.

223. Holland SM, DeLeo FR, Elloumi HZ, Hsu AP, Uzel G, Brodsky N, et al. STAT3 mutations in the hyper-IgE syndrome. *The New England journal of medicine*. 2007 Oct;357(16):1608–19.
224. Minegishi Y, Saito M, Tsuchiya S, Tsuge I, Takada H, Hara T, et al. Dominant-negative mutations in the DNA-binding domain of STAT3 cause hyper-IgE syndrome. *Nature*. 2007;448(7157):1058–62.
225. Khourieh J, Rao G, Habib T, Avery DT, Lefèvre-Utile A, Chandesris MO, et al. A deep intronic splice mutation of STAT3 underlies hyper IgE syndrome by negative dominance. *Proceedings of the National Academy of Sciences*. 2019 Aug 13;116(33):16463–72.
226. Giacomelli M, Tamassia N, Moratto D, Bertolini P, Ricci G, Bertulli C, et al. SH2-domain mutations in STAT3 in hyper-IgE syndrome patients result in impairment of IL-10 function. *European Journal of Immunology*. 2011;41(10):3075–84.
227. Heimall J, Davis J, Shaw PA, Hsu AP, Gu W, Welch P, et al. Paucity of genotype'phenotype correlations in STAT3 mutation positive Hyper IgE Syndrome (HIES). *Clinical Immunology*. 2011;139(1):75–84.
228. He J, Shi J, Xu X, Zhang W, Wang Y, Chen X, et al. STAT3 mutations correlated with hyper-IgE syndrome lead to blockage of IL-6/STAT3 signalling pathway. *Journal of Biosciences*. 2012;37(2):243–57.
229. Mackie J, Ma CS, Tangye SG, Guerin A. The ups and downs of STAT3 function: too much, too little and human immune dysregulation. *Clinical and Experimental Immunology*. 2023 Jan 18;uxad007.
230. Tangye SG, Cook MC, Fulcher DA. Insights into the Role of STAT3 in Human Lymphocyte Differentiation as Revealed by the Hyper-IgE Syndrome¹. *The Journal of Immunology*. 2009 Jan 1;182(1):21–8.
231. Yang XO, Panopoulos AD, Nurieva R, Chang SH, Wang D, Watowich SS, et al. STAT3 Regulates Cytokine-mediated Generation of Inflammatory Helper T Cells *. *Journal of Biological Chemistry*. 2007 Mar 30;282(13):9358–63.
232. Egwuagu CE. STAT3 in CD4+ T helper cell differentiation and inflammatory diseases. *Cytokine*. 2009 Sep 1;47(3):149–56.
233. Toussiroot E. The IL23/Th17 Pathway as a Therapeutic Target in Chronic Inflammatory Diseases. *IADT*. 2012 Apr 1;11(2):159–68.
234. Jin W, Dong C. IL-17 cytokines in immunity and inflammation. *Emerg Microbes Infect*. 2013 Sep;2(9):e60.
235. Muranski P, Restifo NP. Essentials of Th17 cell commitment and plasticity. *Blood*. 2013 Mar 28;121(13):2402–14.
236. Holland SM, DeLeo FR, Elloumi HZ, Hsu AP, Uzel G, Brodsky N, et al. STAT3 Mutations in the Hyper-IgE Syndrome. *New England Journal of Medicine*. 2007 Oct 18;357(16):1608–19.
237. He J, Shi J, Xu X, Zhang W, Wang Y, Chen X, et al. STAT3 mutations correlated with hyper-IgE syndrome lead to blockage of IL-6/STAT3 signalling pathway. *Journal of biosciences*. 2012 Jun;37(2):243–57.
238. Dmitrieva NI, Walts AD, Nguyen DP, Grubb A, Zhang X, Wang X, et al. Impaired angiogenesis and extracellular matrix metabolism in autosomal-dominant hyper-IgE syndrome. *Journal of Clinical Investigation*. 2020;140(8):4167–81.

239. Gasteiger E, Hoogland C, Gattiker A, Duvaud S, Wilkins MR, Appel RD, et al. Protein Identification and Analysis Tools on the ExPASy Server. In: Walker JM, editor. *The Proteomics Protocols Handbook*. Totowa, NJ: Humana Press; 2005. p. 571–607.
240. Kelly SM, Jess TJ, Price NC. How to study proteins by circular dichroism. *Biochimica et Biophysica Acta - Proteins and Proteomics*. 2005;1751(2):119–39.
241. Kelly S, Price N. The Use of Circular Dichroism in the Investigation of Protein Structure and Function. *Current Protein & Peptide Science*. 2005;1(4):349–84.
242. Micsonai A, Wien F, Kernya L, Lee YH, Goto Y, Réfrégiers M, et al. Accurate secondary structure prediction and fold recognition for circular dichroism spectroscopy. *Proceedings of the National Academy of Sciences of the United States of America*. 2015;112(24):E3095–103.
243. Micsonai A, Wien F, Bulyáki É, Kun J, Moussong É, Lee YH, et al. BeStSel: A web server for accurate protein secondary structure prediction and fold recognition from the circular dichroism spectra. *Nucleic Acids Research*. 2018;46(W1):W315–22.
244. Butturini E, Gotte G, Dell'Orco D, Chiavegato G, Marino V, Canetti D, et al. Intermolecular disulfide bond influences unphosphorylated STAT3 dimerization and function. *Biochemical Journal*. 2016;473(19):3205–19.
245. Butturini E, Darra E, Chiavegato G, Cellini B, Cozzolino F, Monti M, et al. S-glutathionylation at Cys328 and Cys542 impairs STAT3 phosphorylation. *ACS Chemical Biology*. 2014;9(8):1885–93.
246. Ma X, Sayeski PP. Identification of Tubulin as a Substrate of Jak2 Tyrosine Kinase and Its Role in Jak2-Dependent Signaling. *Biochemistry*. 2007 Jun 1;46(24):7153–62.
247. Trenkenschuh E, Richter M, Heinrich E, Koch M, Fuhrmann G, Friess W. Enhancing the Stabilization Potential of Lyophilization for Extracellular Vesicles. *Advanced Healthcare Materials*. 2021;2100538.
248. Schulz E, Karagianni A, Koch M, Fuhrmann G. Hot EVs – How temperature affects extracellular vesicles. *European Journal of Pharmaceutics and Biopharmaceutics*. 2020;146(December 2019):55–63.
249. Préal C de, Hadam MR, Mach B. Regulation of Genes for HLA Class II Antigens in Cell Lines from Patients with Severe Combined Immunodeficiency. *New England Journal of Medicine*. 1988 May 19;318(20):1295–300.
250. Yang F, Moss LG, Phillips GN. The Molecular Structure of Green Fluorescent Protein. *Structure*. 2011;14(October):1–14.
251. Ward WW, Prentice HJ, Roth AF, Cody CW, Reeves SC. Spectral Perturbations of the Aequorea Green-Fluorescent Protein. *Photochemistry and Photobiology*. 1982;35:803–8.
252. Darnell JE, Kerr Ian M, Stark GR. Jak-STAT Pathways and Transcriptional Activation in Response to IFNs and Other Extracellular Signaling Proteins. *Science*. 1994 Jun 3;264(5164):1415–21.
253. Escola JM, Kleijmeer MJ, Stoorvogel W, Griffith JM, Yoshie O, Geuze HJ. Selective Enrichment of Tetraspan Proteins on the Internal Vesicles of Multivesicular Endosomes and on Exosomes Secreted by Human B-lymphocytes *. *Journal of Biological Chemistry*. 1998 Aug 7;273(32):20121–7.
254. Bachurski D, Schuldner M, Nguyen PH, Malz A, Reiners KS, Grenzi PC, et al. Extracellular vesicle measurements with nanoparticle tracking analysis—An accuracy and repeatability comparison between NanoSight NS300 and ZetaView. *Journal of Extracellular Vesicles*. 2019 Jan 1;8(1).

255. O'Brien K, Ughetto S, Mahjoun S, Nair AV, Breakefield XO. Uptake, functionality, and re-release of extracellular vesicle-encapsulated cargo. *Cell Reports*. 2022;39(2):110651.
256. Choi D, Go G, Kim DK, Lee J, Park SM, Di Vizio D, et al. Quantitative proteomic analysis of trypsin-treated extracellular vesicles to identify the real-vesicular proteins. *Journal of extracellular vesicles*. 2020;9(1):1757209.
257. Tsien RY. The Green Fluorescent Protein. *Annu Rev Biochem*. 1998 Jun 1;67(1):509–44.
258. Beer L, Mildner M, Gyöngyösi M, Ankersmit HJ. Peripheral blood mononuclear cell secretome for tissue repair. *Apoptosis*. 2016 Dec 1;21(12):1336–53.
259. Rajendran L, Bali J, Barr MM, Court FA, Krämer-Albers EM, Picou F, et al. Emerging Roles of Extracellular Vesicles in the Nervous System. *The Journal of Neuroscience*. 2014 Nov 12;34(46):15482 LP – 15489.
260. Paolicelli RC, Bergamini G, Rajendran L. Cell-to-cell Communication by Extracellular Vesicles: Focus on Microglia. *Neuroscience*. 2019;405:148–57.
261. Nimmerjahn A, Kirchhoff F, Helmchen F. Resting Microglial Cells Are Highly Dynamic Surveillants of Brain Parenchyma in Vivo. *Science*. 2005 May 27;308(5726):1314–8.
262. Awada R, Saulnier-Blache JS, Grès S, Bourdon E, Rondeau P, Parimisetty A, et al. Autotaxin Downregulates LPS-Induced Microglia Activation and Pro-Inflammatory Cytokines Production. *Journal of Cellular Biochemistry*. 2014;115(12):2123–32.
263. Garção P, Oliveira CR, Agostinho P. Comparative study of microglia activation induced by amyloid-beta and prion peptides: Role in neurodegeneration. *Journal of Neuroscience Research*. 2006;84(1):182–93.
264. Taylor RA, Sansing LH. Microglial Responses after Ischemic Stroke and Intracerebral Hemorrhage. *Journal of Immunology Research*. 2013 Oct 10;2013:e746068.
265. Wang G, Zhang J, Hu X, Zhang L, Mao L, Jiang X, et al. Microglia/Macrophage Polarization Dynamics in White Matter after Traumatic Brain Injury. *Journal of Cerebral Blood Flow & Metabolism*. 2013;33(12):1864–74.
266. Block ML, Zecca L, Hong JS. Microglia-mediated neurotoxicity: uncovering the molecular mechanisms. *Nat Rev Neurosci*. 2007 Jan;8(1):57–69.
267. Muzio L, Viotti A, Martino G. Microglia in Neuroinflammation and Neurodegeneration: From Understanding to Therapy. *Frontiers in Neuroscience*. 2021;15.
268. Hu X, Herrero C, Li WP, Antoniv TT, Falck-Pedersen E, Koch AE, et al. Sensitization of IFN- γ Jak-STAT signaling during macrophage activation. *Nat Immunol*. 2002 Sep;3(9):859–66.
269. Butturini E, Boriero D, Carcereri de Prati A, Mariotto S. STAT1 drives M1 microglia activation and neuroinflammation under hypoxia. *Archives of Biochemistry and Biophysics*. 2019;669(January):22–30.
270. Butturini E, Cozzolino F, Boriero D, Carcereri de Prati A, Monti M, Rossin M, et al. S-glutathionylation exerts opposing roles in the regulation of STAT1 and STAT3 signaling in reactive microglia. *Free Radical Biology and Medicine*. 2018;117(February):191–201.
271. Boriero D, Carcereri de Prati A, Antonini L, Ragno R, Sohji K, Mariotto S, et al. The anti-STAT1 polyphenol myricetin inhibits M1 microglia activation and counteracts neuronal death. *FEBS Journal*. 2021;288(7):2347–59.